THE BEHAVIOR OF PRESTRESSED HIGH PERFORMANCE CONCRETE BRIDGE GIRDERS FOR US HIGHWAY 401 OVER THE NEUSE RIVER IN RALEIGH, NC

By

Mervyn J. Kowalsky
Co-Principal Investigator

Paul Zia
Co-Principal Investigator

Matthew C. Wagner
Graduate Research Assistant

Bruce A. Warren
Graduate Research Assistant

Research Project 23241-97-8

Final Report

In cooperation with the

North Carolina Department of Transportation

And

Federal Highway Administration
The United States Department of Transportation

Department of Civil Engineering
North Carolina State University
Raleigh, N.C. 27695-7908

November 2001

Technical Report Documentation Page

1. Report No. **FHWA/NC/2002-003**	2. Government Accession No.	3. Recipient's Catalog No.
4. Title and Subtitle **The Behavior of Prestressed High Performance Concrete Bridge Girders for US Highway 401 over the Neuse River in Raleigh, NC**		5. Report Date **May 2, 2002**
		6. Performing Organization Code
7. Author(s) Mervyn J. Kowalsky, Paul Zia, Matt C. Wagner, and Bruce A. Warren		8. Performing Organization Report No.
9. Performing Organization Name and Address **North Carolina State University, Box 7908, Raleigh, NC**		10. Work Unit No. (TRAIS)
		11. Contract or Grant No.
12. Sponsoring Agency Name and Address Office of Bridge Technology Federal Highway Administration 400 Seventh Street, NW Washington D.C., 20590		13. Type of Report and Period Covered **Final Report** **August, 1998 - July, 2001**
		14. Sponsoring Agency Code **1997-08**

15. Supplementary Notes

This project was fully funded by a federal ISTEA grant through the FHWA.

16. Abstract

High performance concrete (HPC) with higher compressive strength (in the range of 8,000 to 10,000 psi) and increased durability is rapidly gaining acceptance for bridge construction. The goal of this project was to implement and demonstrate the economic benefits of the HPC technology in bridge design and construction in North Carolina, thereby providing a greater value to the public. Specifically, the project monitored the production of HPC in typical plant and field conditions, confirmed the feasibility of producing HPC bridge girders and decks, and validated the expected behavior of bridge superstructures built with HPC girders and decks.

17. Key Words **High performance concrete, bridges, prestressed, field monitoring.**	18. Distribution Statement		
19. Security Classif. (of this report)	20. Security Classif. (of this page)	21. No. of Pages **140**	22. Price

Form DOT F 1700.7 (8-72) **Reproduction of completed page authorized**

DISCLAIMER

The contents of this report reflect the views of the author(s) and not necessarily the view of the University. The author(s) are responsible for the facts and the accuracy of the data presented herein. The contents do not necessarily reflect the official views or policies of either the North Carolina Department of Transportation or the Federal Highway Administration at the time of publication. This report does not constitute a standard, specification, or regulation.

ACKNOWLEDGMENTS

The research documented in this report was sponsored by the Federal Highway Administration through its High Performance Concrete Implementation Program and the North Carolina Department of Transportation. A Technical Advisory Committee composed of representatives of the two agencies provided guidance for the research project. The authors are indebted to many individuals for their support at the various stages of the research. They included J. L. Smith, Bill Rogers, Jimmy Lee, Dick Reaves, Pat Strong, Mohammed Mustafa (deceased), Tim Rountree, Cecil Jones, Ron Hancock, Moy Biswas, David Greene, Owen Cordle, Robert Woodruff, Rodger Rochelle, and Tom Koch of NCDOT, and Paul Simon of FHWA. The assistance of Leif Wathne and Gene Clark of the FHWA Mobile Concrete Laboratory in conducting match-curing of the concrete as well as some of tests to determine the concrete properties during and after the casting of the HPC girders is greatly appreciated.

The authors would like to thank the technical staff of the NCSU Constructed Facilities Laboratory, in particular, Jerry Atkinson who assisted in various aspects of instrumentation at the laboratory. The authors also received invaluable help from both Adrian Durham and Bryan Ewing prior to and during the casting of the HPC girders.

Finally, the cooperation of the personnel of Carolina Prestress in Charlotte, during the casting and instrumentation of the prestressed concrete girders is also gratefully acknowledged.

SUMMARY

As of December 1999, 29% of the nation's 585,542 highway bridges have been rated structurally or functionally deficient, according to the Federal Highway Administration (http://www.fhwa.dot.gov////bridge/defbr99.htm). To replace some of these deficient bridges or to construct new bridges, it has been found that high performance concrete (HPC) can be utilized to great advantage in terms of structural efficiency and durability. However, there is a need for more field data on high performance concrete and on the structural behavior when high performance concrete is used.

In 1997, the Federal Highway Administration (FHWA) initiated a program to demonstrate the application of high performance concrete to bridges throughout the United States. The North Carolina Department of Transportation (NCDOT) participated in that program and chose a bridge on U. S. Highway 401 in Raleigh crossing the Neuse River as the site for demonstration. The original design of the bridge with the conventional concrete called for six lines of girders. By using HPC, it was possible to eliminate one line of girders for the entire length of the bridge, thus achieving significant savings for the initial cost of the bridge.

The objective of this research is to monitor the behavior of four prestressed HPC bridge girders used in this NCDOT demonstration project during their casting and to study the properties of the concrete used in the girders. This report provides details of the testing of the concrete and field instrumentation of the bridge girders. Comparisons are made between the experimental and theoretical results.

TABLE OF CONTENTS

LIST OF TABLES

LIST OF FIGURES

1. INTRODUCTION

1.1 Overview

In May 1997, the Federal Highway Administration (FHWA) established the High Performance Concrete (HPC) Bridge-Technology Delivery Team (TDT). One goal of the HPC Bridge TDT is to have at least one such bridge project in every state by the year 2002. The FHWA shares funding for such a bridge with each individual state in which the project is located (http://www.tfhrc.gov/structur/hpc/research.htm). The North Carolina Department of Transportation (NCDOT) chose a bridge on Highway 401 over the Neuse River in Raleigh as the demonstration site. As part of this program, North Carolina State University (NCSU) undertook a research project that consisted of the tasks of providing instrumentation and monitoring four prestressed HPC girders used in the bridge.

This report covers phase two of three phases in the implementation effort. In phase one, Warren (2000) assembled a data acquisition system and developed the necessary computer code for the CR323X data logger (Campbell Scientific Inc.) to accumulate data. The work presented in this report involved the use of the data acquisition system to monitor the short-term behavior of the girders during and after their casting along with the properties of the concrete used. Phase three will involve installing instrumentation in the bridge deck and monitoring the long-term performance of the girders and bridge superstructure using the same data acquisition system. Phase three is currently underway as part of a new NCDOT sponsored research project.

1.2 High Performance Concrete

High performance concrete (HPC) is any concrete that satisfies certain performance requirements that cannot be achieved by conventional concrete. There is no unique definition of HPC. The American Concrete Institute (ACI) defines HPC "as concrete which meets special performance and uniformity requirements that cannot always be achieved routinely by using only conventional materials and normal mixing, placing, and curing practices" (Zia et al. 1997). HPC does not simply mean high strength concrete, but also includes other enhanced material properties such as early-age strength, increased flowability, high modulus of elasticity, low permeability, and resistance to chemical and physical attack (increased durability). "HPC is composed of the same materials used in normal concrete, but proportioned and mixed so as to yield a stronger, more durable product" (Vanikar 1996). HPC is usually high strength concrete (HSC), but HSC may not always be of high performance (Zia et al. 1997).

HSC has generally been defined as a concrete with a compressive strength of 8,500 psi (60 MPa) up to 18,500 psi (130 MPa) (the practical limit for concrete with ordinary aggregates). In Japan, HSC was achieved as early as the 1930s (Nagataki 1994). As mentioned above, compressive strength alone is not sufficient for distinguishing the various properties of HPC. Shah (1999) states that, "knowledge about relating other attributes of concrete to its composition is still inadequate, and therefore we continue to evaluate other properties in terms of compressive strength." In many cases, HSC is referred to as HPC when its only attribute is high compressive strength. This report will sometimes use compressive strength as a criterion for HPC.

Optimal HPC designs reduce construction material and installation costs. HSC offers the potential for cost savings in construction due to reduced member dimensions. Concrete of very early strength needs less time for curing than conventional concrete. This is beneficial in transportation as it shortens traffic delays. In addition, for general construction, formwork can be removed at a faster pace to accommodate rapid construction schedules. Most importantly, the increased durability of HPC produces structures with enhanced service life (Ehlen 1997).

1.3 Literature Review: High Performance Concrete

HPC is concrete with properties or attributes, which satisfy certain performance criteria, including high strength (see Section 1.2). In North American practice, high strength concrete is usually considered to have a 28-day compressive strength of at least 6000 psi (Shah 1999). There is currently an extensive volume of literature on the subject of HPC. In this section, only those HPC concrete attributes investigated in this research will be discussed.

An important aspect of HPC is its stress-strain relationship. The stress-strain behavior of concrete is dependent on a number of parameters, including aggregate type, age at testing, loading rate, and strain gradient. Figure 1.1 shows the influence of aggregate type on the ascending portion of the stress-strain curve of concrete (Shah and Ahmad 1994).

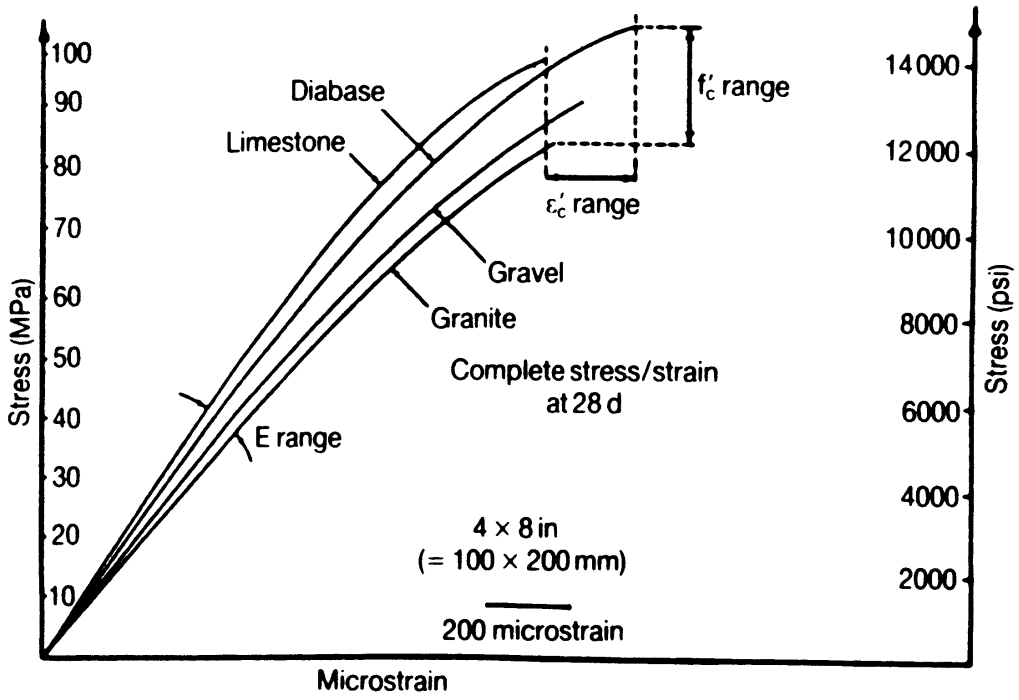

Figure 1.1 Effect of the aggregate type on the ascending portion of the stress-strain curves of concrete at 28 days (Shah and Ahmad 1994)

Shah and Ahmad (1994) also give the following equation for determining the compressive stress at a given strain.

$$f_e = (f'_c)\frac{A(e/e'_c)+(B-1)(e/e'_c)^2}{1+(A-2)(e/e'_c)+B(e/e'_c)} \qquad \text{(Eq. 1.1)}$$

in which

$$A = E_c\frac{e'_c}{f'_c} \qquad \text{(Eq. 1.2)}$$

$$B = 0.88087 - 0.57\times10^{-4}(f'_c) \qquad \text{(Eq. 1.3)}$$

$$e'_c = 0.001648 + 1.14\times10^{-7}(f'_c) \qquad \text{(Eq. 1.4)}$$

$$E_c = 27.55w^{1.5}\sqrt{f'_c} \qquad \text{(Eq. 1.5)}$$

where

w = weight of the concrete (lb/ft^3)

f'_c = ultimate compression strength of the concrete (psi)

The parameters A, B, e'_c, and E_c were determined from a statistical analysis of the experimental results on 3×6 in. (75×152 mm) concrete cylinders with compressive strengths ranging from 3,000 to 11,000 psi (20 to 75 MPa) (Shah and Ahmad 1994). Once *w* and f'_c are known, f_e (the compressive stress at a given strain) can be determined.

The ductility of HPC is an important aspect that must not be overlooked. Gowripalan and Zou (1997) conducted a study examining the flexural behavior and ductility of prestressed beams made with HSC. The curvature of the pretensioned beams tested decreased with increasing concrete strengths (from 8,000 psi to 15,250 psi or 55 to 105 MPa) over the entire loading range from service to ultimate load. The tests showed that ductility reduced with increasing concrete strength.

Research has also been performed to determine the best combination of steel and concrete in regards to the strengths of these materials. Yamada and Matsuura (1999) carried out tests on simple beams constructed of HSC with high strength steel as reinforcement with and without prestressing. In conjunction with this, beams made of normal strength concrete as well as ordinary reinforcing steel were tested for comparison. The tests revealed that the best combination of materials is high strength concrete and high strength steel or normal strength concrete and reinforcement. However, the use of high strength concrete along with high strength steel is expected to have less ductility.

Another important ingredient of HPC is pozzolans. Pozzolans such as silica fume and fly ash are added to portland cement to reduce permeability and, in turn, enhance durability. Silica fume is a by-product of the smelting process used to produce silicon metal and ferrosilicon alloys. Norway produces about 50 % of the world's supply

(Helland 1997). Alshamsi (1997) examined the influence of silica fume and curing temperature on the strength of HSC. Two mixes were examined, one containing silica fume and portland cement, and the other with only normal portland cement. A water cement ratio of 0.27 and slump of 40-60 mm were kept constant using a superplasticizer. The results indicated that while high curing temperature results in greater strength at an early age, it has an adverse effect on concrete at a more mature age. This adverse effect was greater in the concrete mix containing silica fume. Figure 1.2 shows that this is most notable between tests at ages 56 and 90 days.

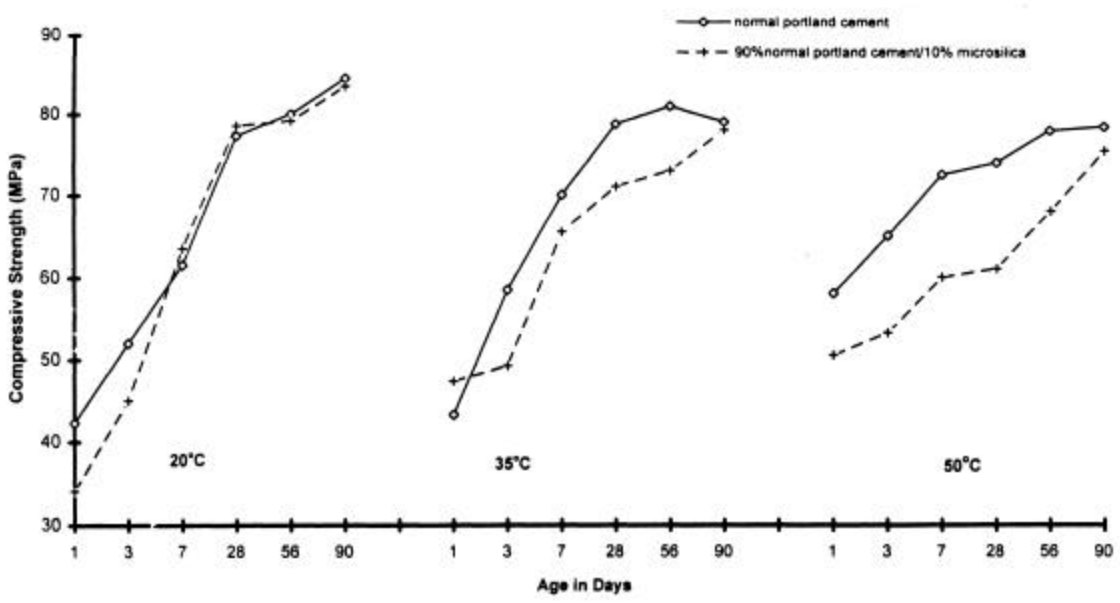

Figure 1.2 The effect of silica fume on the strength of HSC at 20° C, 35° C and 50° C (Alshamsi 1997)

Not only the stress-strain relationship, from which the modulus of elasticity (MOE) is determined, but also the cause of compression failure is important for HPC. A test program was performed on HPC mixes in a study performed by French et al. (1997). Nearly 7,000 specimens were tested from 142 HPC mixes with w/c ratios between 0.28

and 0.32. The results indicated that the aggregate was the dominant variable. They concluded that, "For high strength concrete, the strength of the paste and paste aggregate interface are sufficiently increased such that the strength becomes limited by failure of the aggregate."

HPC is beneficial in nearly every aspect. Across the United States, it has been found that obtaining the longer life and increased durability of bridges built with HPC can come at no additional initial cost. Mary Lou Ralls of the Texas DOT notes that, "Although HPC mixes cost more than conventional mixes, overall bridge costs can be lower because fewer beams and supports are needed" (Halkyard 1996).

1.4 Literature Review: High Performance Bridges

Since the increasing cost of materials can be offset by an increase in strength and a corresponding reduction in material quantities, high performance structures are becoming increasingly popular (Price et al. 1999). This discussion is not intended to list all bridges constructed using HPC, but to highlight some important structures which exemplify the use of HPC in bridge structures.

In 1973, the first generation of HSC bridges was built for the Japan National Railway. The second Ayaragigawa Bridge used post-tensioned bulb T-beams with 8,600 psi (60 MPa) concrete. The Iwahana Bridge was a single span Warren truss made with over 11,500 psi (80 MPa) concrete. The Otanabe Bridge was a single span Howe truss built with a HSC mix of the same strength. These historically significant bridges utilized HSC in order to lower dead load, reduce deflection and reduce vibration and noise (Zia et al. 1997). Since their construction, these bridges have performed to all expectations.

HSC bridges have also been constructed in France, Norway, Denmark, and Germany. The Elorn Bridge in France was completed in 1994. This cable-stayed bridge spans 1,320 ft (400 m) and utilizes silica fume to achieve a concrete strength of 13,900 psi (97 MPa) and increased durability. The Stovset Bridge, a prestressed cantilever, was completed in Norway in 1993. The lightweight high strength mix had a concrete strength of 10,600 psi (74 MPa) to reduce weight and increase strength. In Germany, the Dwutzer Bridge was built in 1978 to cross the Rhine close to Cologne. "The bridge is a free cantilever construction with three spans of 435, 610, and 399 ft (132, 185, and 121 m). Two hundred feet (61 m) of the middle span was cast with a lightweight concrete and the rest of the bridge with a normal weight concrete" (Zia et al. 1997). The field strength of the concrete reached 9,890 psi (69 MPa) for the normal weight concrete and 10,500 psi (73 MPa) for the lightweight concrete (Zia et al. 1997). Completed in 1998, the Great Belt Bridge consists of two 26,247 ft (8000 m) railway tunnels and a 5,328 ft (1624 m) suspension bridge. Three hundred and sixty-three feet (110 m) precast concrete girders were used in the structure.

Canada also boasts a fair share of HPC bridges. The Portneuf Bridge in Quebec, for one, constructed in 1992, uses precast post-tensioned beams of 81.5 ft (24.8 m) with an average concrete strength of 10,750 psi (75 MPa), a w/c of 0.29 and 5-7% air content. Through the use of this mix, prestress loss was reduced, and enhanced durability extended the service life of the structure. This is an important bridge and will be discussed again in the ensuing section.

The Cross Westchester Expressway Bridge in Westchester County, New York exhibits the benefits of using HPC. The New York State Department of Transportation

designed two viaduct replacement structures using steel box girders composite with a cast-in-place concrete deck. A precast, post-tensioned deck was proposed as an alternate to the cast-in-place concrete deck to speed up the construction and provide a more durable structure by utilizing HPC. The viaducts consist of spans ranging in lengths of 110 ft (33.5m) to 184 ft (56.1m). The typical 28-day strength of the concrete mix is 6,300 psi (43.4 MPa). Though this seems to reside on the lower end of compressive strength for a HPC, the mix is considered of high performance due to other factors. Reduced permeability, enhanced workability, controlled heat of hydration, and reduced creep and shrinkage effects are all very important considerations that were incorporated into the design of this mix. The mix is shown below in Table 1.1.

Table 1.1 Cross Westchester Expressway Bridge HPC Mix

Cement content (lbs per cy)	536
Fly ash content (lbs per cy)	145
Microsilica content (lbs per cy)	44
Sand percent total aggregate (solid volume)	45.8
Designed water/total cementitious content of 725 lbs (weight)	0.4
Target air content (%)	7.5
Target Slump (inches)	3

The Cross Westchester Expressway shows that using a precast, post-tensioned, high performance concrete deck system results in an accelerated construction schedule, better quality control, a more durable structure, and the same approximate cost as a cast-in-place deck (Price et al. 1999).

1.5 Literature Review: Instrumented Structures

With 29% of the nation's 585,542 highway bridges rated structurally or functionally deficient (http://www.fhwa.dot.gov////bridge/defbr99.htm), instrumentation

of bridge structures is one of the best means of identifying bridges in need of repair and monitoring current and future projects.

The Sunshine Skyway Bridge, which spans the Tampa Bay, is one of the longest clear-span concrete bridges built in North America. The bridge has four different types of spans: trestle approach spans, low-level approach spans, high-level approach spans, and three cable-stayed spans. Standard I-girders are used for 128 of the trestle approach spans. The bridge was instrumented in order to measure strain and temperature gradients. Seventeen precast bridge segments, three pylon sections, and 11 sections of two main piers were instrumented. Carlson strain meters were installed horizontally to measure longitudinal movements and thermocouples were placed in the bridge superstructure for monitoring temperature effects (Shahawy and Aarockiasamy 1996a). A computer-controlled automatic data acquisition system (ADAS) was used to collect the data during and after construction. The data correlated very well with analytical models developed by Shahawy and Aarockiasamy (1996a).

Short-term and long-term tests were performed on twenty-four 6 x 12 inch concrete cylinders. Short-term tests included measurements of concrete compressive strength, modulus of elasticity, and coefficient of thermal expansion. Vibrating wire gages (type VCE 4200) were positioned at the center of cylinders before casting to measure strains during testing (Shahawy and Aarockiasamy 1996a). Long-term tests consisted of measurements of time-dependent shrinkage and creep. Shrinkage measurements began three days after casting, and creep measurements began 28 days after casting (Shahawy and Aarockiasamy 1996a).

In the case of the Sunshine Skyway Bridge, an estimate of forces and moments in the bridge were based on a number of analyses considering different percentages of prestress losses (Shahawy and Aarockiasamy 1996b). Losses in the pylon sections and bridge segments were estimated at 20% for analytical models considering time-dependent strains. These estimates compared well with the measured data.

Another instrumented structure is the Bi-Tan Bridge, located in Taiwan. It was designed by T.Y. Lin International and was constructed by the Continental Construction Company of Taiwan. It has a total span of about 2,625 ft (800 m), a horizontal radius of curvature of about 2,461 ft (750 m), and is a continuous prestressed concrete bridge. The 160-meter arch-shaped center span was constructed using prestressed concrete box girders. This bridge was instrumented with a static and dynamic monitoring system to verify design assumptions and to determine the stress distribution in the structure during and after construction. The system was also used to collect data for analysis and use as a reference for development of bridge maintenance, and to assess damage of the bridge due to prestress loss, earthquakes, or traffic overloads (Tarricone 1990). The center portion of the Bi-Tan Bridge was instrumented with concrete strain gages, thermocouples, inclinometers, and creep and shrinkage compensation gages for static monitoring. "The static instrumentation and analysis is emphasized on studying the long-term behavior of the bridge due to creep and shrinkage of the concrete" (Tarricone 1990). These gages were all embedded in the box girders. Dynamic monitoring was desired as dynamic loading can affect the long-term operation of a bridge. Identifying earthquake damage quickly, and determining damage due to traffic overload will help assess the health of the

bridge. In the case of the Bi-Tan Bridge, accelerometers were placed along the bridge. The locations of these gages were determined based on finite element analyses.

Vibrating wire gages (extensometers) are another means of measuring strain and even temperature within concrete. The Portneuf Bridge mentioned in the previous section represents one of the first air-entrained HPC bridges located in North America. The deck slab was instrumented with 24 thermocouples and 24 vibrating wire extensometers that were connected to a remote data acquisition system directly linked by modem to a computer at the Universite de Sherbrooke (Lachemi et al. 1996). This project tested the reliability of thermocouples and vibrating wire extensometers on a real structure. It was successful, and the results from this study presented a clear observation of the temperature variation on the slab's behavior.

Thermocouples are used not only to measure the temperatures within a structure throughout its life, but sometimes more importantly to measure the temperatures during cement hydration. This is because the heat of hydration can be the cause of cracking in concrete at early age as well as long-term strength problems as concrete ages (Gilliland and Dilger 1997). A short-term temperature-monitoring project on the Confederation Bridge, crossing the Northumberland Strait in Atlantic Ocean, Canada was undertaken to determine the effects of heat of cement hydration on bridge members. Thermocouples were placed throughout the piers of the structure, both vertically and horizontally. Temperatures inside some members did not approach ambient levels until one month after casting of concrete. The study did conclude that, "Overall, little cracking has occurred despite large thermal gradients and high maximum temperatures" (Gilliland and Dilger 1997).

Through the efforts of the FHWA, there is a large number of HPC bridges in the United States both constructed and under construction. Rather than discuss in detail every HPC bridge that has been constructed and in most cases instrumented in the United States, Table 1.2 gives a summary of some notable bridges and their attributes. The table lists both instrumented and non-instrumented HPC bridge structures. Compressive strength is the sole concrete property listed, however most of these structures have other enhanced properties such as permeability limitations in their HPC mix. In some cases, these other properties are the reason why these structures are deemed high performance.

With ever increasing technological advancements, we enter the new millennium with more tools than ever before for determining what is taking place within structures. Fiber-optic gages, which have greater capacity and speed than standard gages, are now available (Fuhr et al. 1998). Acoustic gages and wireless data acquisition systems are also being used (Anon 1997a). There are gages that can measure corrosion as well as strains and temperature. These gages and instruments are the wave of the future (Anon 1997b).

Table 1.2 HPC Bridges in the United States as of April 2001

Bridge	State	Status	Girder Length and Type	28-day Compressive Strength	Instrumentation	Benefits of using HPC & Comments
Alabama Highway 199 over Uphaupee and Bulger Creek, Macon County	Alabama	Open April 2000	34.7 m AASHTO BT-54	f'_c= 69 MPa, (10,000 psi)	Thermocouples, ERSGs, VWG, external gages.	Eliminates one pier and requires 35-34.7m girders instead of 40-30.5m girders.
Interstate 25 Over Yale Avenue, Denver	Colorado	Open June 1998	34.5m and 30m Box	f'_c= 69 MPa, (10,000 psi)	Yes, but undecided	Eliminates two column/pier lines. More durable-resistant to wear and de-icing chemicals.
Bridge Over Interstate 75, Henry County	Georgia	Not yet open	Still being designed.	Possibly f'_c= 97 MPa, (14,000 psi)	Thermocouples, VWG, external gages.	Smaller girder depth. Increased durability.
120th Street and Giles Road Bridge, Sarpy County	Nebraska*	Opened to traffic in 1996	22.9m NU1100 (metric Bulb-Tee)	f'_c= 83 MPa, (12,000 psi)	Thermocouples, ERSGs, VWG, external gages.	Fewer girders. Increased durability
Route 104 Bridge over the Newfound River, Bristol	New Hampshire	Opened in 1996	20m Type III AASHTO	f'_c= 55 MPa, (8,000 psi	None	Concrete material properties measured at casting to determine durability.
Route 3A Bridge over the Newfound River, Bristol	New Hampshire	Opened to traffic 6/25/99	18.3m NE Bulb-Tee	f'_c= 55 MPa, (8,000 psi	VWGs, thermistors.	Strong field basis for monitoring structure in harsh northern climate.
State Route 22 at Mile Post 6.57, Guernsey County	Ohio	Opened Nov, 1998	36m 1219mm x 1067mm deep box beams	f'_c= 69 MPa, (10,000 psi)	Yes, but undecided	Eliminates two substructure units with a single-span.
Louetta Road Overpass State Highway 249, Houston	Texas*	Opened to traffic in May, 1998	40m U-shaped	f'_c= 69-90 MPa, (10,000-13,000 psi)	None	Allowed for simple-span construction eliminating more complicated/costly substructure. U-beams & single pier aesthetically pleasing.

Table 1.2 (continued)

Bridge	State	Status	Girder Length and Type	28-day Compressive Strength	Instrumentation	Benefits of using HPC & Comments
San Angelo Bridge, US Route 67, San Angelo	Texas*	Opened to traffic in Jan 1998	19.4-47.9m Type IV AASHTO	f'_c= 40-101 MPa, (5,800-14,700 psi)	None	Reduced number of beams and reduction of one span. Improved durability.
Route 40 Over the Falling River, Lynchburg District	Virginia	Open to traffic in May, 1996	24.4m Type IV AASHTO	f'_c= 55 MPa, (8,000 psi)	None	Five girders instead of seven. Four percent savings over normal bridge material.
Virginia Avenue Over the Clinch River, Richlands	Virginia	Opened to traffic in Dec, 1997	22.6m Type III AASHTO	f'_c= 69 MPa, (10,000 psi)	None	Four girders instead of seven.
Eastbound State Route 18 Over State Route 515, King County	Washington	Opened to traffic in Jan, 1998	42m and 24m WSDOT W74G I-girders	f'_c= 69 MPa, (10,000 psi)	None	Five lines of girders instead of seven.

*All girders are prestressed using 15.2mm strand (0.6 in) except in Nebraska and Texas. 12.7mm (0.5 in) strand was used in Nebraska, and in Texas both size strands were used, depending on span length.

1.6 Objectives and Scope of Work

The purpose of this research is to develop data on the properties of the concrete used for this bridge demonstration project and to evaluate the structural behavior of the bridge girders. As mentioned previously, there is an abundance of laboratory information regarding HPC, a need exists for specific data on HPC actually used in the field.

To achieve this objective, AASHTO Type III and Type IV girders were instrumented with thermocouples, electrical resistance strain gages (ERSGs), and vibrating wire gages (VWGs). Transfer length, prestress loss, heat of hydration, and creep and shrinkage of the concrete are determined through field data obtained from the instrumented girders. Compressive strength, modulus of elasticity (MOE), modulus of rupture (MOR), coefficient of thermal expansion and chloride permeability of the concrete are determined from cylinders and prisms cast on site during the casting of the actual girders. Shrinkage and creep are measured from cylinders, prisms as well as "mock-up" girders.

The field observation was accomplished by using a previously developed comprehensive data acquisition program, which utilizes Campbell Scientific software and equipment (data loggers).

2. MATERIAL PROPERTIES

2.1 Introduction

Tests were conducted on the HPC to evaluate its compressive strength, flexural strength, modulus of elasticity, creep, shrinkage, thermal properties, and chloride permeability. In all cases, the concrete was taken from batches of material used in the casting of the bridge girders in October of 2000. The October casting was the second attempt to cast the girders due to an unsuccessful casting at Carolina Prestress in March of 2000[1].

It should be noted that these material tests were not used for designing the concrete mix, but for analysis of the concrete. The mix design was produced before casting and was "tested" on a mock-up girder, which will be discussed in Section 3.4.

Numerous 4 x 8 in (102 x 203 mm) cylinders, six 3 x 3 x 11 ¼ in (76 x 76 x 286 mm) prisms, and six 6 x 6 x 20 in (152 x 152 x 508 mm) prisms were cast for the material testing. Figure 2.1 shows the casting of the test specimens for the Type III girders. All specimens were made using three lifts of concrete and rodded after each lift. Once all specimen molds were full, the exposed surface was smoothed with a trowel. After the concrete had developed its initial set, the specimens were placed on the side forms of the girders to keep the curing temperatures for the specimens as close as possible to those of the actual girders (see Figure 2.2).

[1] During the March casting, the concrete became overly stiff and resulted in honeycombing after removal of the forms. The NCDOT also made a mistake in approving a larger aggregate than the specifications allowed.

Figure 2.1 Casting Cylinder and Prism Specimens

Figure 2.2 Specimen Curing Before Placement of Tarp and Moist Cure

One concern in the use of HSC is that standard cylinder tests may not provide an accurate measure of the in-place strength of the concrete. High temperatures generated during hydration can affect the in-place strength of HPC. For this reason, it was desirable to match-cure the cylinders that were to be used for compression test and the determination of the modulus of elasticity. The match curing was performed with the help of the FHWA Mobile Concrete Laboratory. A thermocouple was placed at mid-span near the bottom flange of the girder and connected to a control box, which regulated the cylinder mold temperature. This thermocouple was used as the datum to ensure that the cylinders were cured at the same temperature as the concrete in the girder. Four cylinders were match-cured for each girder, for a total of 16. The match-cured cylinders were prepared in the same fashion as standard non-match-cured cylinders. Figure 2.3 shows the set-up of the match-cured cylinders and control boxes.

Figure 2.3 Match Cured Cylinders and Control Boxes

This chapter also presents the predicted values of the material properties of the concrete using various equations, tables, and figures. These values are discussed at the end of each section where applicable.

2.2 HPC Mix

The performance requirements of the HPC mix are listed in Table 2.1. Not all performance criteria were evaluated and the testing was carried out either by NCSU or by the FHWA, as shown in the table. Table 2.2 shows the mix proportion of the concrete that was used for the girders, including the mock-up girder discussed in Section 3.4. Table 2.3 lists the laboratory test results for the concrete. It should be noted that the addition of superplasticizer is very important for this mix as it increases the slump from zero to seven inches.

The producer's quality control personnel measured the slump of the concrete and the air content as ready-mix concrete trucks arrived on site. Table 2.4 shows the field data acquired on the concrete. Concrete from every other ready-mix truck was tested to determine its air content and the slump was tested for the concrete from two trucks for both the Type III and Type IV girders. Both the air content and the slump met the requirements of the specifications.

Table 2.1 HPC Target Performance Criteria

Material Characteristic	Value	If tested, by whom
Strength	$10 \leq x \leq 11$ ksi ($69 \leq x \leq 76$ MPa)	NCSU
Modulus of Elasticity	$6 \leq x \leq 7.5 \times 10^6$ psi ($41 \leq x \leq 52$ GPa)	NCSU
Shrinkage	$x < 400$ microstrain	NCSU
Creep	($0.31 \geq x > 0.21$/psi ($45 \geq x > 30$/MPa)	NCSU
Freeze-Thaw Durability (x = relative dynamic modulus of elasticity after 300 cycles)	$x \geq 80\%$	
Chloride Permeability (x = coulombs)	$800 \leq x \leq 2000$	FHWA
Scaling Resistance (x = visual rating of surface after 50 cycles)	$x = 2.3$	
Abrasion resistance (x = average depth of wear in inches)	$x < 0.02$	
Resistance to Internal Chemical Attack (x = alkali in cement)	$x < 0.4\%$	

Table 2.2 HPC Mix Proportion (per cubic yard)

Materials Used to Produce the Mix, Quantity SSD	
Water/cementitious materials	0.305
Cement, Type I/II, lbs (Holnam, Holly Hill, S. C.)	900
Coarse Aggregate (78m), lbs (Arrowood, Martin Marietta)	1550
Coarse Aggregate (67m), lbs (Arrowood, Martin Marietta)	450
Fine Aggregate, lbs (H. V. Hedrick, Piedmont Sand Co.)	905
Water, lbs/gallons	275/33
AEA, Micro-Air, oz. (Master Builder)	6
HRWR, PS 1232, oz. (Master Builder)	81
Retarder, Delvo, oz. (Master Builder)	36
Silica Fume, Rheomac, lbs (Master Builder)	50

Table 2.3 Laboratory Test Data of HPC Mix

Target Slump before/after addition of plasticizer, inches	0/8
Actual Slump before/after addition of plasticizer, inches	0/7
Target Air Content (range), %	3-5
Actual Air Content, %	4.8
Concrete Temperature, ºF	88
Air Temperature, ºF	78
24 hr-Compressive Strength, psi	7800
48 hr-Compressive Strength, psi	8800
7 Days-Compressive Strength, psi	9800

Table 2.4 In-situ Material Properties

	Type III Girders		Type IV Girders	
Truck	**Slump, in (mm)**	**Air Content, %**	**Slump, in (mm)**	**Air Content, %**
1	7.68 (195)	5.4	7.87 (200)	4.3
3		4.5		4.3
5		3.7		4.6
7		4.9		4.5
9	7.87 (200)	4.3		4.7
11	-	-	7.87 (200)	3.8

2.3 Compressive Strength

Several 4 x 8 in cylinders were tested to determine the compressive strength at various ages of the HPC. The measured compressive strengths are summarized in Table 2.5. The cylinders were tested in accordance with AASHTO DESIGNATION: T 22-86 (ASTM DESIGNATION: C 39-83b, REVISED). The specimens were loaded at 26,400 lbs/min. Steel caps containing neoprene pads were used to bring the end plane and to transfer the loads uniformly. As mentioned in Section 2.1, both match-cured cylinders and non-match-cured cylinders were tested. The non-match-cured cylinders were initially cured on the side forms of the girders (see Figure 2.2) and then stored at room

temperature in the laboratory until tested. The match-cured cylinders were also stored in the laboratory at room temperature until tested.

Table 2.5 Cylinder Compression Strength (psi)

	Type III Girders				Type IV Girders			
	Girder C4		Girder D4		Girder A4		Girder B4	
Test Age (days)	Match Cure	Non-match Cure	Match Cure	Non-match Cure	Match Cure	Non-match Cure	Match Cure	Non-match Cure
R	9,030	8,400	8,950	7,700	5,930*	8,080	8,830	9,130
14	-	10,140+	-	10,140+	-	9,650+	-	9,650+
28	10,640	10,170+	10,580	10,170+	10,670*	10,560+	10,450	10,560+
56	-	10,740+	-	10,740+	-	11,070+	-	11,070+
100	10,500	10,700+	10,980	10,700+	9,690*	10,850+	9,750	10,850+

- \- Indicates no cylinders tested.
- * Indicates error in match curing due to failure in temperature control.
- \+ Three cylinders tested from C4/D4 and three from A4/B4.
- R Release of prestressing force.

The average compressive strength of the concrete for both the Type III and Type IV girders met specifications ($10 \leq x \leq 11$ ksi). It should be noted that the 100-day strengths were less than that of the 56-day strengths. This could be attributed to the use of silica fume (see Section 1.2).

2.4 Modulus of Elasticity (MOE)

The MOE represents the stiffness of concrete. In order to determine the MOE of the concrete, 4 x 8 in cylinder specimens were tested in compression with dial gages indicating the axial deformation during loading. The dial gages were mounted on a compressometer, shown in Figure 2.4. The cylinders were loaded at 26,400 lbs/min (as required by ASTM C 469) to a maximum load of $0.4 f'_c$ to ensure that the specimens

were only subjected to elastic deformations. The capping procedure was identical to that of the compression test. The deflection of both dial gages was read every 10,000 lbs. These values were averaged and divided by the five-inch gage length to determine the strain at each load increment (see Equation 2.1). The MOE was determined from the slope of the stress vs. strain plot. An instrumented specimen is shown being loaded in Figure 2.5 and Table 2.6 summarizes the MOE results in ksi.

$$e = \frac{(\Delta_1 + \Delta_2)/2}{L_g} \qquad \text{(Eq. 2.1)}$$

where e = strain at a given stress
Δ_1 = deflection of gage 1 at a given stress
Δ_2 = deflection of gage 2 at a given stress
L_g = gage length = 5 in.

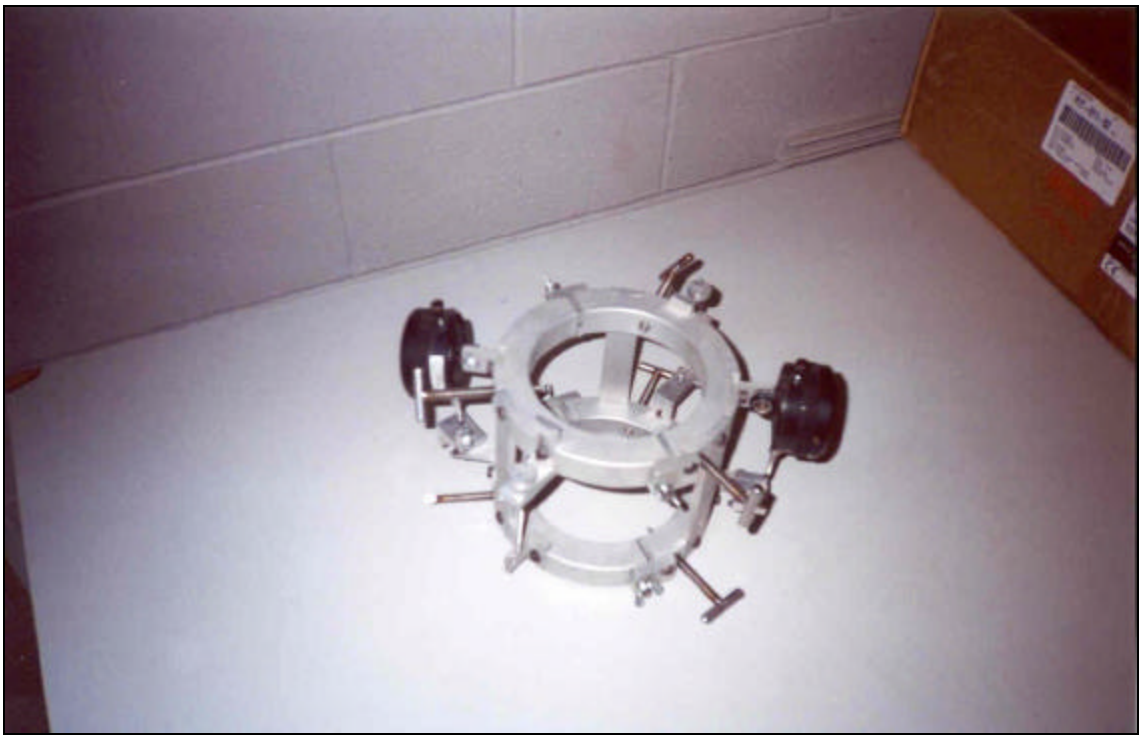

Figure 2.4 Compressometer

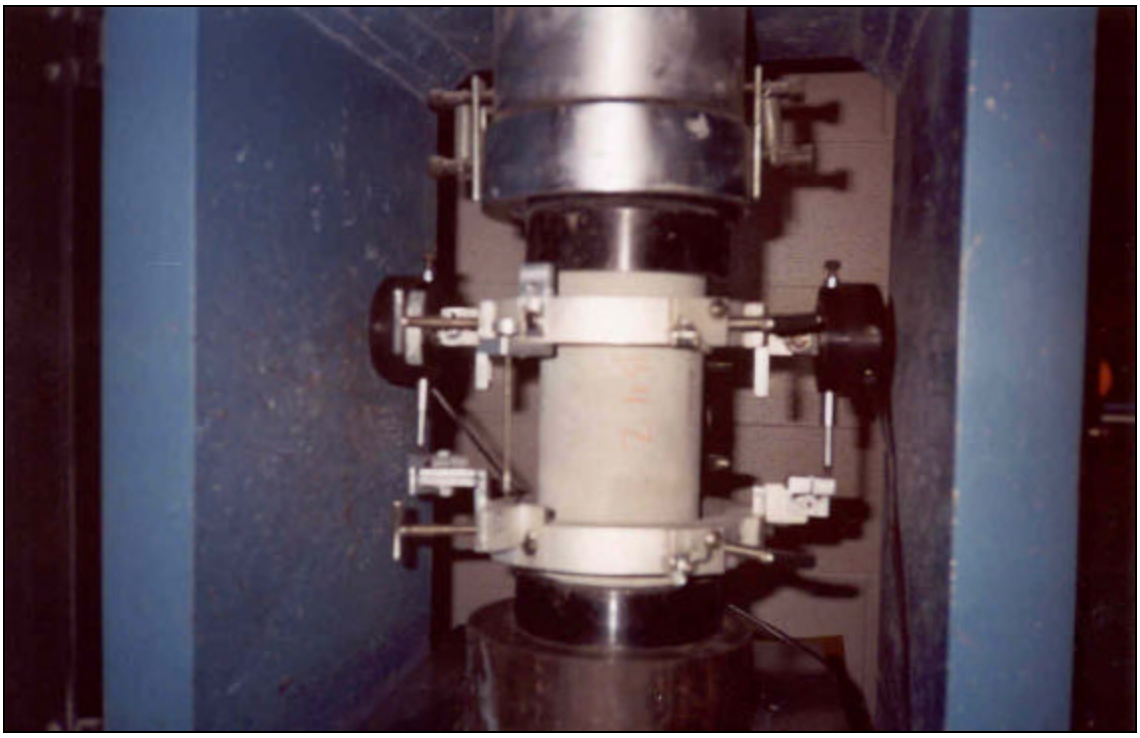

Figure 2.5 Modulus of Elasticity Test in Progress

Table 2.6 Modulus of Elasticity (ksi)

	Type III Girders				Type IV Girders			
	Girder C4		Girder D4		Girder A4		Girder B4	
Test Age (days)	Match Cure	Non-match Cure	Match Cure	Non-match Cure	Match Cure	Non-match Cure	Match Cure	Non-match Cure
R	-	-	-	-	-	-	-	-
14	-	4,421	-	4,721	-	4,958	-	4,134
28	4,547	3,816	4,968	3,860	4,323*	5,240	4,395	4,911
56	-	4,100	-	4,320	-	5,435	-	4,292
100	4,541	4,270	4,960	4,369	4,521*	4,484	4,288	3,935

- \- Indicates no cylinders tested.
- * Indicates error in match curing due to failure of temperature control.
- R Release of prestressing force.

Numerous studies have been conducted to determine a design equation for calculating the MOE of concrete. Both the ACI Code and the PCI Design Handbook recommend using Equation 2.2, based on the work of Pauw (1960).

$$E_c = w^{1.5} 33 \sqrt{f'_c} \qquad \text{lb/ft}^3 \text{ and psi} \qquad \text{(Eq. 2.2)}$$

Collins et al. point out that Equation 2.2 overestimates the MOE of concrete with compression strengths greater than 6000 psi (41 MPa). They recommended an alternate equation for calculating the MOE of normal weight concrete (Equation 2.3):

$$E_c = 40{,}000 \sqrt{f'_c} + 1{,}000{,}000 \qquad \text{psi} \qquad \text{(Eq. 2.3)}$$

Table 2.7 gives the MOE for the compression strengths (from Table 2.5) of both girder types calculated using Equation 2.2. Table 2.8 shows the same, but using Equation 2.3. The unit weight of the concrete used in Equation 2.2 is 153 pcf., the measured unit weight of the concrete.

Table 2.7 Theoretical MOE (ksi) Using Equation 2.2

	Type III Girders				**Type IV Girders**			
	Girder C4		**Girder D4**		**Girder A4**		**Girder B4**	
Test Age (days)	Match Cure	Non-match Cure	Match Cure	Non-match Cure	Match Cure	Non-match Cure	Match Cure	Non-match Cure
R	5,930	5,720	5,910	5,480	4,810*	5,610	5,870	5,970
14	-	6,290+	-	6,290+	-	6,140+	-	6,140+
28	6,440	6,300+	6,420	6,300+	6,450*	6,420+	6,380	6,420+
56	-	6,470+	-	6,470+	-	6,570+	-	6,570+
100	6,400	6,460+	6,540	6,460+	6,150*	6,510+	6,170	6,510+

- \- Indicates no cylinders tested.
- * Indicates error in match curing due to failure of temperature control.
- \+ Based on three cylinders tested from C4/D4 and three from A4/B4.
- R Release of prestressing force.

Table 2.8 Theoretical MOE (ksi) Using Equation 2.3

	Type III Girders				Type IV Girders			
	Girder C4		Girder D4		Girder A4		Girder B4	
Test Age (days)	Match Cure	Non-match Cure	Match Cure	Non-match Cure	Match Cure	Non-match Cure	Match Cure	Non-match Cure
R	4,800	4,670	4,780	4,510	4,080*	4,600	4,760	4,820
14	-	5,030+	-	5,030+	-	4,930+	-	4,930+
28	5,130	5,030+	5,110	5,030+	5,130*	5,110+	5,090	5,110+
56	-	5,150+	-	5,150+	-	5,210+	-	5,210+
100	5,100	5,140+	5,190	5,140+	4,940*	5,170+	4,950	5,170+

- \- Indicates no cylinders tested.
- * Indicates error in match curing due to failure of temperature control.
- \+ Based on three cylinders tested from C4/D4 and three from A4/B4.
- R Release of prestressing force.

Equation 2.2 seems to produce values more in line with the performance criterion (Table 2.1). However, Equation 2.3 gives values that compare better with those obtained from tests. In general, the MOE of the concrete was lower than anticipated. Tables 2.9 and 2.10 show the percent difference between the experimental values and those found using both equations (2.2 and 2.3).

At least three factors may have caused the lower than expected values for the MOE. First, the test specimens were heat cured first followed by air cure instead of moist cure. The difference in curing would cause the specimen to gain its strength faster than its modulus of elasticity. Second, the HPC mix supplied by the producer had a much higher cement content than the HPC mixes used for other recent demonstration projects (see High Performance Concrete, CD produced by Federal Highway Administration, Version 2.0). Higher cement content meant more paste volume in the HPC mix. As a

composite material, the modulus of elasticity of concrete is dependent on the modulus of the paste as well as the aggregates. Since the modulus of the paste is generally lower than that of the aggregates, a concrete mix with a higher cement content (thus a larger volume of paste) would result in lower modulus of elasticity of the concrete. Third, the modulus of elasticity of concrete also depends heavily on the stiffness of the coarse aggregate. The coarse aggregate used in the HPC mix for this project was granite, which may produce a lower modulus of concrete as shown in Figure 1.1.

Table 2.9 Percent Difference in MOE (ksi), Experimental Value vs. Equation 2.2

	Type III Girders				**Type IV Girders**			
	Girder C4		**Girder D4**		**Girder A4**		**Girder B4**	
Test Age (days)	Match Cure	Non-match Cure	Match Cure	Non-match Cure	Match Cure	Non-match Cure	Match Cure	Non-match Cure
R	-	-	-	-	-	-	-	-
14	-	30%	-	25%	-	19%	-	33%
28	29%	39%	23%	39%	33%	18%	31%	24%
56	-	37%	-	33%	-	17%	-	35%
100	29%	34%	24%	32%	26%	31%	31%	40%

- Indicates no cylinders tested.
R Release of prestressing force.

Table 2.10 Percent Difference in MOE (ksi), Experimental Value vs. Equation 2.3

	Type III Girders				**Type IV Girders**			
	Girder C4		**Girder D4**		**Girder A4**		**Girder B4**	
Test Age (days)	Match Cure	Non-match Cure	Match Cure	Non-match Cure	Match Cure	Non-match Cure	Match Cure	Non-match Cure
R	-	-	-	-	-	-	-	-
14	-	12%	-	6%	-	1%	-	16%
28	11%	24%	3%	23%	16%	3%	14%	4%
56	-	20%	-	16%	-	4%	-	18%
100	11%	17%	4%	15%	8%	13%	13%	24%

- Indicates no cylinders tested.
R Release of prestressing force.

2.5 Modulus of Rupture (MOR)

The modulus of rupture (MOR) represents the flexural strength of the concrete, which is defined as the maximum tensile stress in a 20 in. concrete beam failed in pure bending. Six 6 x 6 x 20 in. (152 x 152 x 508 mm) prisms were tested. Three were taken from the same concrete used to cast the Type III girders and three from the concrete used for the Type IV girders. The determination of the MOR was performed in accordance with AASHTO DESIGNATION: T 97-86 (ASTM DESIGNATION C 78-84). Since all specimens fractured in the middle third of the prism, the MOR was determined using Equation 2.4. Figure 2.6 shows the test setup and a loaded specimen is shown in Figure 2.7. Figure 2.8 shows a broken specimen, and the average MOR for each girder type is presented in Table 2.11.

$$MOR = \frac{P \cdot l}{b \cdot d^2} \qquad \text{(Eq. 2.4)}$$

where P = maximum load at fracture
l = clear span
b = base width of prism
d = depth of prism

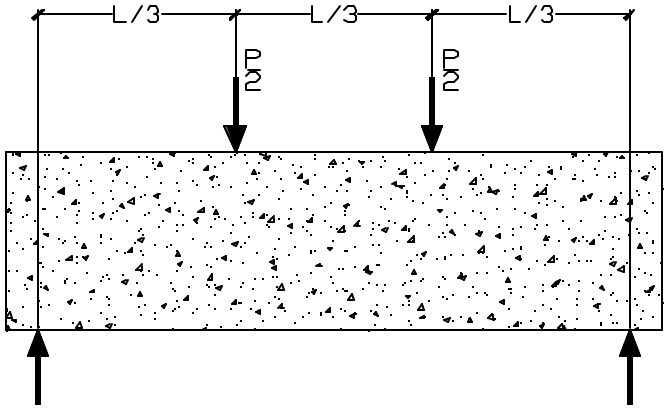

Figure 2.6 MOR Test Setup

Figure 2.7 MOR Specimen Before Loading

Figure 2.8 Fractured MOR Specimen

Table 2.11 Modulus of Rupture (psi)

Type III	Type IV
865	765

The ACI Code (1999) gives the following equation for calculating the modulus of rupture.

$$f_r = 7.5\sqrt{f'_c} \qquad \text{(Eq. 2.5)}$$

where f_r = the modulus of rupture
f'_c = compression strength of the concrete

Using an average value of 10,500 psi for f'_c, Equation 2.5 gives a value of 770 psi, which compares very well with the test results presented in Table 2.11. Modulus of rupture was not specified as a performance criterion.

2.6 Coefficient of Thermal Expansion

Volume changes result from not only creep and shrinkage, but also thermal effects. It is imperative to obtain knowledge of the coefficient of thermal expansion of concrete members that are placed in a structure to mitigate against problems that may result. As with the type VCE 4200 VWGs that were placed in cylinders for the Sunshine Skyway Bridge (see Section 1.5), VWGs (ROCTEST Type EM-5) were placed in the center of 6 x 12 in cylinders in the NCSU laboratory. The EM-5 gage was suspended in place in the center of the mold with six small rubber bands (three at the top and three at the bottom). The VWG lead wire exited the cylinder mold through a hole approximately two inches below the top of the mold. Figure 2.9 shows the gage with lead wire attached and Figure 2.10 shows a prepared mold prior to placing concrete. Embedment ERSGs of

type EGP-5-120 (made by Measurements Group, Inc) were also placed in 6 x 12 in cylinders in the same manner as the VWGs. Figure 2.11 shows both the embedment ERSG, and the cylinder with the gage in place. The purpose of preparing these different cylinders was to compare the data obtained from the two types of gages. Figure 2.12 shows a cylinder with the embedment ESRG.

The VWG not only measures strain, a thermistor located at the center of the gage measures temperature as well. In order to determine the coefficient of thermal expansion of the concrete, the specimens were placed in a freezer for 24 hours and then allowed to warm-up to the room temperature. Initial temperature and strain readings were taken, and then the readings were recorded again after the specimens have been in the freezer for 24 hours. After the specimens were allowed to warm-up to the room temperature, final readings were then recorded. The coefficient of thermal expansion was determined using Equation 2.6. This result, however, is the relative contraction of the concrete to the gage. The coefficient of thermal expansion of the VWG by itself (and the embedment ERSG) had to be determined. The actual coefficient of thermal expansion of the concrete is the summation of the result from the cylinder and the coefficient of thermal expansion of the respective gage. These values can be added because the same gage was used, and therefore the gage length was the same. The test results are listed in Table 2.12.

$$a_T = \frac{m_{e_2} - m_{e_1}}{T_2 - T_1} \qquad \text{(Eq. 2.6)}$$

where a_T = coefficient of thermal expansion
m_{e_2} = final strain
m_{e_1} = initial strain
T_2 = final temperature

T_1 = initial temperature

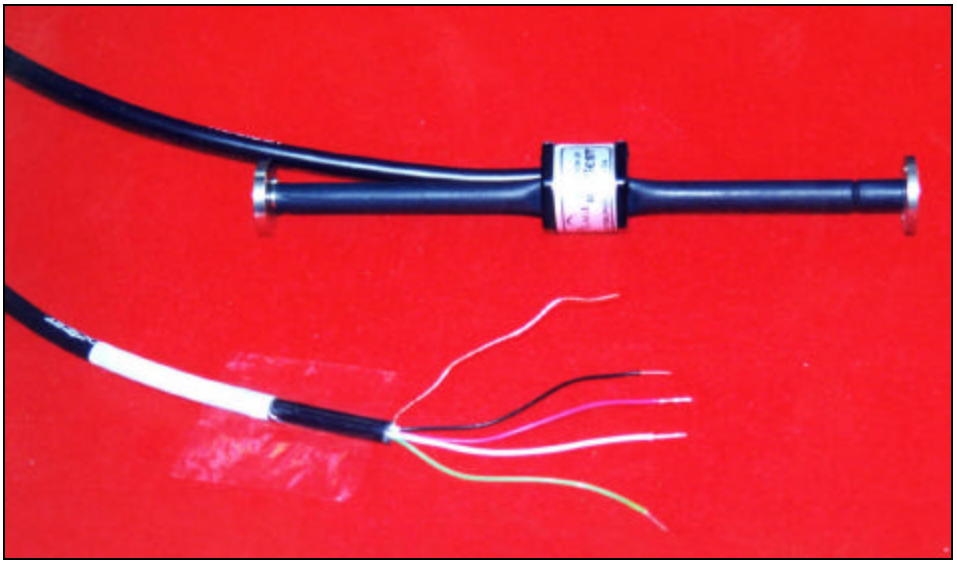

Figure 2.9 VWG, EM-5

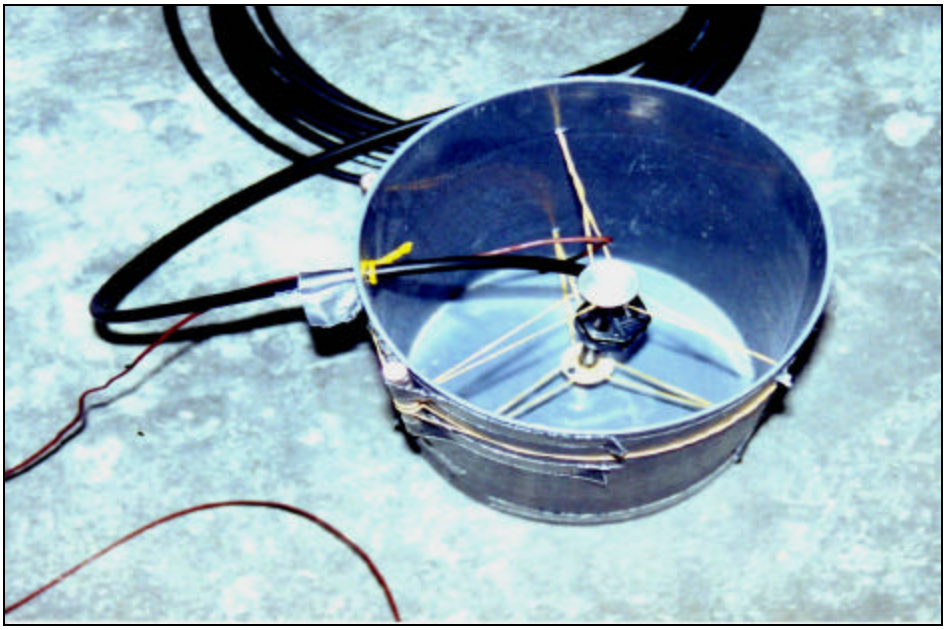

Figure 2.10 VWG in Cylinder

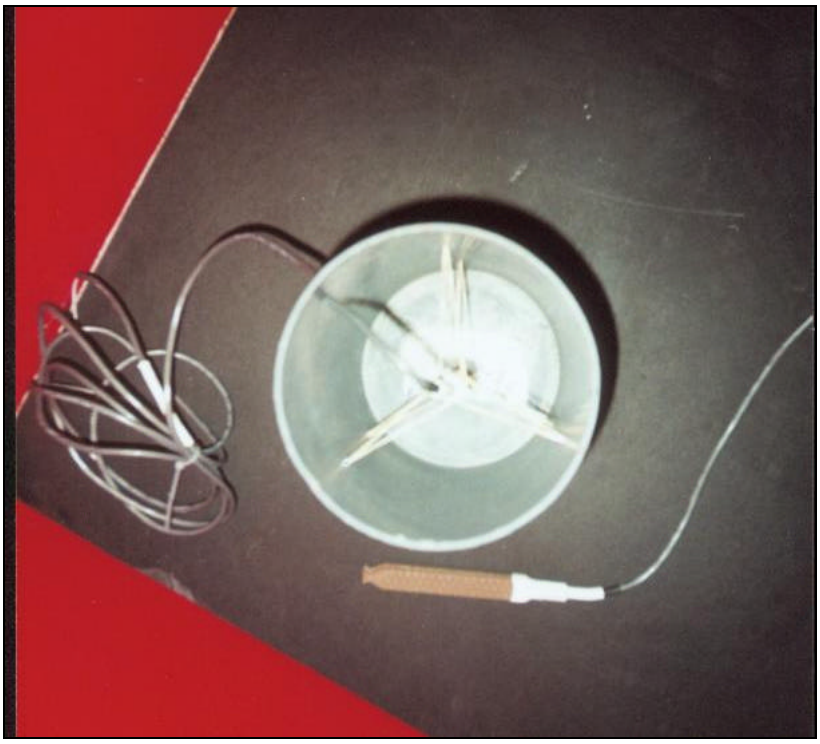

Figure 2.11 Embedment ERSG and Embedment ESRG in Mold

Figure 2.12 Cylinder with Embedment ERSG

Table 2.12 Coefficient of Thermal Expansion

α (in/in/ºC x 10^{-6})	Type III Girders				Type IV Girders			
	Girder C4		Girder D4		Girder A4		Girder B4	
	VWG	ERSG	VWG	ERSG	VWG	ERSG	VWG	ERSG
Gage	6.7	4.9	6.7	4.9	6.7	4.9	6.7	4.9
Cylinder	2.06	4.68	2.14	4.03	2.08	3.74	1.96	3.92
Total	8.76	9.58	8.84	8.93	8.78	8.64	8.66	8.82

The FHWA also performed coefficient of thermal expansion tests on two 4 x 8 in cylinders in accordance with AASHTO P 60; one specimen from the concrete used for the Type III girders and one for the Type IV girders. The results are given below in Table 2.13.

Table 2.13 Coefficient of Thermal Expansion (FHWA, 2001)

	Type III Girder	Type IV Girder
a **(in/in/ºC)**	7.4 x 10^{-6}	8.7 x 10^{-6}

The coefficient of thermal expansion of concrete varies with the type of aggregate used. The range for normal weight concrete made with the same aggregate used in the bridge girders is generally expected to be 9 to 12.5x10^{-6} in/in/°C (5 to 7x10^{-6} in/in/°F) (Collins et al. 1997, PCI Handbook 5th Ed. 1999). So the measured coefficient of thermal expansion for this concrete falls just below the values presented in literature. Coefficient of thermal expansion was not specified as a performance criterion.

2.7 Creep

In prestressed concrete structures, the stress and strain at any section change over time, during which creep and shrinkage of concrete and relaxation of the steel develop

gradually. A stress applied on concrete produces instantaneous strain and if the stress is sustained the strain progressively increases with time due to creep. The instantaneous strain is known as elastic shortening. In prestressed concrete members, creep leads to a substantial loss in prestress. In order to determine the specific creep of the concrete, two creep rigs were used (see Figure 2.13). A constant load was applied to two cylinder specimens (for Type IV girders) between two steel plates by a hydraulic ram above the middle plate and then the load was locked in by three nuts as shown in Figure 2.13. A strain gage box can be seen at the base of the second rig for another set of specimens (for Type III girders). Railroad car coil springs are located at the bottom of each rig to maintain a "constant" load as the specimens shorten. ERSGs were applied to the threaded steel rods, and the load on the cylinders was determined by measuring the strain in the steel rods. The strain gages were read with the strain gage box.

Once the cylinders were brought back from the prestressing plant to NCSU, they were immediately prepared for loading in the creep rigs. First, sulfur caps were applied to both ends of each cylinder to achieve two parallel and uniform loading surfaces. Demec points were then epoxied to both sides of the cylinder. Figure 2.14 shows the prepared cylinders before loading. As shown in Figure 2.13, two cylinders for each girder type were placed in a rig. One cylinder remained uncapped and unloaded in order to record the shrinkage of the specimen. The specimens for the Type III girders were placed in the rig five days after casting and the specimens for the Type IV girders were placed in the rig three days after casting.

Figure 2.13 Creep Rigs

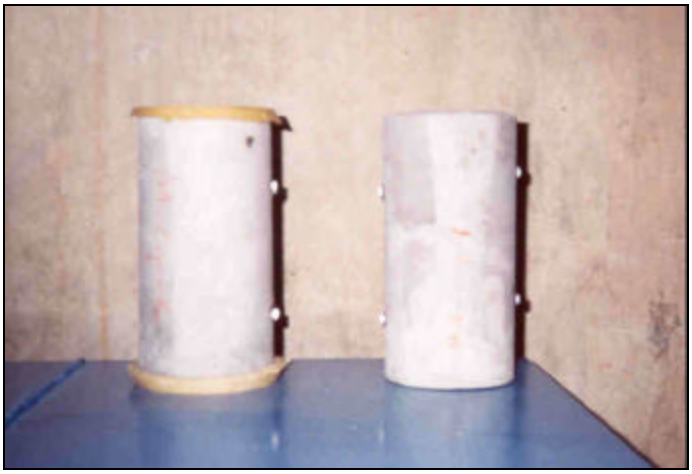

Figure 2.14 Creep and Shrinkage Cylinders

The specimens were loaded to the stress level similar to the concrete stress in the girder at the center of gravity of the prestressing steel. The stress was calculated using the following Equation 2.7.

$$s_{net} = \frac{P}{A} + \frac{P \cdot e}{S} - \frac{M_{DL}}{S} \qquad \text{(Eq. 2.7)}$$

where $P =$ total prestressing force
$A =$ cross sectional area of girder
$e =$ eccentricity of the prestressing force
$S =$ section modulus, $\left(\frac{I}{e}\right)$
$M_{DL} =$ moment induced by the dead load of the girder at mid-span

For the Type III girders, the net compressive stress is 1.75 ksi after detensioning. For the Type IV girders, the corresponding stress is 2.87 ksi. Figure 2.15 shows the cylinder with the applied stress and Demec points. The strain gages on the creep rigs were frequently checked to ensure that the load remained constant as time elapsed. It was necessary to periodically tighten the nuts on the rigs to maintain a constant applied stress.

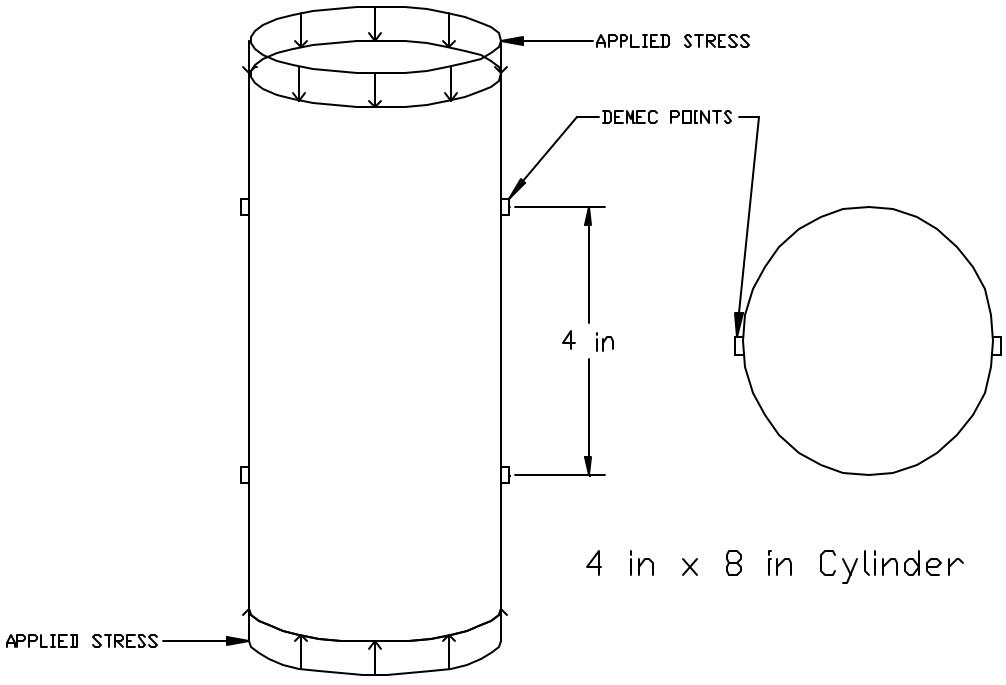

Figure 2.15 Demec Point Locations and Applied Stress on Creep Cylinder

A Demec mechanical gage was used to monitor the deformation in both the creep and shrinkage cylinders. Initial elastic shortening and shrinkage strains were subtracted from the strain readings of the cylinders in the rigs. These net creep strains are plotted in Figures 2.16 and 2.17. During the 3rd to 30th days of loading, applied loads decreased unexpectedly until it was discovered on the 30th day. At this time, the creep rigs were adjusted to re-establish the required loading. This is reflected in the graphs. The dotted lines represent a prediction of the creep strain had the load adjustment not occurred.

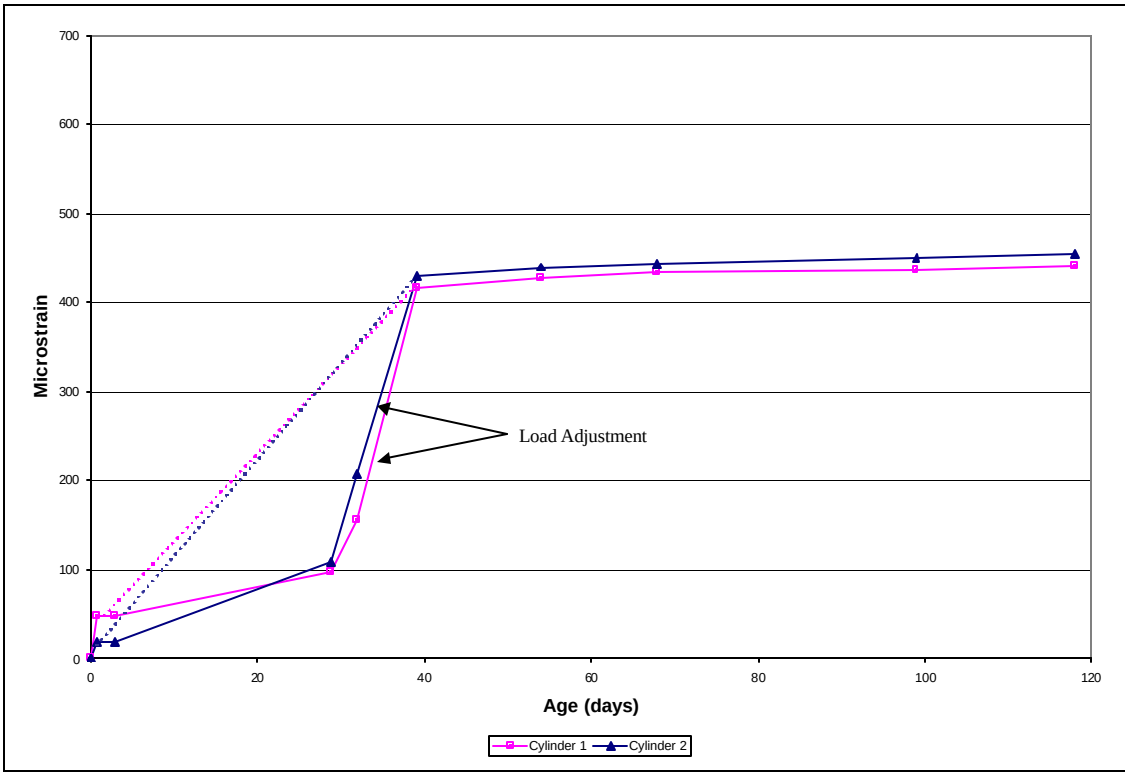

Figure 2.16 Creep Cylinder Strains for Type III Girder

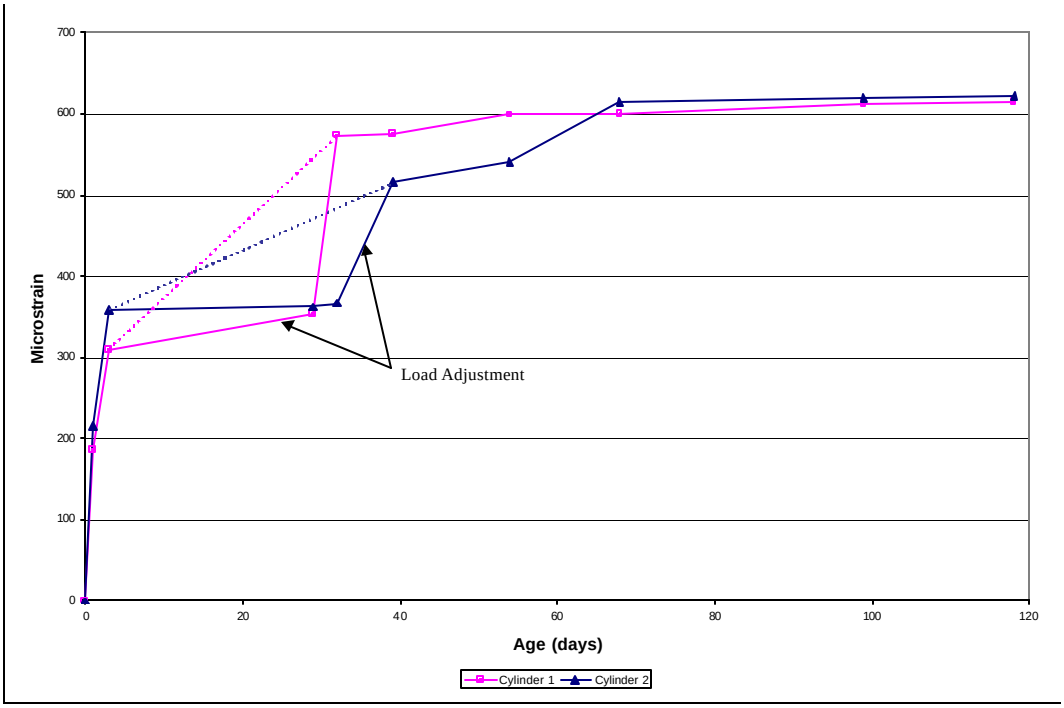

Figure 2.17 Creep Cylinder Strains for Type IV Girder

The average creep of the concrete for the Type III girders is 445 microstrain and that for the Type IV girders is 615 microstrain. The specific creep was calculated using Equation 2.8. The creep coefficient was calculated using Equation 2.9.

$$S_c = \frac{e}{s_{net}} \qquad \text{(Eq. 2.8)}$$

where: S_c = specific creep
e = creep strain
s_{net} = applied stress

$$C_c = \frac{e_{c,ult}}{e_{ci}} \qquad \text{(Eq. 2.9)}$$

where: C_c = creep coefficient
$e_{c,ult}$ = ultimate creep strain

e_{ci} = initial strain due to elastic shortening

The specific creep of the concrete for the Type III girders is 0.254 in/in/psi and that for the Type IV girders is 0.214 in/in/psi. These values met the performance criteria ($0.31 \geq x > 0.21$/psi). The average creep coefficient of the concrete for the Type III girders is 1.85 and that for the Type IV girders is 1.94. These values are slightly lower than the average value of 2.35 as recommended by the ACI Code (1999). However, it should be noted that the ACI Code only considers concrete strengths up to 6000 psi. Naaman (1982) gives values that decrease as the strength of the concrete increases (see Table 2.14). The creep coefficients obtained in this study follow quite well the trend presented in Table 2.14.

Table 2.14 Creep Coefficients (Naaman, 1982)

Compressive Strength		**Creep Coefficient,** C_c
Psi	**MPa**	
3000	20.7	3.1
4000	27.6	2.9
5000	34.5	2.65
6000	41.4	2.4
7000	48.3	2.2
8000	55.2	2.0

2.8 Shrinkage

During casting of the girders, shrinkage prisms and shrinkage girders (i.e. short sections of girder cast for shrinkage measurement) were made. The shrinkage prisms were stored in the laboratory and the shrinkage was measured with a shrinkage stand. The stand, shown in Figure 2.18, measured length change using a dial gage. Figures 2.19 and 2.20 show the shrinkage values of the concrete used in both types of girders. Six 3 x

3 x 11 ¼ in. prisms (76 x 76 x 286 mm) were monitored, three specimens for each girder type. The average shrinkage strain of the concrete for the Type III girders is 510 microstrain, and that for the Type IV girders is 470 microstrain. In calculating the average shrinkage strain for the Type III prisms, only the strain values for specimens one and two were considered as the values for specimen three are inconsistent with those of specimens one and two.

Figure 2.18 Shrinkage Prism in Stand

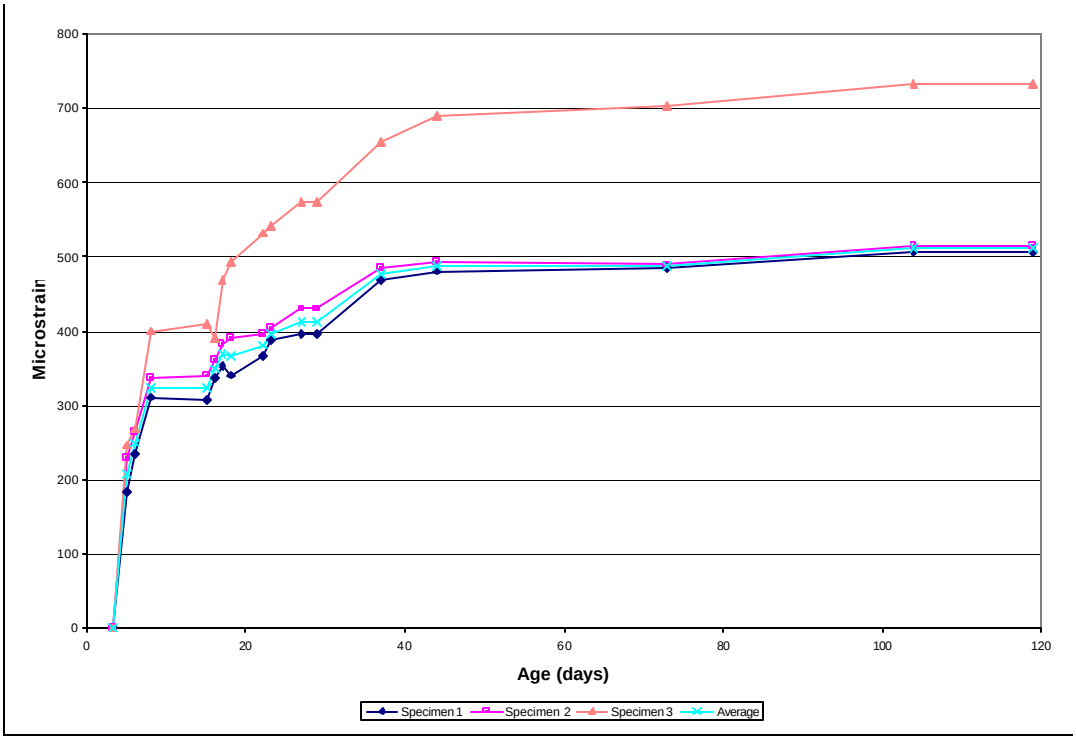

Figure 2.19 Shrinkage Prism Strains for Type III Girder

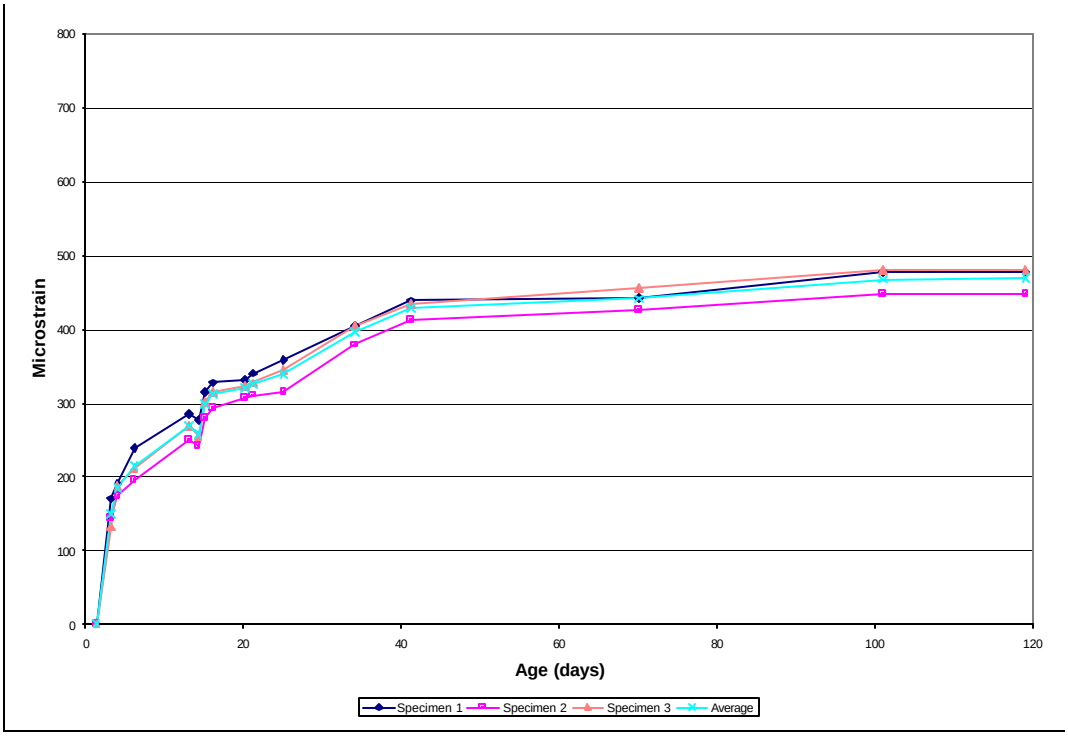

Figure 2.20 Shrinkage Prism Strains For Type IV Girder

Although concrete prisms are generally used to measure the shrinkage of concrete, these specimens are usually stored in the laboratory and contain no reinforcement. However, the specimen size and the environmental conditions affect the shrinkage of concrete. In order to obtain more realistic assessment of shrinkage, two five-foot long shrinkage girders were cast at the same time as the instrumented bridge girders. One was cast in the Type III girder bed and one in the Type IV girder bed. The shrinkage girders not only reside in outdoor conditions, but they have similar steel configurations as that of the actual girders. The embedded steel will provide some restraint to shrinkage.

The shrinkage girders were instrumented at mid-span with VWGs to measure temperature and strain change. One gage was placed at the center of gravity of the top flange, one at mid-height of the web, and one at the center of gravity of the bottom flange (see Figure 2.21). Figure 2.21 shows the Type III shrinkage girder before the side forms were set. Figure 2.22 shows the girder after casting.

Measured shrinkage from the two shrinkage girder specimens are shown in Figures 2.23 and 2.24. The average shrinkage for the Type III girder is 44 microstrain and 86 microstrain for the Type IV girder.

Figure 2.21 Type III Shrinkage Girder Prior to Form Setting

Figure 2.22 Type III Shrinkage Girder

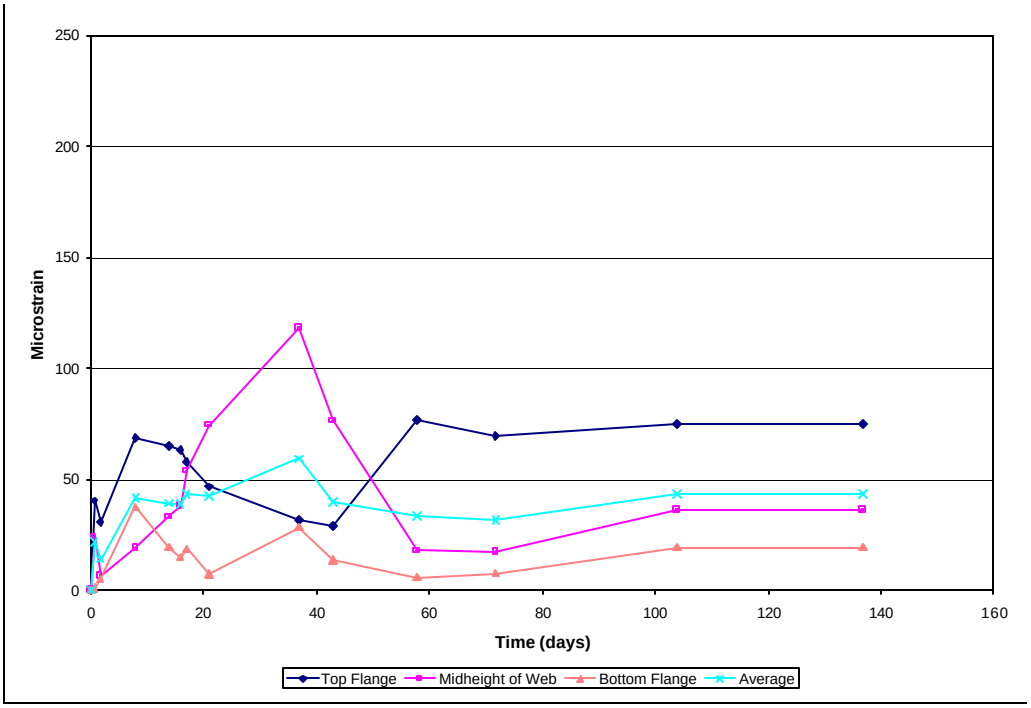

Figure 2.23 Type III Shrinkage Girder Strains

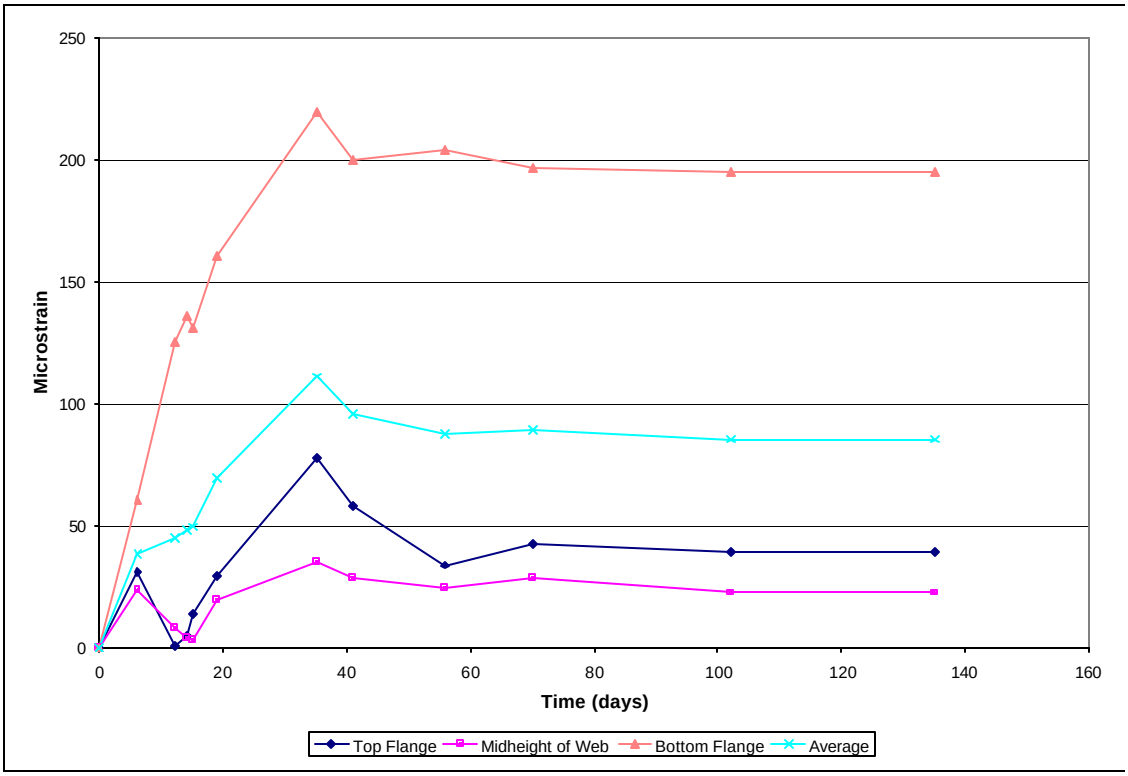

Figure 2.24 Type IV Shrinkage Girder Strains

The shrinkage strains obtained from the prisms exceeded the performance criterion (x < 400 microstrain), however the shrinkage strains obtained from the shrinkage girders were well within the criterion. Table 2.15 gives a summary of the results of shrinkage measurements.

The PCI Design Handbook gives a value of 450 microstrain for a concrete with a surface to volume ratio of 1.5 at 70% relative humidity at 150 days. This value is somewhat lower than the results obtained from shrinkage prisms presented in Table 2.15, and much larger than the shrinkage strains determined from the shrinkage girders.

Table 2.15 Measured Shrinkage

	Microstrain (Average)	
	Type III Girder	**Type IV Girder**
Shrinkage Prisms	510	470
Shrinkage Girders	45	85

2.9 Rapid Chloride Permeability Test

The rapid chloride permeability test provides an indication of the durability of a concrete. The FHWA performed this test in accordance with AASHTO T 277 by slicing standard 4 x 8 in cylinders into thirds and testing the top and middle thirds. The results are given below in Table 2.16.

Table 2.16 Results of Rapid Chloride Permeability Test

Age (days)	Charge Passed (Coulombs)			
	Concrete for Type III Girder		Concrete for Type IV Girder	
	Top	**Middle**	**Top**	**Middle**
56		3704		4557
90	3055	2530	1261	1257

It is noted that the permeability at 56 days did not meet the performance criteria (see Table 2.1) for both concrete. However, the concrete for the Type IV girder met the criteria at 90 days, and the concrete for the Type III girder could likely meet the criteria at a later age.

The higher than expected values of permeability are most likely due to the higher cement content of the HPC mix and the use of heat and air cure of the test specimens. Both of these two factors could cause more and coarser pore structures of the concrete paste, which in turn would increase the permeability of the concrete.

3. GIRDER BEHAVIOR

3.1 Introduction

As mentioned in Section 1.1, NCDOT and NCSU chose the bridge as a demonstration project. A single line of girders was instrumented in order to monitor temperature and strains within the girders. There are five girder lines, each with four spans: 91.9 ft., 91.9 ft., 57.4 ft., and 57.4 ft. The longer spans use Type IV AASHTO girders and the shorter spans use Type III AASHTO girders. Figure 3.1 shows a layout of the bridge. The instrumented girders are designated A4, B4, C4, and D4. The bridge is described in greater detail in the following section.

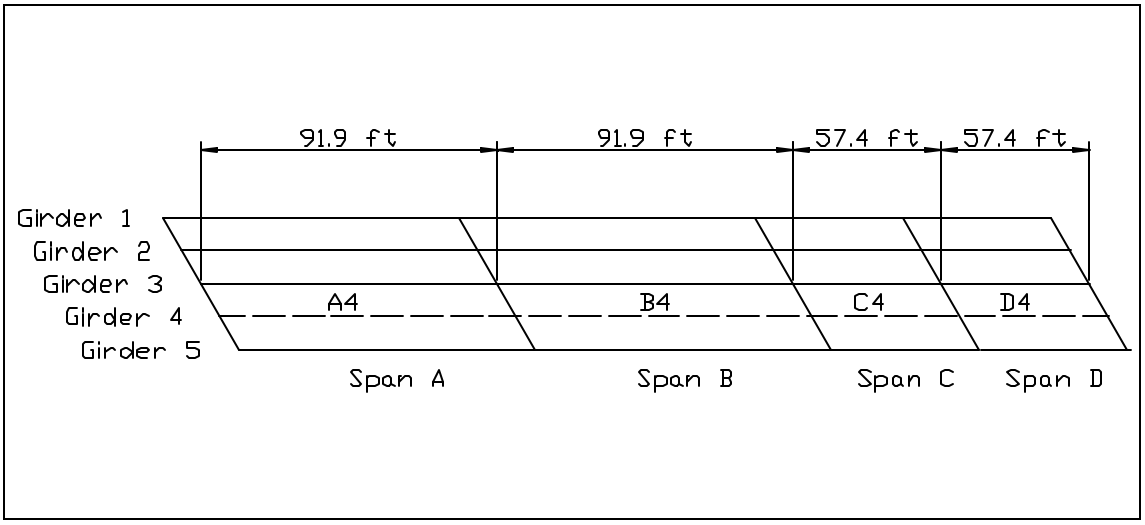

Figure 3.1 US 401 Southbound Bridge Over the Neuse River

In August 2000, a five-foot long test girder was cast in order to provide the fabricator (Carolina Prestress) with experience in handling the material, to monitor concrete temperatures during hydration, and to ensure workability of the concrete mix. Such a test girder was called for by the specifications and especially due to the

unsuccessful casting in March 2000, as mentioned previously. The girders cast in March were rejected for use in the bridge due to honeycombing. The test girder will be discussed in Section 3.4. For the instrumentation of the girders cast in October, PVC piping was used to protect the lead wires of the gages (see Section 3.3).

During the casting of the girders, several instruments were used to determine various properties of the girders. These properties included prestress loss, transfer length, strain and thermal changes during curing, and camber. This chapter discusses these girder behaviors and also presents the predicted values of the material properties of the concrete based on various equations, tables, and figures.

3.2 Description of the Bridge

The bridge is located just north of Raleigh, North Carolina on US Highway 401 over the Neuse River in Wake County. The structure is a four-span bridge that will carry three lanes of the southbound traffic of the divided highway. Both the girders and the deck are of HPC. A separate and parallel bridge that carries three northbound lanes has been completed and the bridge is temporarily carrying both northbound and southbound traffic. Figures 3.2 and 3.3 show the bridge viewed from the northeast. The bridge for the southbound lanes was to be erected in the summer of 2001. Figure 3.4 shows the bridge for the northbound lanes, viewed from the northwest, and also the groundbreaking for the new bridge that will carry the southbound traffic. Figure 3.5 shows the site plan of both bridges and Figure 3.6 shows a typical section of the southbound bridge.

Figure 3.2 Northbound Bridge Looking Southwest

Figure 3.3 Northbound Bridge Superstructure Looking Southwest

Figure 3.4 Northbound Bridge Looking Southeast Showing Southbound Site

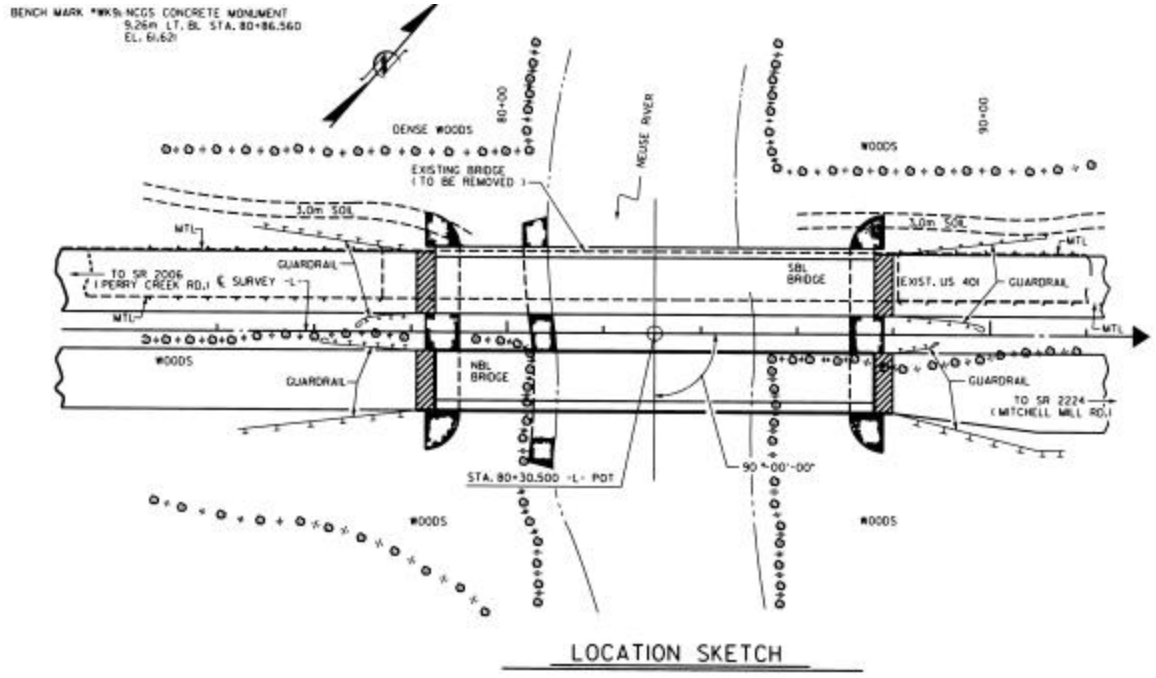

Figure 3.5 Plan View of Entire Bridge Structure

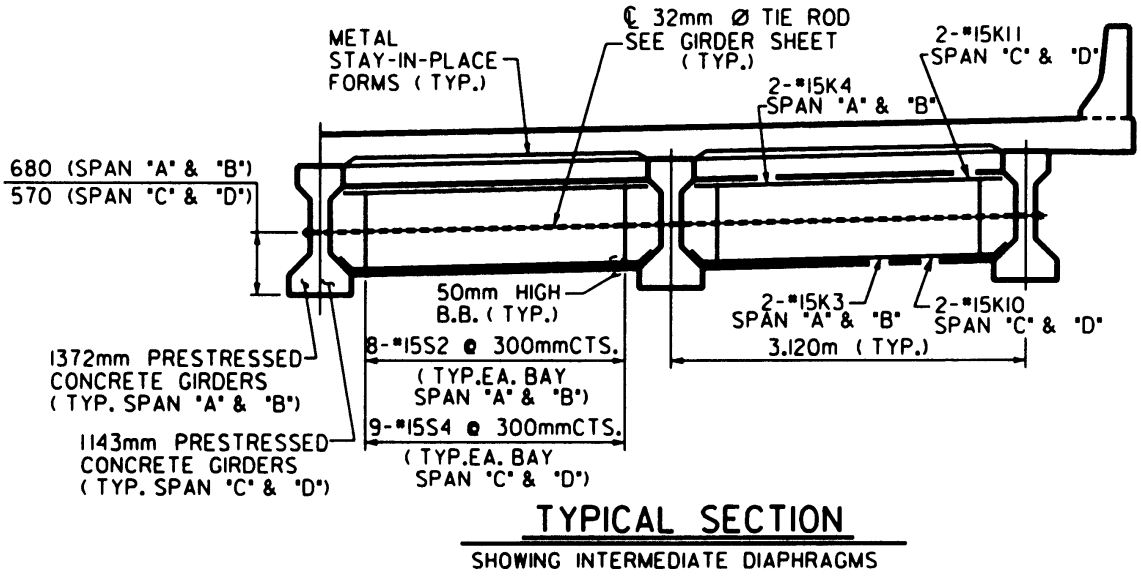

Figure 3.6 Typical Section of Southbound Bridge

The prestressed girders, using the HPC mix discussed in Chapter 2, were fabricated at Carolina Prestress, south of Charlotte, North Carolina. The use of this HPC mix eliminated one line of girders and increased transverse girder spacing from the original design using the conventional concrete. The strength requirement for the girders was 10,000 psi at 28 days. Figures 3.7 and 3.8 show the cross-sections of the instrumented girders. Figures 3.9 and 3.10 show the elevation and plan views of the girders.

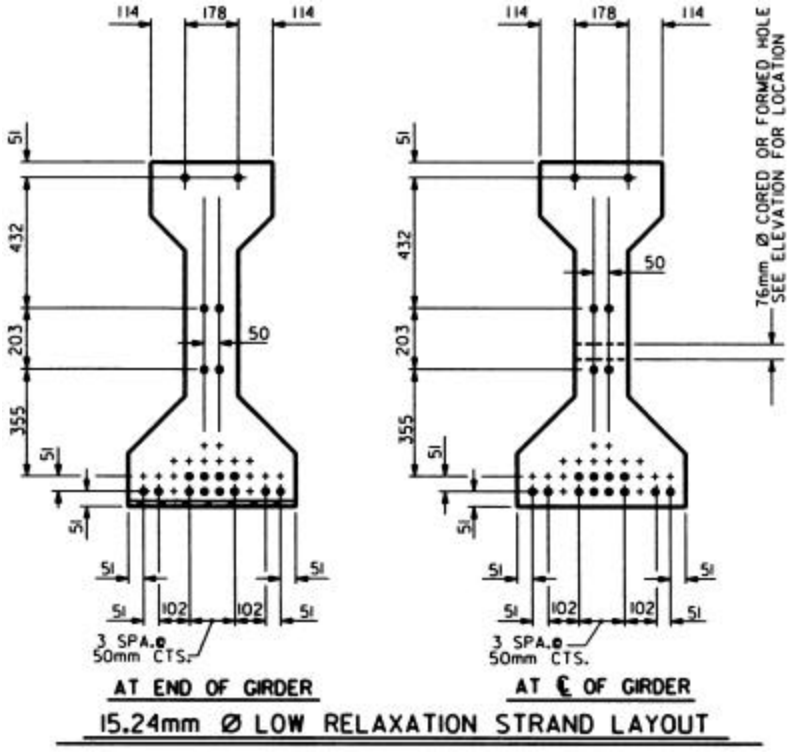

Figure 3.7 Cross-Sections, Type III Girder for Spans C and D

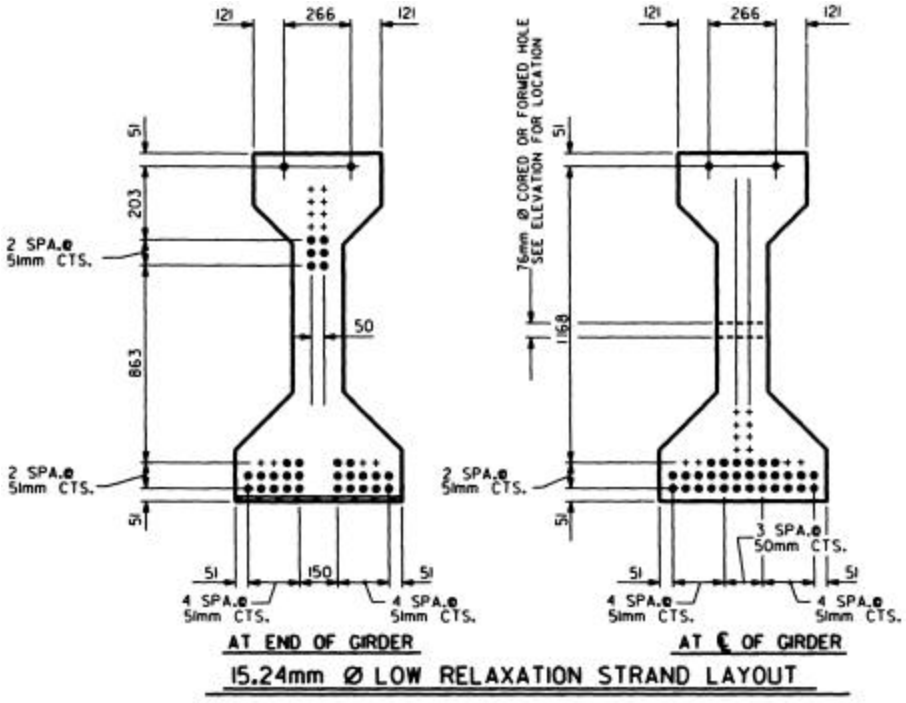

Figure 3.8 Cross-Sections, Type IV Girder for Spans A and B

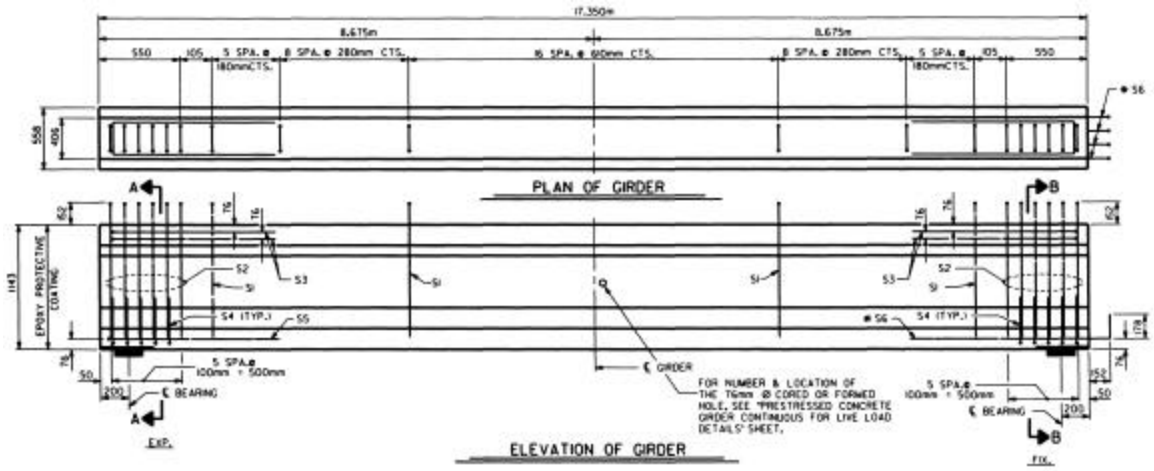

Figure 3.9 Elevation and Plan of Type III Girder

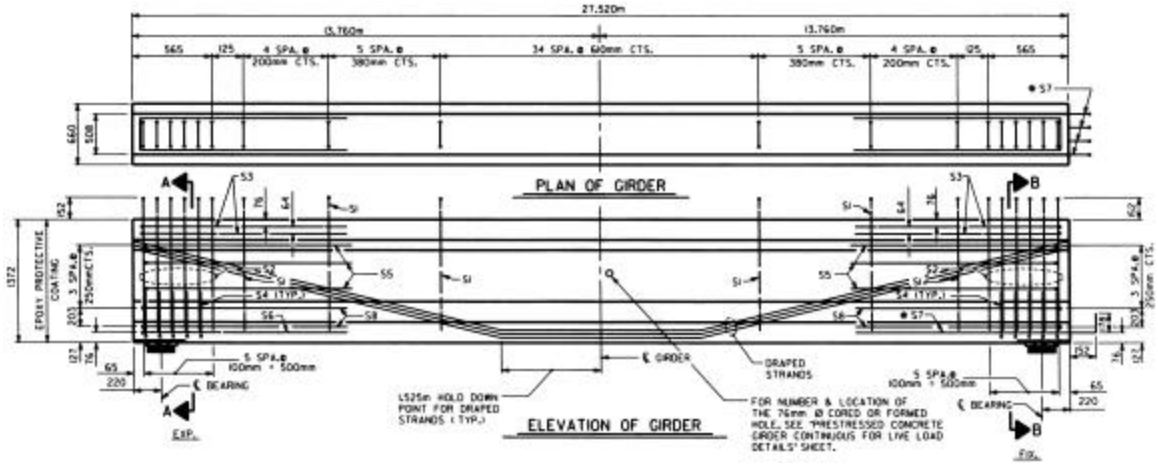

Figure 3.10 Elevation and Plan of Type IV Girder

3.3 Instrumentation

As usually is the case, a major limitation on bridge instrumentation and long-term monitoring and analysis is the budget constraint. Since the bridge consists of five girder lines of 4 spans each, it was not economically feasible to instrument the entire bridge. Only the girders on line #4 were instrumented (see Figure 3.1).

Since changes in temperature gradient in bridge cross sections can cause deformation and stress redistribution in a bridge, thermocouples were installed throughout the girders. Strains were measured using embedded ERSGs and VWGs. Dynamic monitoring was not considered in the instrumentation plan, but accelerometers or inclinometers could be added at any time after the bridge is in service. Prestressing force was measured with load cells (Section 3.3.4) and transfer length was determined from strains measured by using an embedded steel bar with attached strain gages (Section 3.3.5).

3.3.1 Gage Preparation

During the casting in March 2000, many gages were damaged and rendered useless due to loose wiring. Based on that experience, an improvement was made for the October 2000 casting. The instrumentation was pre-assembled at NCSU before it was taken to the prestressing plant in Charlotte. Schedule 40 PVC pipes (1 ¼ in. O.D.) and stiff black tubing (3/4 in.) were used to protect the gage wiring within the girder. The PVC pipe and black tubing were cut to length and the lead wires for the gages were fed through the piping using steel electrician's tape (commonly known as fish tape). Each gage exited the tubing at its desired location. The tubing was used not only for gage protection, but also to facilitate delivery of the gages to the casting site and to aid in the insertion into the girders. Figures 3.11 and 3.12 show the completed gage assembly. Set for transportation, the white PVC pipe is overlapped on itself and the black tubing is coiled. The prefabricated instrumentation assemblies were tied to the prestressed strands in the top flange of the girders, and the excess lead wire was run down stirrups to the

desired location for each gage.

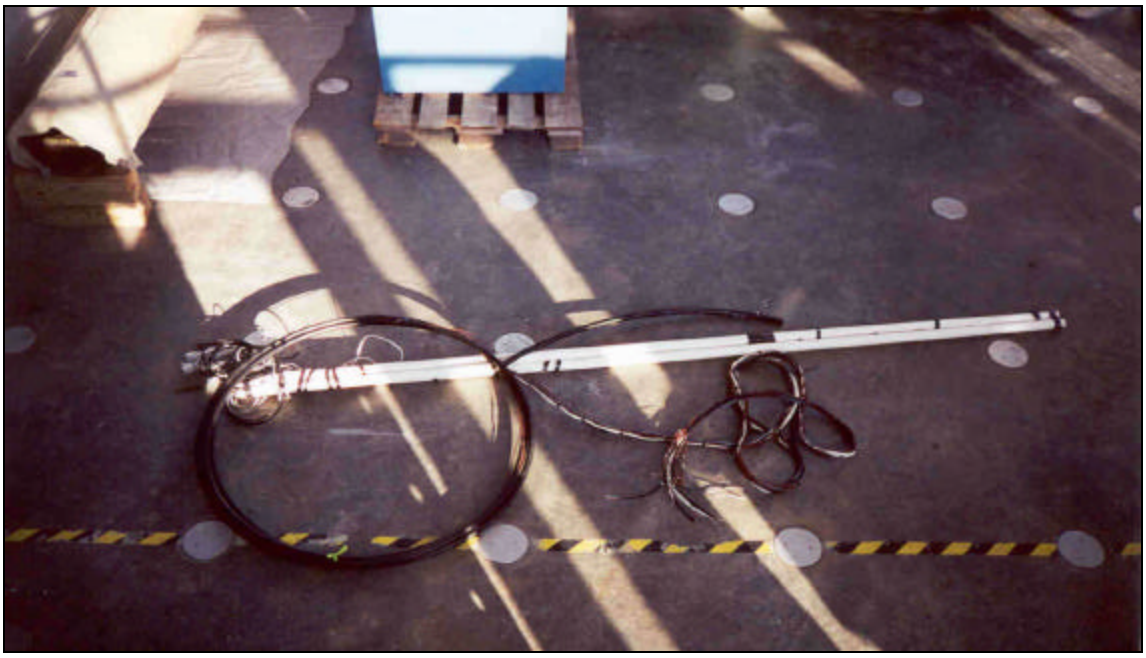

Figure 3.11 Fabricated Instrumentation Assembly Prior to Transport to Site

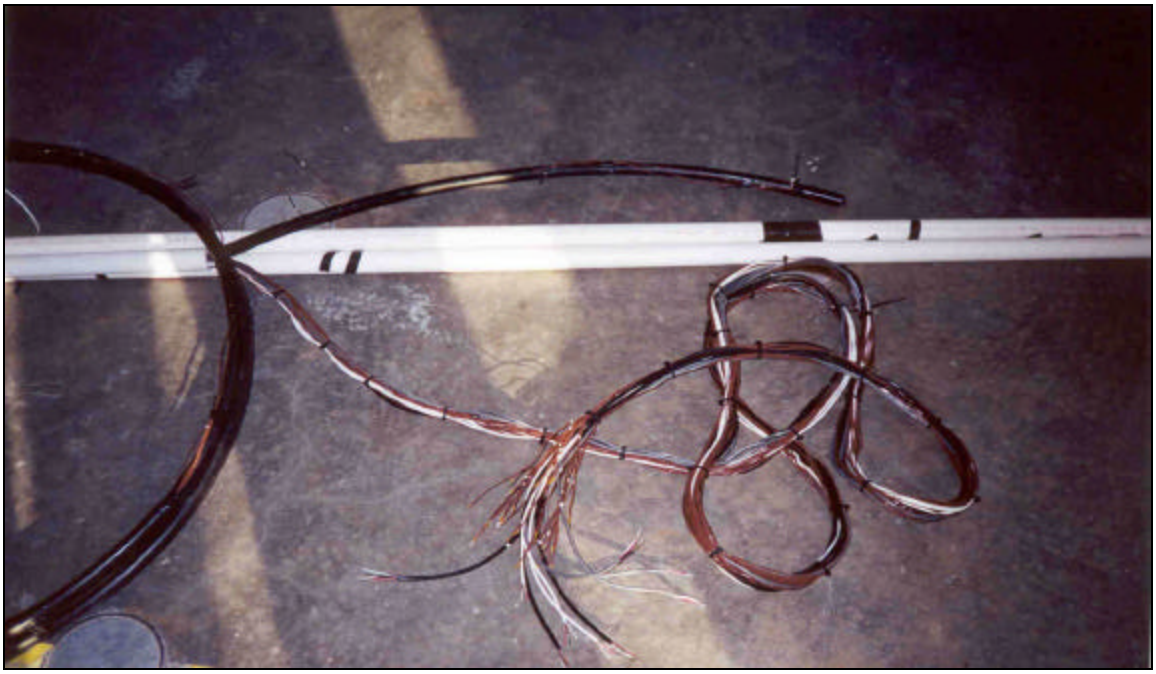

Figure 3.12 Fabricated Instrumentation Assembly Prior to Transport to Site (Close-up)

3.3.2 Temperature Measurement

In order to monitor the temperature gradients within the structure both during the cement hydration and the long-term, a total of 22 thermocouples (Omega FF-K-24) were placed at five cross-sections of each of the four girders. Ten thermocouples were placed at mid-span, three at quarter span, three at ¾ span, and three at a distance of L/50 from either end (where L is the girder span). Figure 3.13 shows the locations of the instrumented cross-sections. Figure 3.14 gives the locations of the thermocouples at each of these cross-sections.

The thermocouples recorded temperatures during the hydration of the cement and will monitor temperature changes throughout the life of the structure. The results of curing temperatures are discussed in Section 3.6.1.

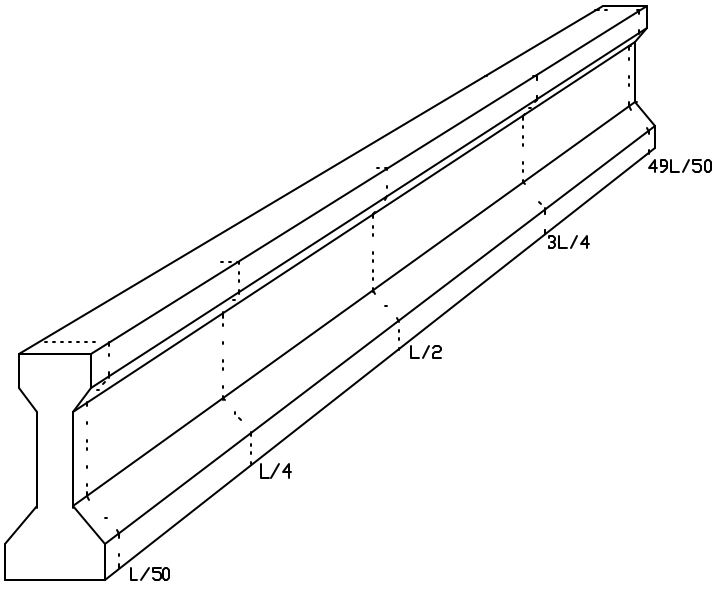

Figure 3.13 Location of Thermocouples

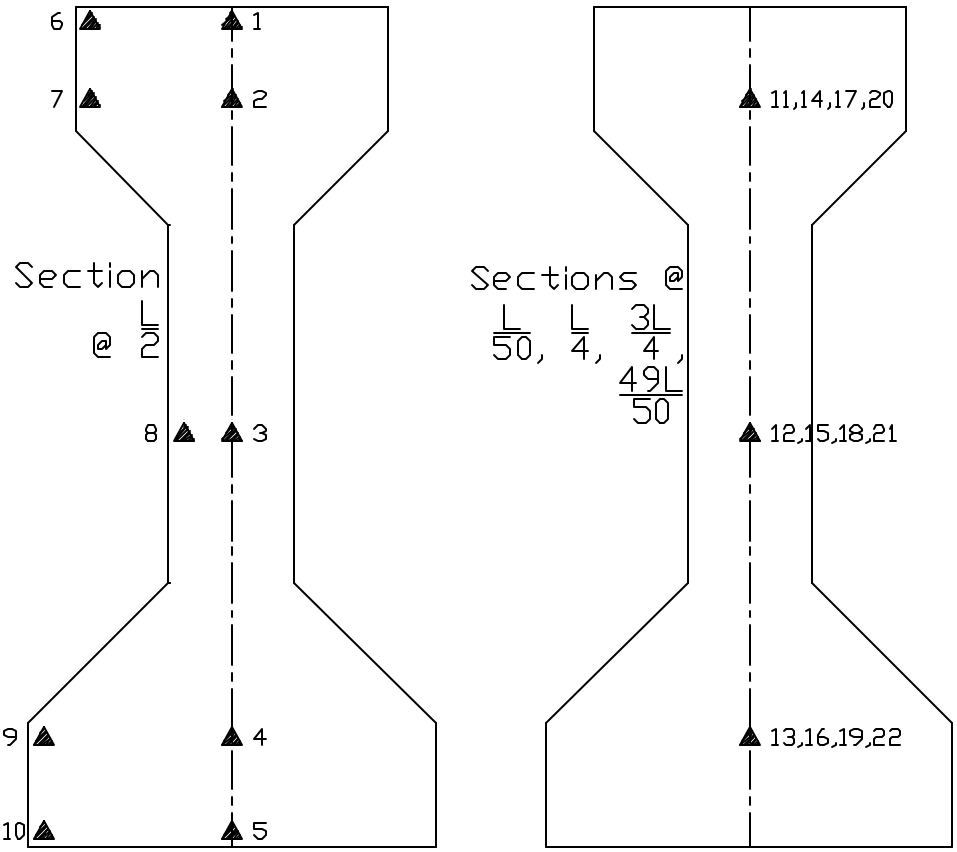

Figure 3.14 Location of Thermocouples at Five Different Cross-Sections

3.3.3 Strain Measurement

A structure experiences internal stresses and strains due to physical loading and thermal effects. Strains developed in concrete are of two categories: short-term and long-term. Short-term strains are a result of changes in loading, such as strand detensioning, initial loading and daily temperature cycles. Long-term strains result from seasonal temperature changes and creep and shrinkage in structures.

In these girders, two types of ERSGs were used to measure short-term strain. Embedment ERSGs were cast directly in the concrete and in cylinders (see Section 2.6) and standard ERSGs were placed on reinforcing steel and a fabricated steel rod to

measure transfer length (see Section 3.3.5).

A fundamental assumption made in structural design is that plane sections remain plane. The girders were instrumented in order to validate this assumption. ERSGs were placed on standard No. 4 reinforcing bars in the laboratory, with the necessary lead wire attached. Three of these instrumented bars were placed at mid-span of each of the four girders (see Figure 3.15). One instrumented bar was placed at the center of gravity of the top flange, one at mid-height of the web, and one just above the center of gravity of the prestressing steel. The sole purpose of these instrumented bars was to determine the strain profile of the section to see if the section remains plane under loading. These gages are named plane strain bars. Figures 3.16 and 3.17 show the instrumented bars as prepared in the laboratory.

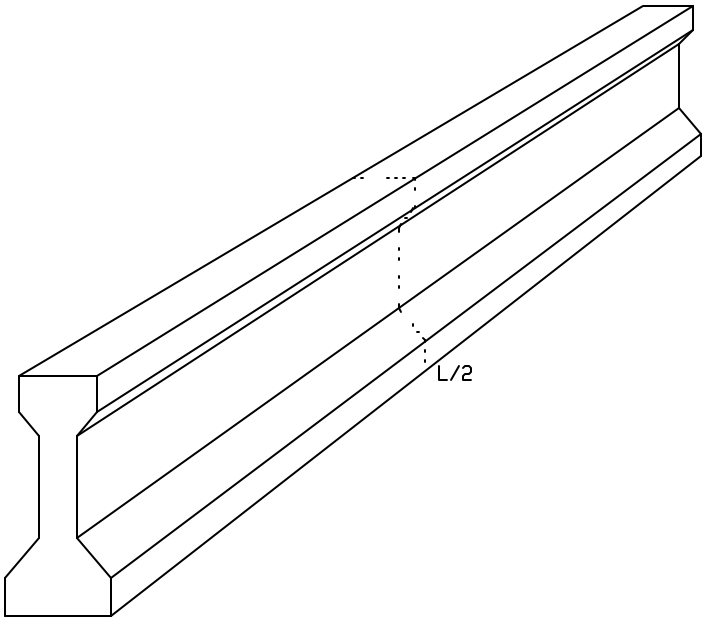

Figure 3.15 Location of Plane Strain Bars

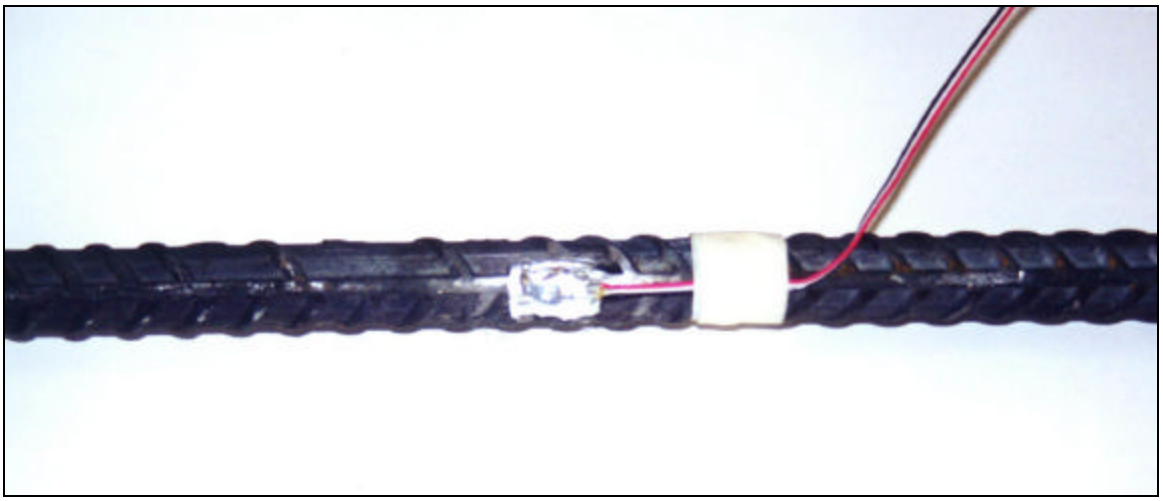

Figure 3.16 ERSG Applied to No. 4 Reinforcing Bar

Figure 3.17 Protected ERSG with Lead Wire Attached

Generally, long-term strains are measured using Carlson Strain Meters and/or VWGs. For this project, VWGs (Roctest EM-5) were placed at the center of gravity of

the prestressing strands at mid-span and five feet in either side from mid-span to measure long-term strains, see Figure 3.18. A typical Roctest EM-5 VWG is shown in Figure 2.9. Each VWG contains a thermistor that measures temperature. The strains measured during curing will be discussed in Section 3.6.2.

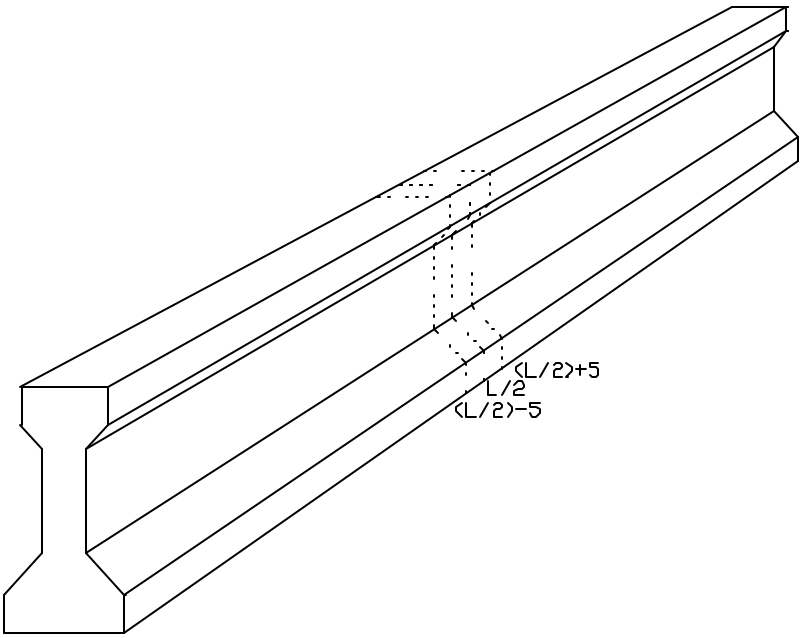

Figure 3.18 Locations of VWGs

3.3.4 Prestress Measurement and Losses

Pretensioning jacks are usually connected to a dial gage to determine the jacking force on a prestressing strand. However, the dial gage indicates only the force at the live (jacking) end of the casting bed. In a long casting bed, the force at the dead (anchoring) end usually is not the same as that at the live end due to strand relaxation, friction, slip, and temperature variations. Load cells placed at the dead end can measure the prestressing force after the jack is removed, as well as after curing, and immediately prior

to detensioning of the strands. For this project, Strainsert model PC-50 (50,000 lb capacity) load cells were placed on four strands on each of the casting beds (Type III and Type IV). Figure 3.19 shows the locations of the load cells for the Type III and Type IV girders. Tables 3.1 and 3.2 give the load cell readings at various times after tensioning.

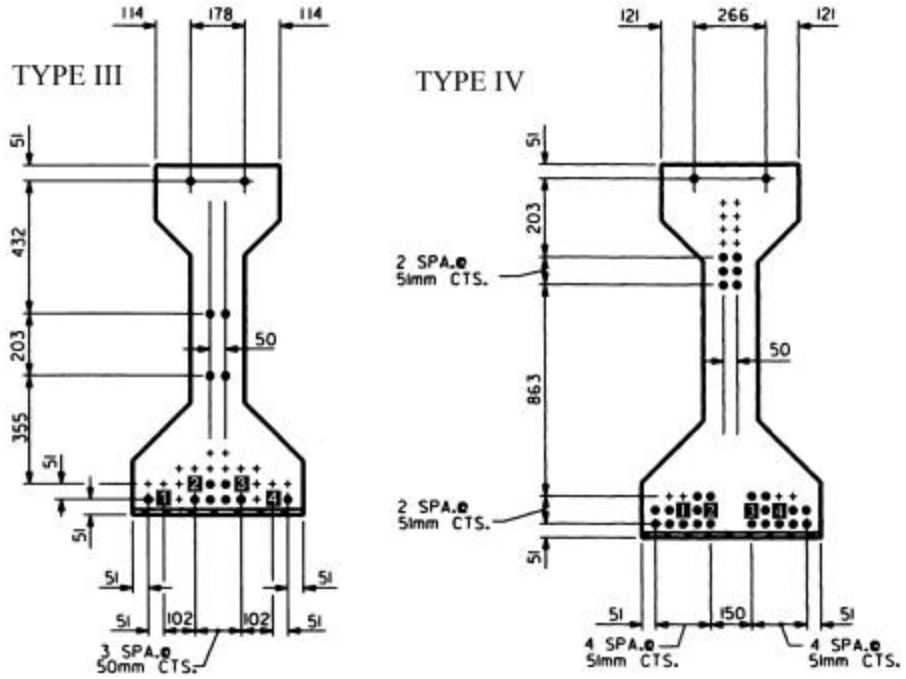

Figure 3.19 Load Cell Locations for Type III and Type IV Girders

Table 3.1 Load Cell Readings for Type III Girders

Time	Temp (°F)	Strand ID (Load in kips)					Comments
		1	2	3	4	Average	
Initial	62	42.8	42.7	42.5	42.9	42.7	Just after tensioning
24 hrs	60	41.0	41.3	40.9	42.1	41.3	
48 hrs	60	39.6	39.8	39.4	40.2	39.8	
55 hrs	70	42.6	43.2	42.5	43.3	42.9	Before detensioning

Table 3.2 Load Cell Readings for Type IV Girders

Time	Temp (ºF)	Strand ID (Load in kips)					Comments
		1	2	3	4	Average	
Initial	85	42.2	42.6	41.2	41.7	41.9	Just after tensioning
17 hrs	60	43.8	43.7	42.4	43.2	43.3	
40 hrs	60	43.7	43.7	42.4	43.2	43.3	
64 hrs	60	42.3	42.3	40.9	41.8	41.8	Before detensioning

The specified initial prestressing force is 44.5 kips. This is what the dial gage on the live end indicated for every strand when it was fully tensioned. From the data given in Tables 3.1 and 3.2, it can be seen that for every strand, there is not only a loss of prestress from the live end to the dead end of the girder, but also a variation of forces over time. It is noted that for calculations involving prestessing force, an average value of the initial tension at the live end and the load cell reading at the dead end was used. The average value for the Type III girder is 43.7 kips and that for the Type IV girder is 43.2 kips.

Table 3.3 presents the various prestress losses. Detailed calculations of the losses can be found in the Appendix.

Equation 3.1 was used to calculate the concrete stress due to prestressing force and the dead load moment. Equation 3.2 was used to calculate the loss of prestress in the strand due to elastic shortening. Equations 3.3a and 3.3b were used to calculate the prestress losses in the strand due to creep and shrinkage, respectively.

$$f_c = \frac{F}{A_t} + \frac{F \cdot e^2}{I_t} - \frac{M_{DL} \cdot e}{I_t} \qquad \text{(Eq. 3.1)}$$

$$\Delta f_s = E_s \frac{f_c}{E_{ci}} \qquad \text{(Eq. 3.2)}$$

$$\Delta f_s = E_s e_s \quad \text{(Eq. 3.3a)}$$

$$\Delta f_s = E_s e_c \quad \text{(Eq. 3.3b)}$$

where: f_c = stress in concrete at center of gravity of strands at mid-span
Δf_s = loss of prestress in strand due to elastic shortening, shrinkage, or creep
F = initial prestressing force
A_t = transformed cross-sectional area of girder
I_t = transformed moment of inertia of girder
e = eccentricity of the prestressing force
M_{DL} = dead load moment of the girder at mid-span
E_{ci} = initial modulus of elasticity (taken as 3,900 ksi for Type III girders and 4,100 ksi for Type IV girders)
E_s = modulus of elasticity of the prestressing strand (taken as 28,500 ksi)
e_s = strain due to shrinkage
e_c = strain due to creep

Table 3.3 Prestress Loss (ksi)

Cause of Loss	Type III Girder	Type IV Girder
Elastic Shortening	12.0	18.1
Creep	12.7	17.5
Shrinkage	1.3	2.4
Total Loss	**26.0 (12.9%)***	**38.0 (19.1%)***

*Based on initial prestress of 201.4 ksi for the Type III girder and 199.1 ksi for the Type IV girder.

3.3.5 Transfer Length Measurement

The transfer length of prestressing strands at the ends of a pre-tensioned girder depends on a number of variables including the concrete strength, the strand size, the prestressing force, the method of detensioning, etc. In this project, two methods were used to measure the transfer length: (1) a "strain gage bar" (SGB) was prefabricated and

embedded in the girder, and (2) standard Demec points were applied on the vertical surfaces of the bottom flange of the girder, using a spacer and applicator.

The SGB, fabricated in the laboratory, was made of a series of washers welded onto a standard 3/8" hot rolled smooth steel bar of 60 in. long. Spaced at six-inch apart, the washers serve as mechanical anchors of the bar to the concrete. A pair of ERSGs was then placed on opposite sides of the bar at midpoint between every two adjacent washers. The gages were protected and sealed, with 12 feet of lead wire attached. A complete SGB is shown in Figure 3.20. The gages were read with a standard strain gage indicator box after the concrete had cured and just before detensioning, in order to obtain the initial readings. The gages were then read immediately after detensioning. The change in strain for each gage is plotted in relation to its distance from the end of the girder in Figures 3.21 and 3.22. The average strain is also plotted in these figures.

To determine the transfer length from the measured concrete strains, it is necessary to establish a strain plateau. Since there are usual variations of the measured strains within the strain plateau as shown in Figures 3.21 and 3.22, a method similar to that proposed by Oh and Kim (2000) is followed to establish the strain plateau. The strain plateau is obtained by drawing a horizontal line at 95% of the maximum value of the plotted average. The transfer length is taken as the horizontal distance from the origin (i.e. the end of the girder) to where the horizontal line intersects the plotted average strain profile. Table 3.4 lists the transfer length for each girder.

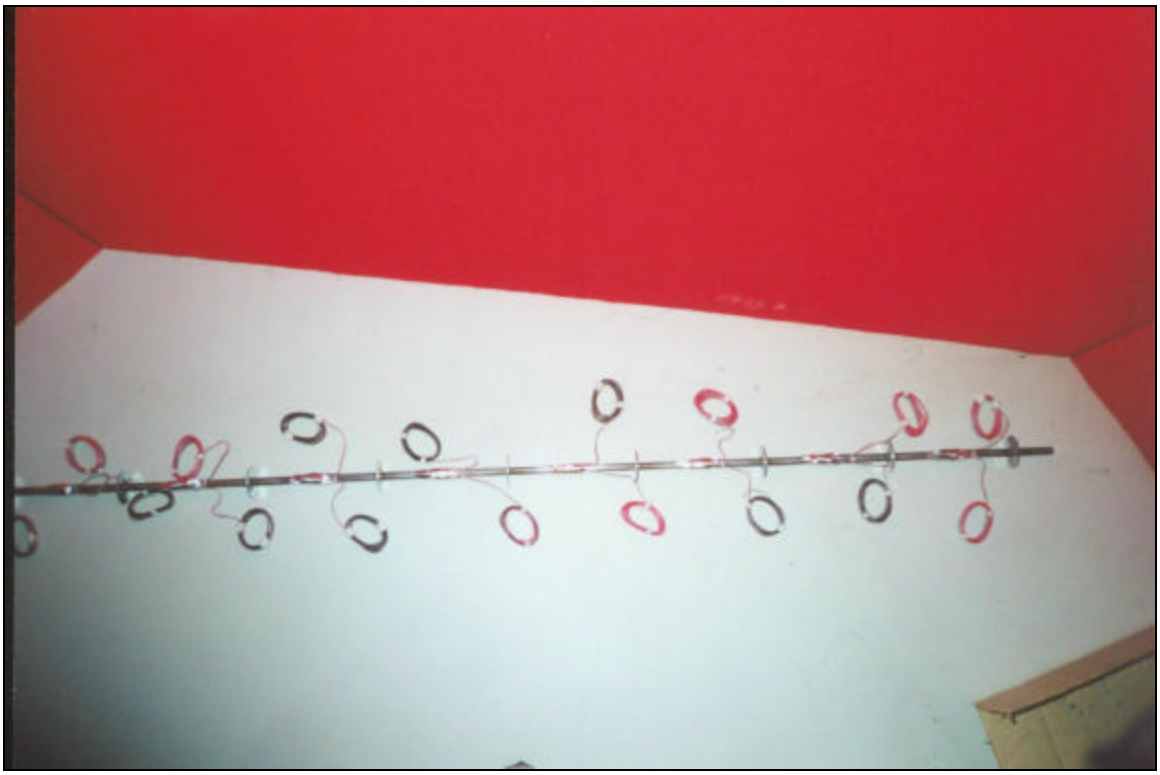

Figure 3.20 Strain Gage Bar

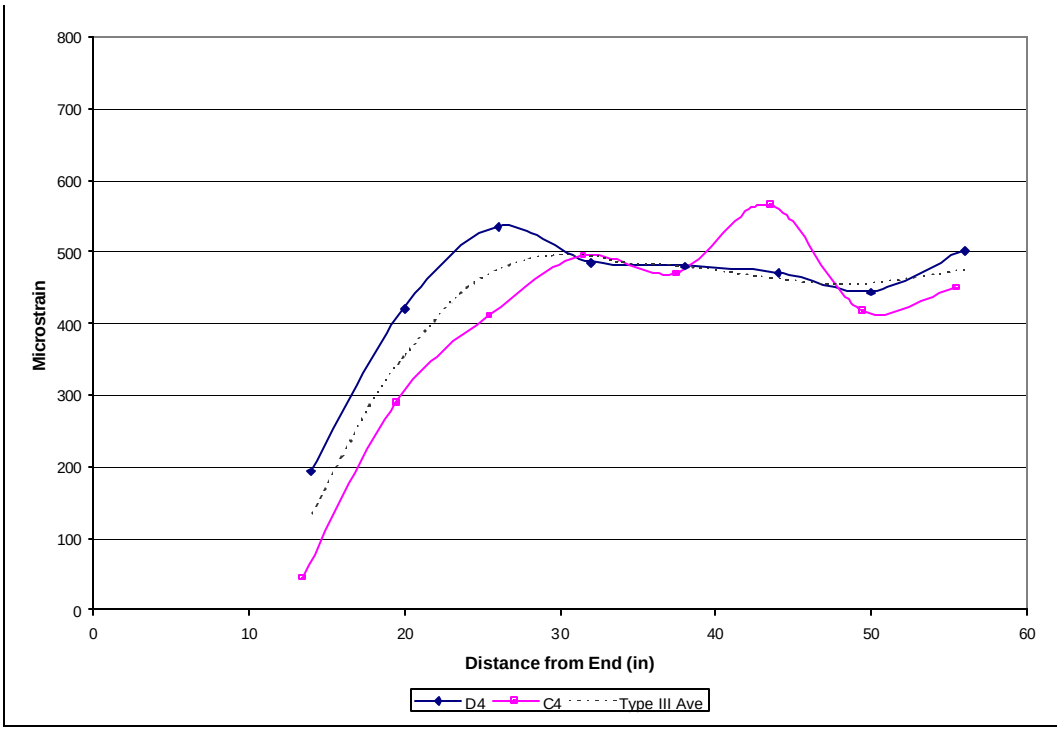

Figure 3.21 Transfer Length for Type III Girder

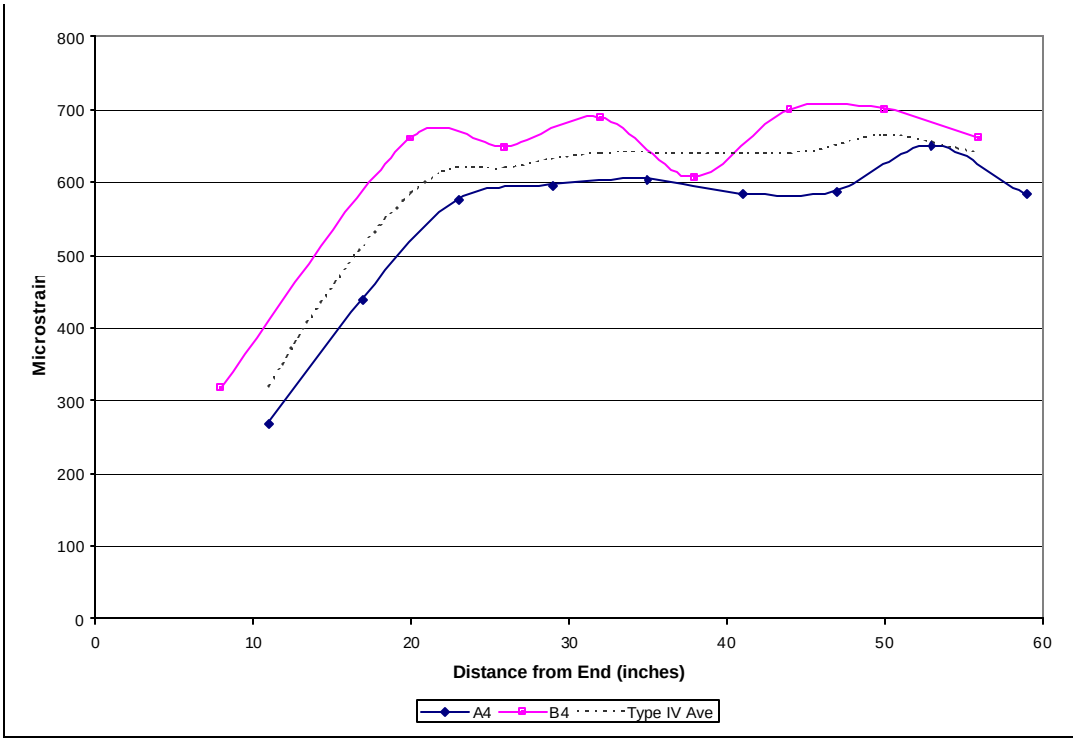

Figure 3.22 Transfer Length for Type IV Girder

Table 3.4 Transfer Length (inches) of 0.6 inch Strands

Type III Girder	Type IV Girder
28	26

The common method of applying Demec points to the exterior of the girder was attempted. A special spacer and applicator was designed in order to apply the Demec points as quickly as possible, due to the time limitation imposed by Carolina Prestress. Epoxy was applied and the gage applicator was pressed against the girder as shown in Figure 3.23. Figure 3.24 shows the Demec points in place, at the end zone of girder C4. Even with the quick set epoxy, this process failed due to the high ambient temperature and the fact that the epoxy needed a longer setting time. In the end, only data was acquired from the SGB.

Figure 3.23 Applying Demec Points

Figure 3.24 Demec points on Girder

It is generally understood that smaller diameter strands will require shorter transfer lengths. The ACI Code recommends that the transfer length be taken as 50 strand diameters for strands and 100 wire diameters for individual wires. For 0.6 inch strand, this equates to a transfer length of 30 inches. Design Aid 11.2.6 in the PCI Design Handbook, 5th Ed. also gives a value of 30 inches for 0.6 inch diameter strand.

3.4 HPC Mock-up Girder

3.4.1 Casting and Instrumentation

A five-foot mock-up girder was cast on August 17, 2000 in order to determine the workability of concrete, thermal gradient during hydration, air content, and slump. NCDOT personnel instrumented this Type IV AASHTO girder with thermocouples installed at locations shown in Figure 3.25. Figure 3.26 shows the thermocouples being installed, and Figure 3.27 shows the data acquisition system (DAQ) used to record the temperatures during curing.

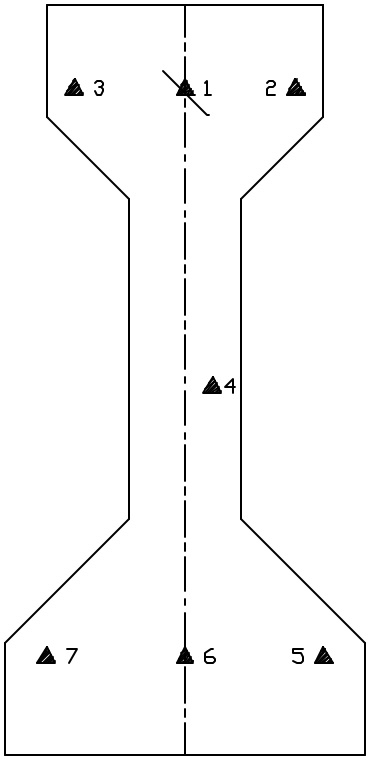

Figure 3.25 Thermocouple Locations in Mock-up Girder

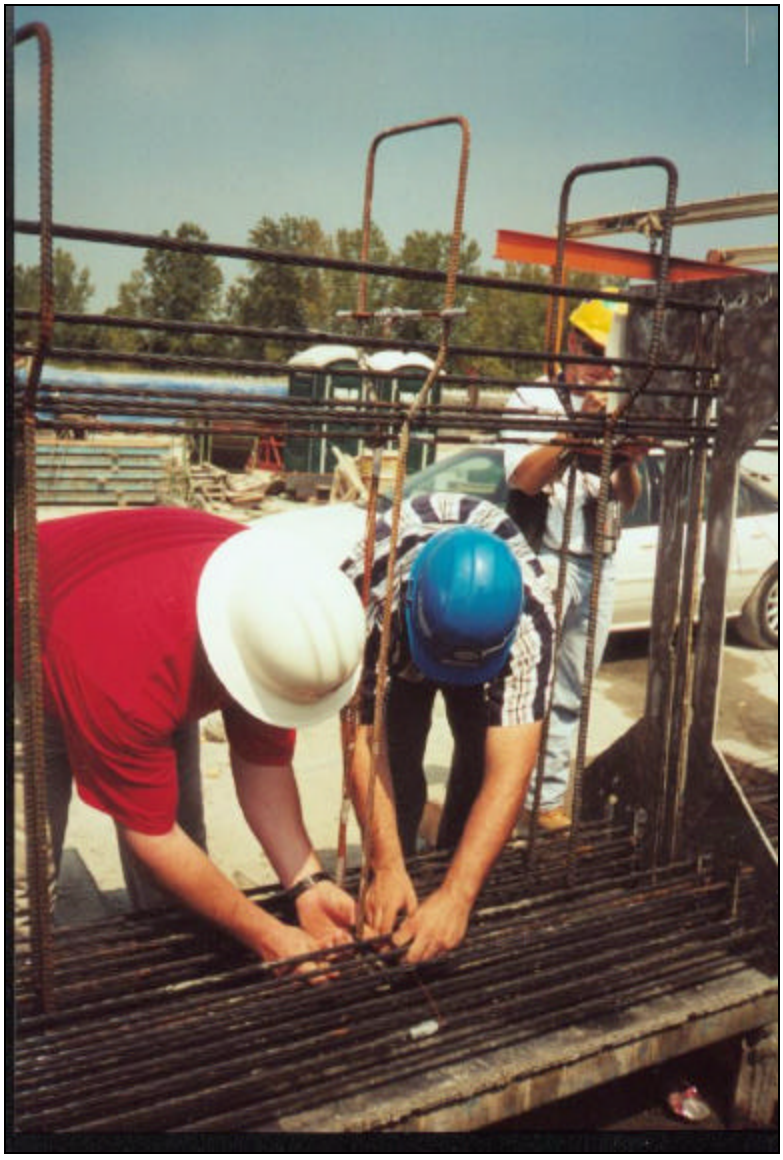

Figure 3.26 Installing Thermocouples

Figure 3.27 Thermocouples Exiting Girder to Data Acquisition System

3.4.2 Material Properties and Results

The HPC target performance criteria and the mix proportions have been provided in Tables 2.1 and 2.2, respectively. The in-situ material properties are provided below in Table 3.5. The NCDOT DAQ recorded temperature data from the time the concrete was placed until 7 a.m. the following morning (16 hours later). One thermocouple was left in

the open air to monitor the ambient temperature, and one was placed underneath the tarp cover on top of the girder. A plot of the curing temperatures is given in Figure 3.28. There was a malfunction in thermocouple No. 1 and therefore no data was collected at that location.

Table 3.5 HPC Mock-up Girder Concrete Material Properties

Air content (%)	3.6
Slump (inches)	6.75

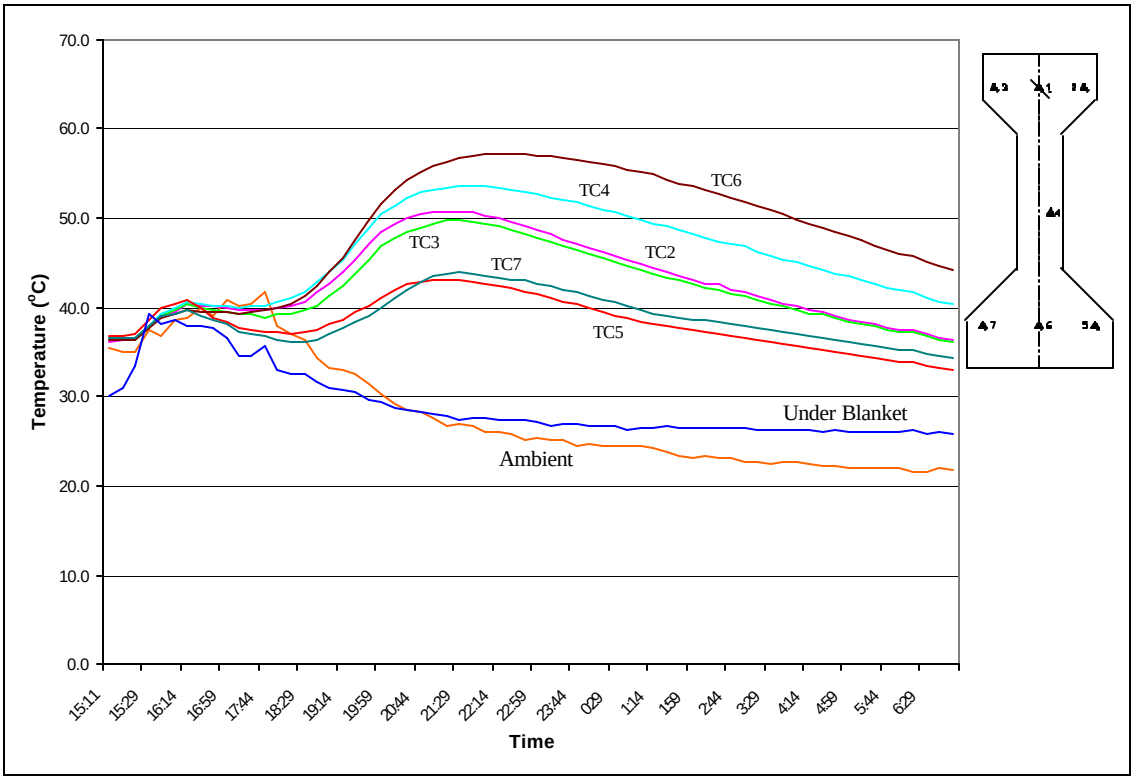

Figure 3.28 Curing Temperatures for mock-up Girder

After reviewing the data it was determined that the concrete was acceptable and would be used for the casting of the actual bridge girders in October.

3.5 Casting of Bridge Girders

3.5.1 Field Instrumentation

Section 3.3 discussed the specifics of the gages and the laboratory fabrication. The following discussion covers the procedure on how the gage assemblies were placed in the girders.

Once the load cells were put in place, the strands were tensioned one by one. After all strands were tensioned, No. 4 reinforcing bar was hung transversely from the strands in the top flange at five-foot increments. The gage assemblies (see Section 3.3.1) were laid out alongside the girder and then tied to the No. 4 bar at the center of the top flange. Carolina Prestress personnel placed the stirrups and the gages were positioned in their correct locations. All lead wires were tied to the stirrups and/or prestressing strand to avoid being damaged during the concrete placement. Figure 3.29 shows the PVC pipe and black tubing connection at mid-span, as well as the stirrups and gages in place. Duct tape was used to seal the connection. Figure 3.30 shows a close-up of the embedment ERSG and VWG at mid-span and Figures 3.31 and 3.32 show all the gages placed in their final designated locations. Lastly, the SGBs were set in place (see Figure 3.33).

Figure 3.29 Field Instrumentation at Mid-span

Figure 3.30 Embedment ERSG and VWG at Mid-span

Figure 3.31 Gages at Mid-span and Five Foot Offset

Figure 3.32 All Gages in Place at Mid-span

Figure 3.33 SGB in Place

3.5.2 Casting

The Type III girders were cast on October 3rd and 4th, 2000 in a single bed and the Type IV girders on October 5th and 6th in another bed. The concrete was tested for slump and air content on site in accordance with AASHTO and NCDOT standards. The concrete was placed into the forms using an overhead bucket. Both standard vibrators and an external vibrator on the side-form were utilized to ensure proper placement. Figure 3.34 shows the placement in progress, the match cured cylinders being made, and the monitoring of the DAQ and solar panels. The girders were covered with burlap, water hoses were placed on the burlap for the moist cure, and then tarps were laid over

the girders on the casting bed as shown in Figure 3.35. The wires that exited the girder were fed through 1-½ inch stiff black tubing for protection (see Figure 3.36).

Figure 3.34 Comprehensive Casting Photo

Figure 3.35 Covered Casting Bed

Figure 3.36 Protection of Lead Wires Exiting Girder

3.6 Behavior During Initial Curing

A Campbell Scientific, Inc. DAQ was used to monitor the instrumentation during initial curing of the girders. Warren (2000) details the specifics of this system. The general premise is that solar panels provide power to a battery, which supplies power to a data logger. The data logger collects data from multiplexer in accordance with a preprogrammed computer code. The gage lead wires are connected to the multiplexer channels. Figure 3.37 shows the entire setup. Figure 3.38 shows the battery and data logger, and Figure 3.39 shows the multiplexers with the gage lead wires connected.

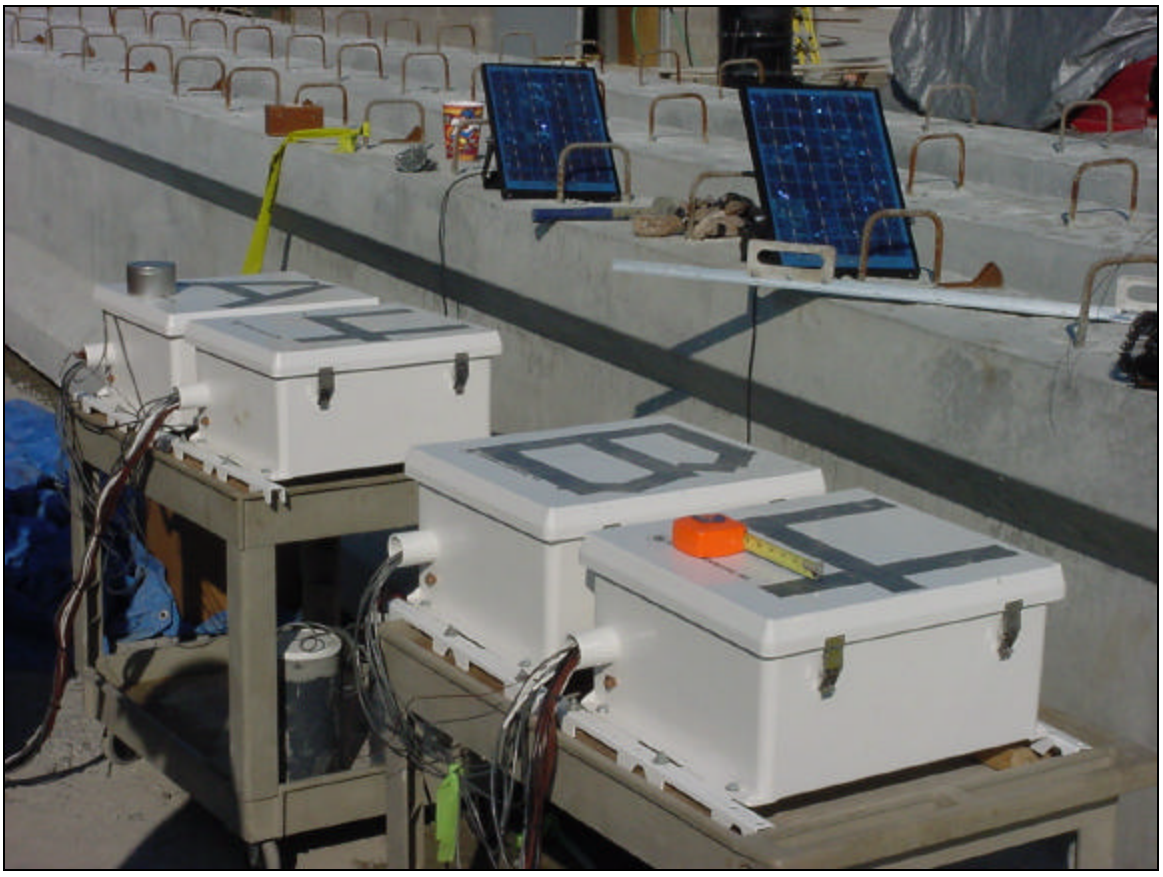

Figure 3.37 Data Acquisition System Boxes and Solar Panels

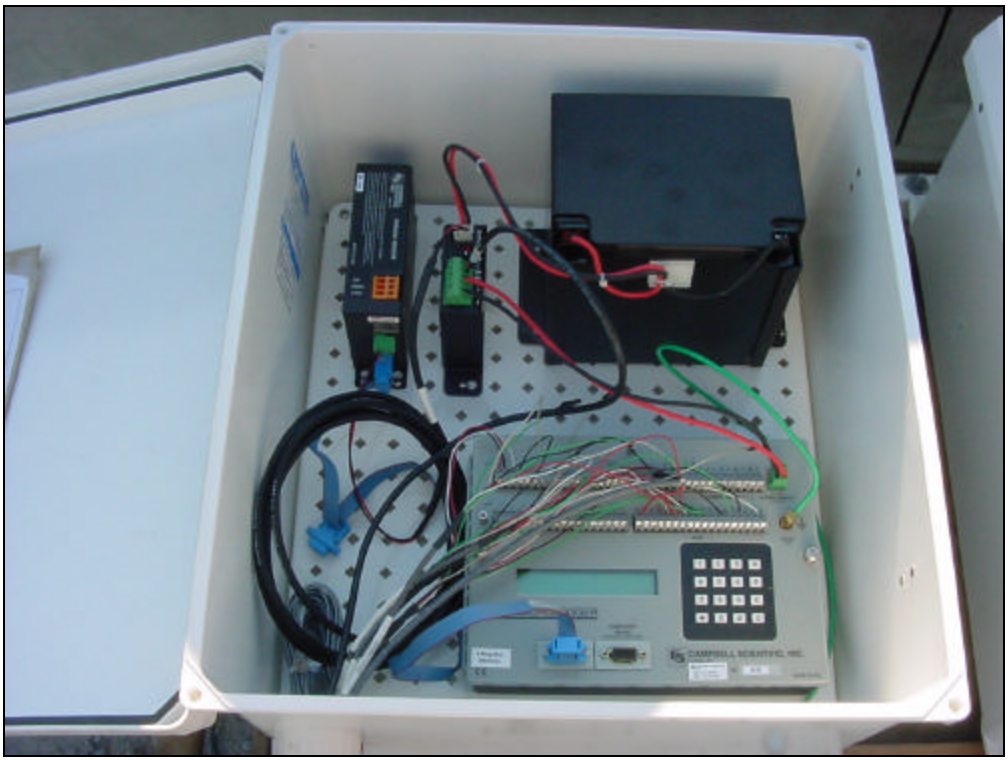

Figure 3.38 Data Logger and Battery

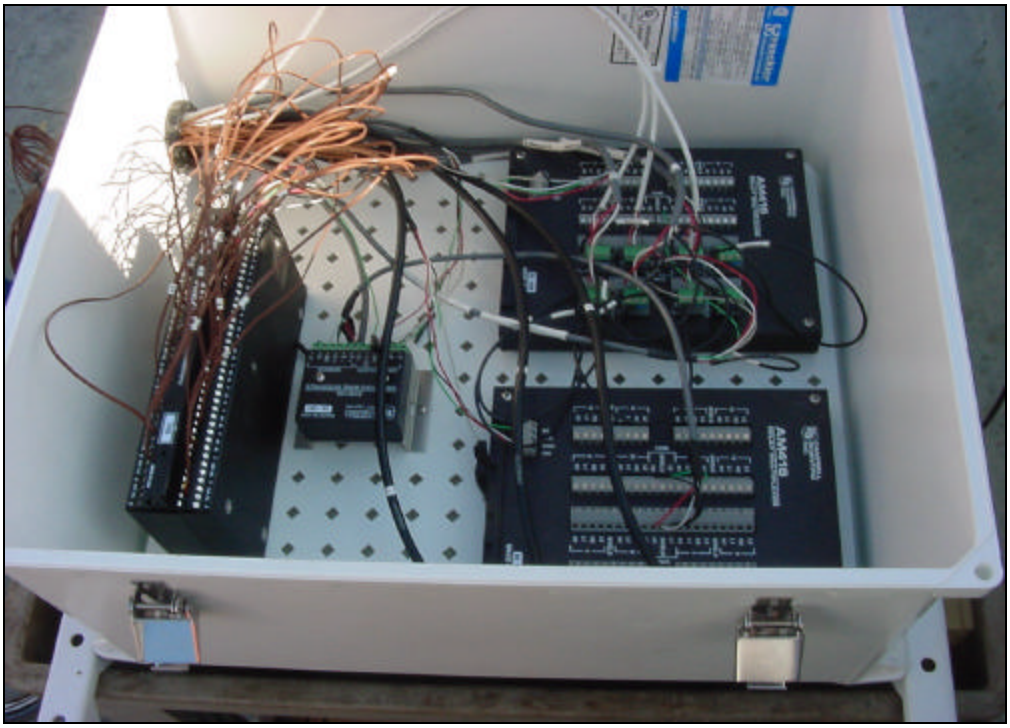

Figure 3.39 Multiplexers

The Campbell Scientific software does not contain a user-friendly output program for organizing and viewing data. For this reason, an Excel spreadsheet was created to reduce the data that was recorded. The behavior of the girders during initial casting and initial curing is given in the following sections.

3.6.1 Thermal Gradients

The following figures (Figures 3.40-3.83) show the thermal gradients during casting. The curing temperatures for each girder at specific cross-sections as well as the temperatures at a specific location of the cross-section compared with those along the length of the girder are shown. The ambient temperature is also plotted on all graphs. The numbers in the legend are located in the cross-sections shown. All gages are shown except thermocouple No. 4 for girder C4. This thermocouple was damaged during casting and no longer functions. The data for the Type III girders is given first followed by the data for the Type IV girders.

Similar trends are found in the results. Examining the ambient temperatures, it can be noticed that the temperatures rise during the midday heat and fall towards evening. The temperature beneath the blanket is similar to the ambient temperature at first, but then increases and remain constant. This higher temperature is a direct result of the heat of hydration. The embedded thermocouples also show a similar trend. Initially, the temperatures rise slowly but then increase rapidly as hydration occurs. The concrete reaches its peak temperature about seven hours after casting and then the heat of hydration slowly reduces.

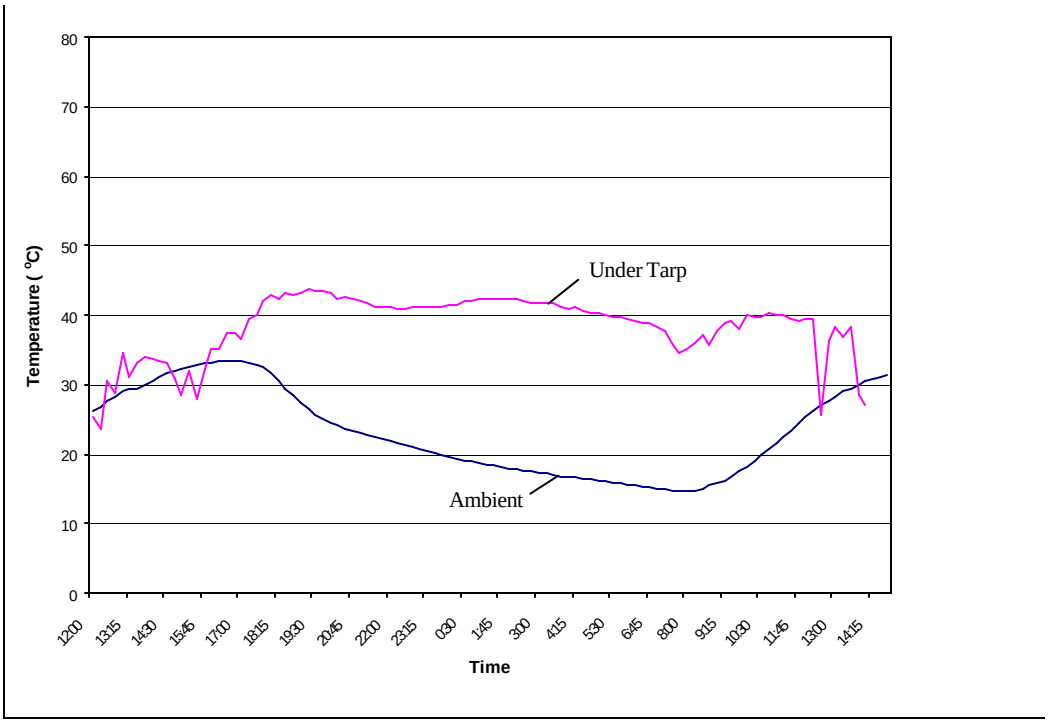

Figure 3.40 Reference Temperatures for Girder C4

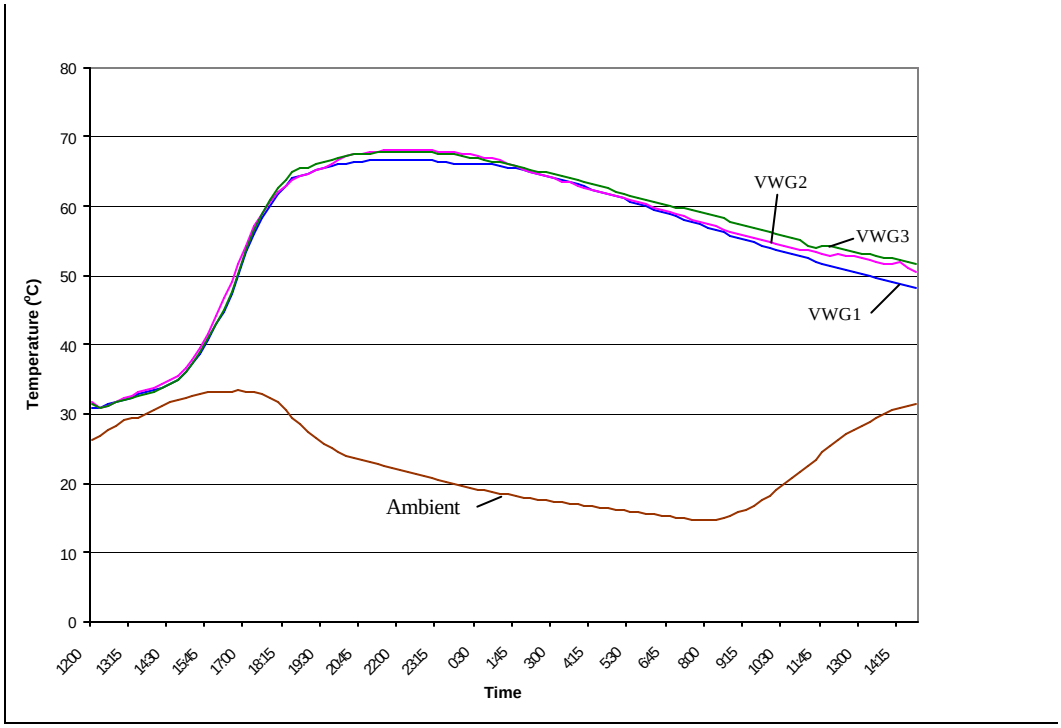

Figure 3.41 VWG Temperatures for Girder C4 (see Figure 3.18 for gage location)

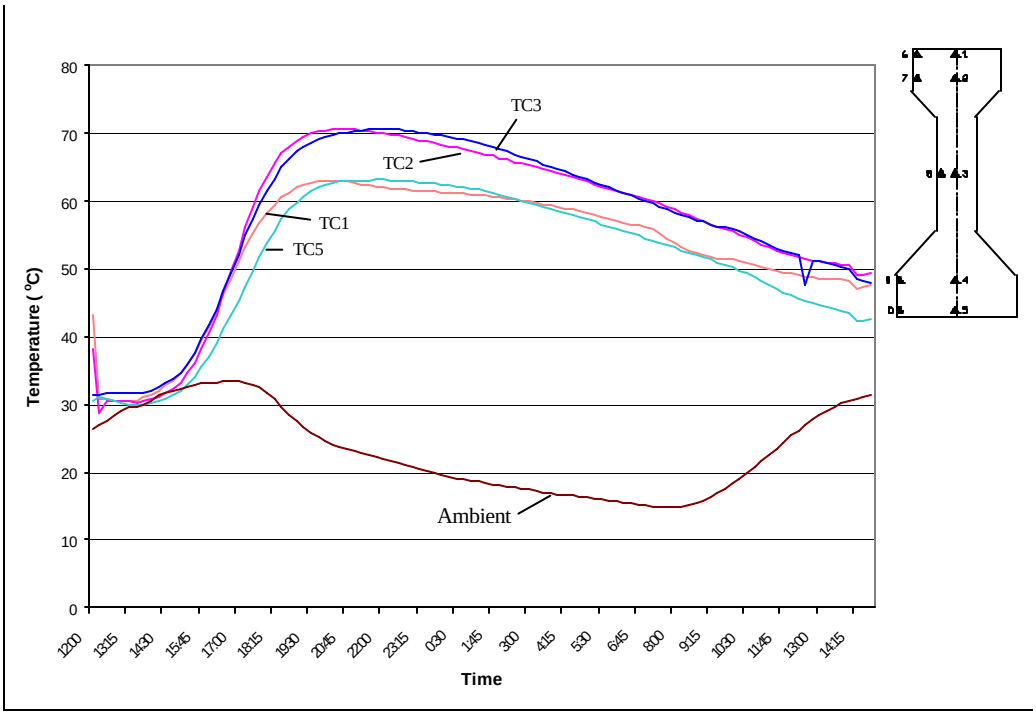

Figure 3.42 Thermocouples 1-5 for Girder C4 at Mid-span

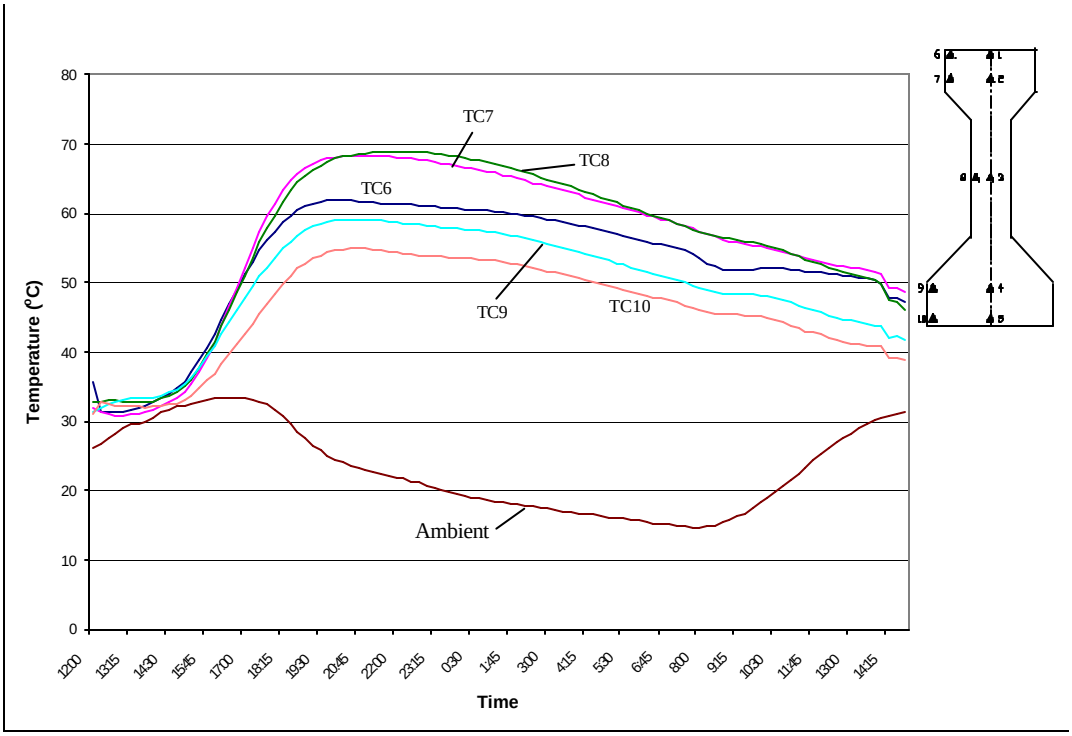

Figure 3.43 Thermocouples 6-10 for Girder C4 at Mid-span

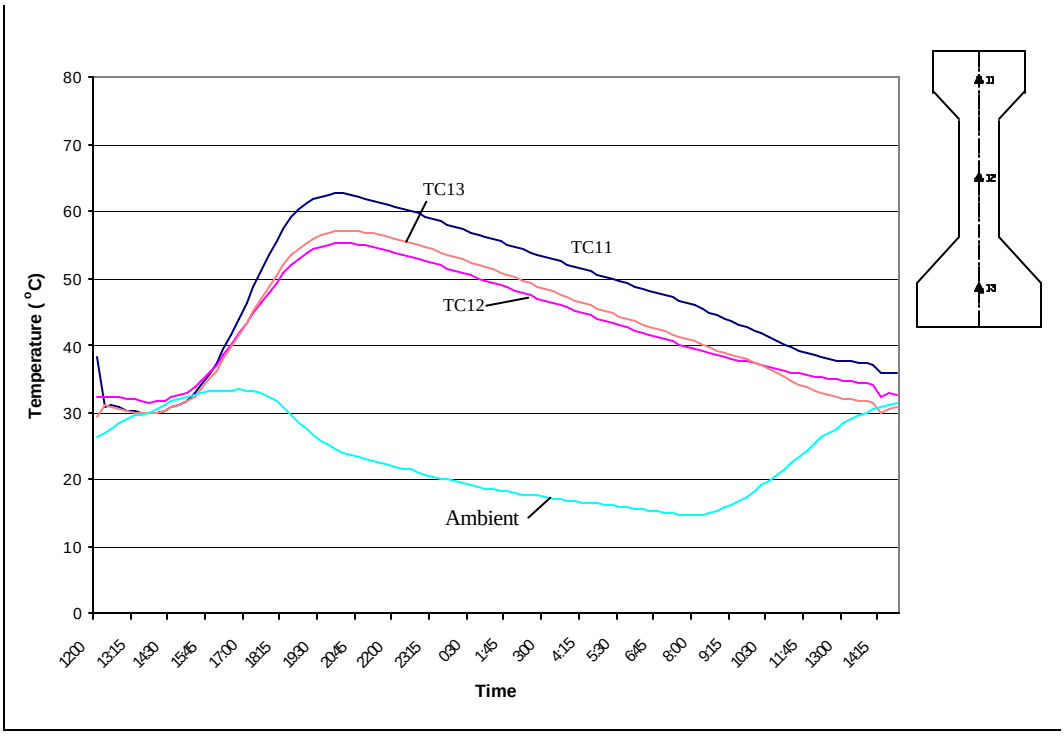

Figure 3.44 Thermocouples 11-13 for Girder C4 at L/50

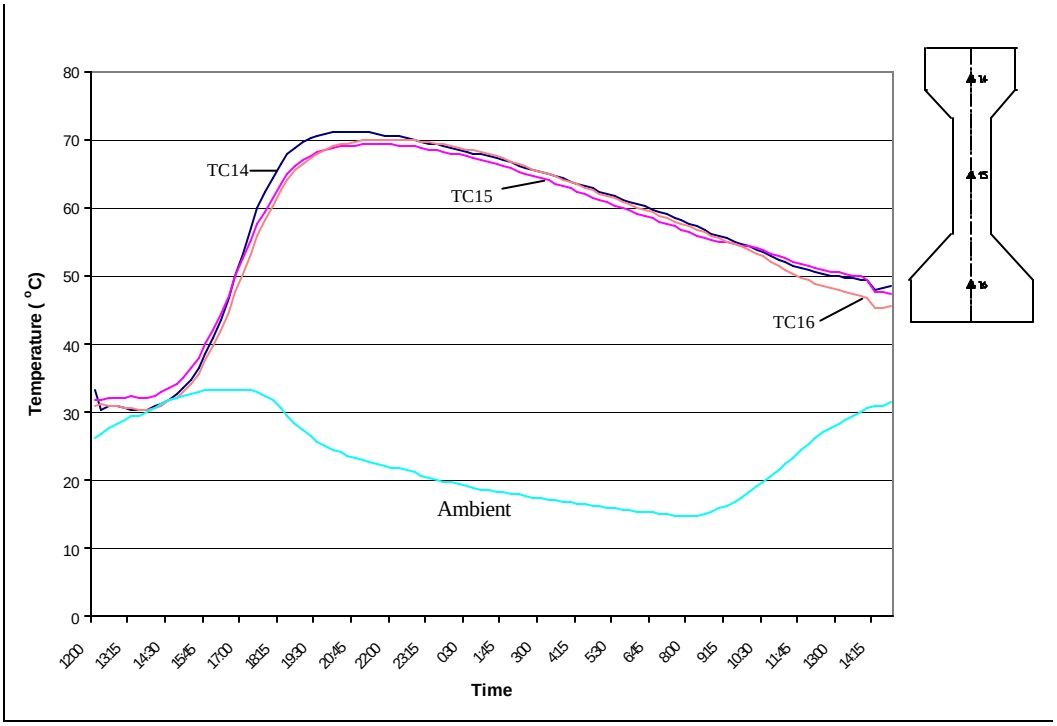

Figure 3.45 Thermocouples 14-16 for Girder C4 at L/4

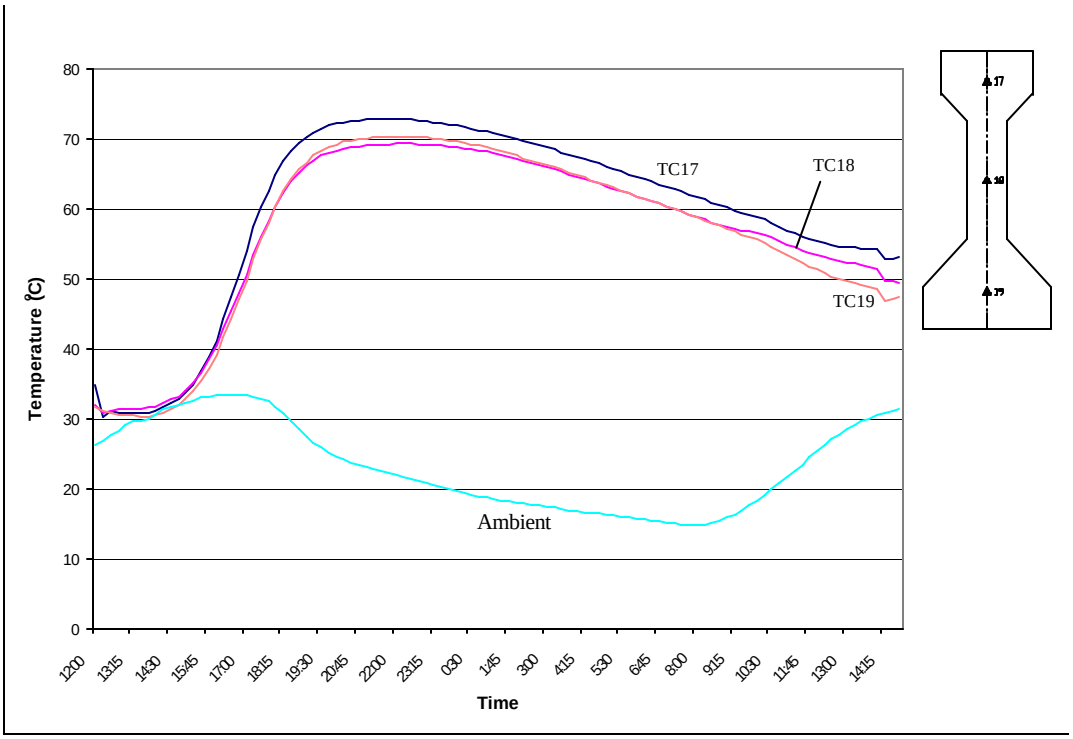

Figure 3.46 Thermocouples 17-19 for Girder C4 at 49L/50

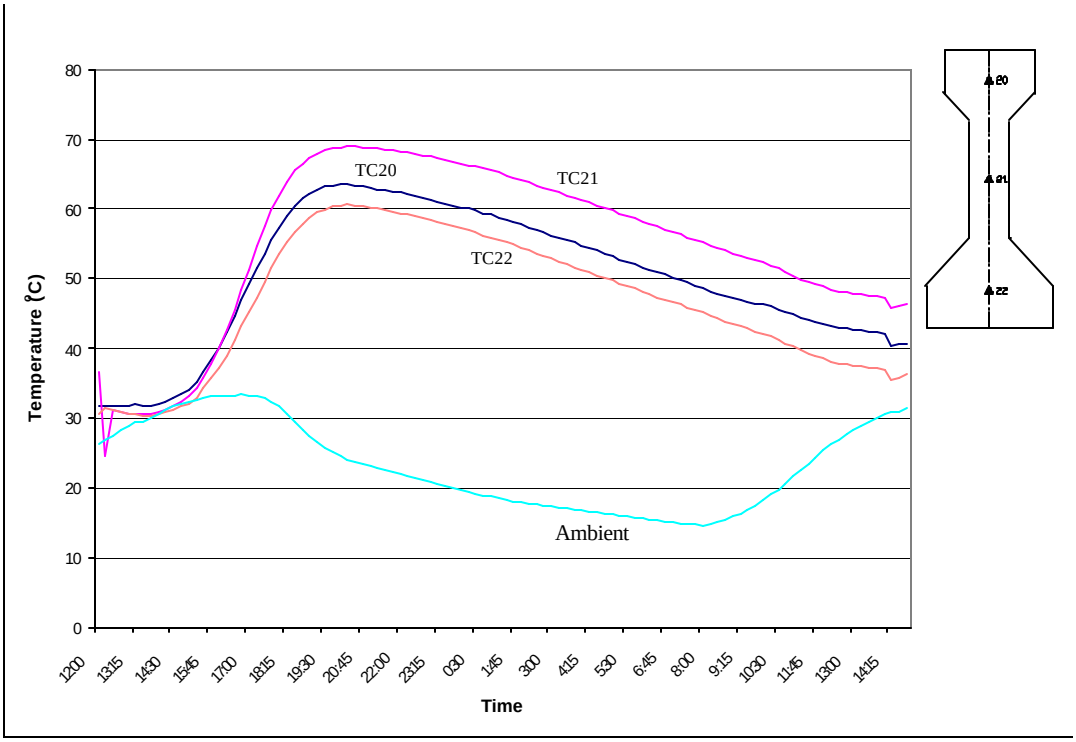

Figure 3.47 Thermocouples 20-22 for Girder C4 at 3L/4

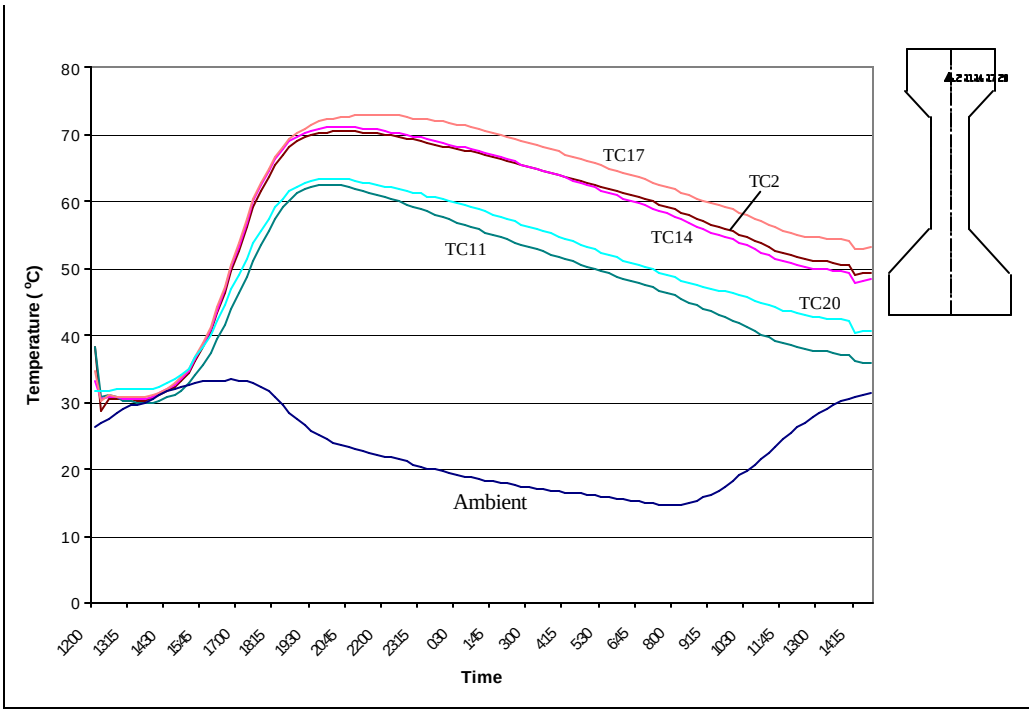

Figure 3.48 Thermocouples in Top Flange for Girder C4

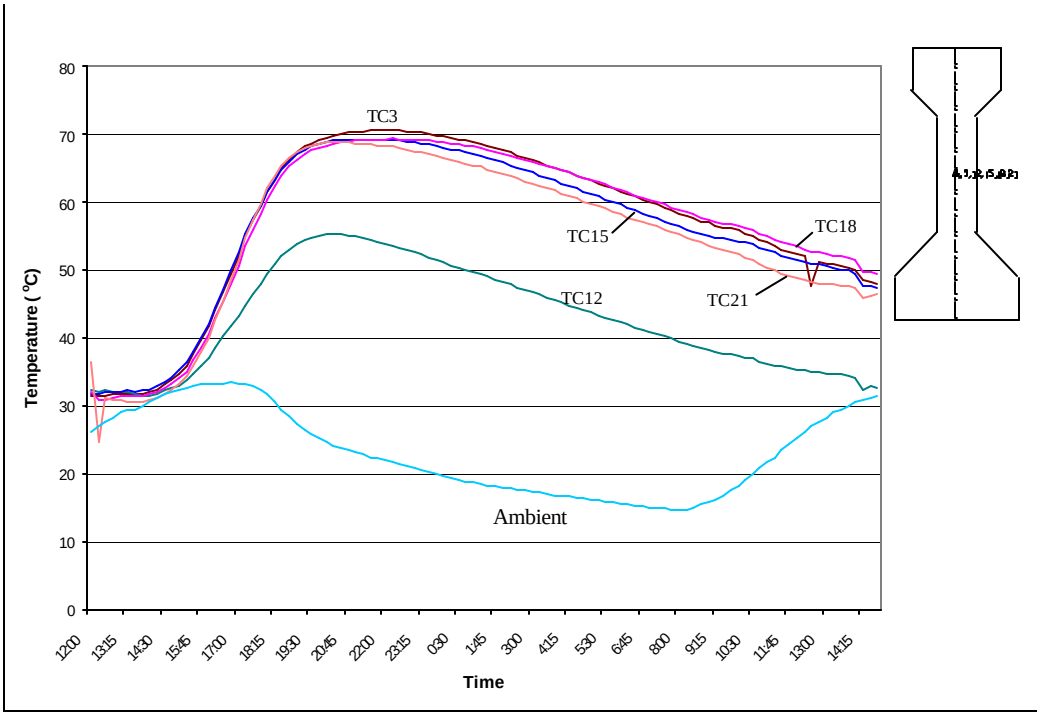

Figure 3.49 Thermocouples at Mid-height of Web for Girder C4

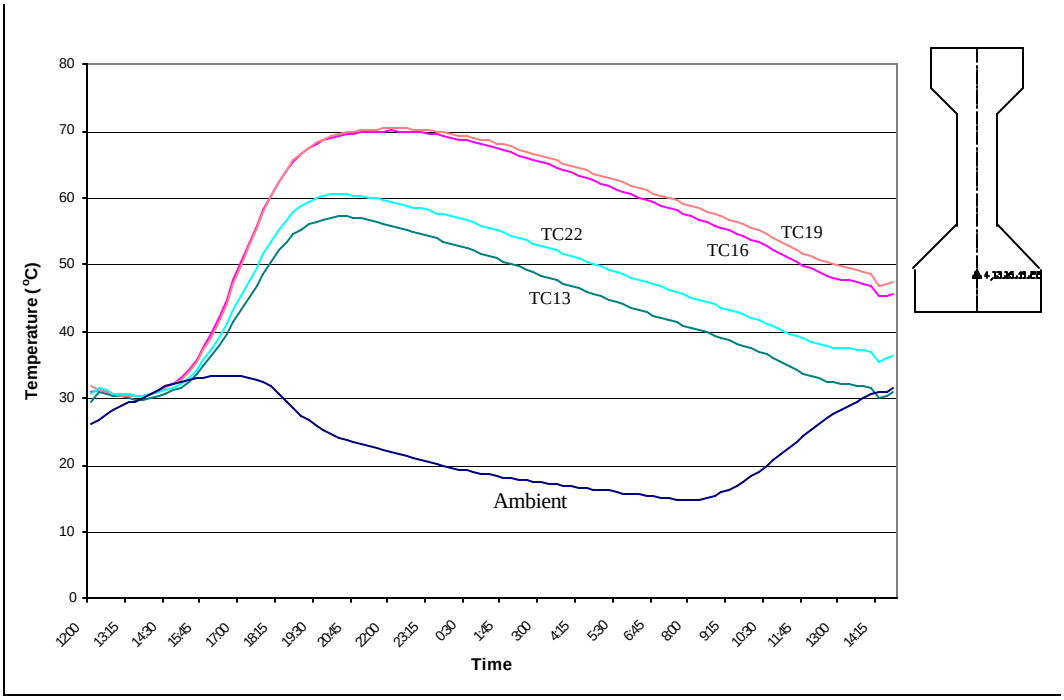

Figure 3.50 Thermocouples in Bottom Flange for Girder C4

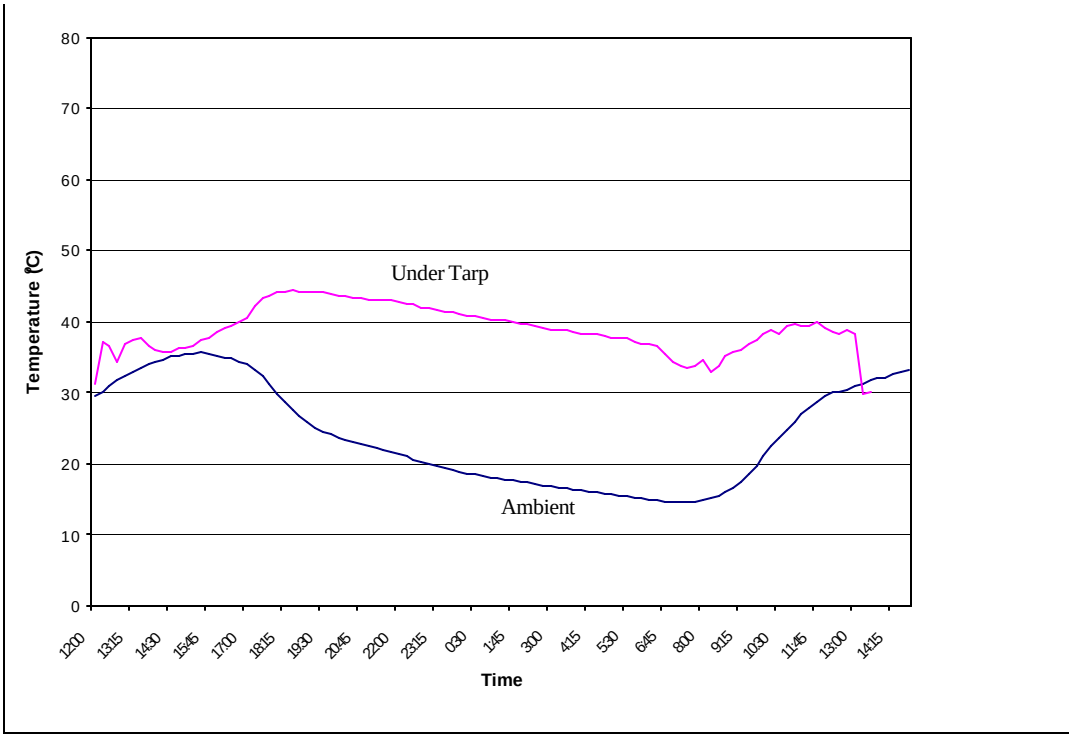

Figure 3.51 Reference Temperatures for Girder D4

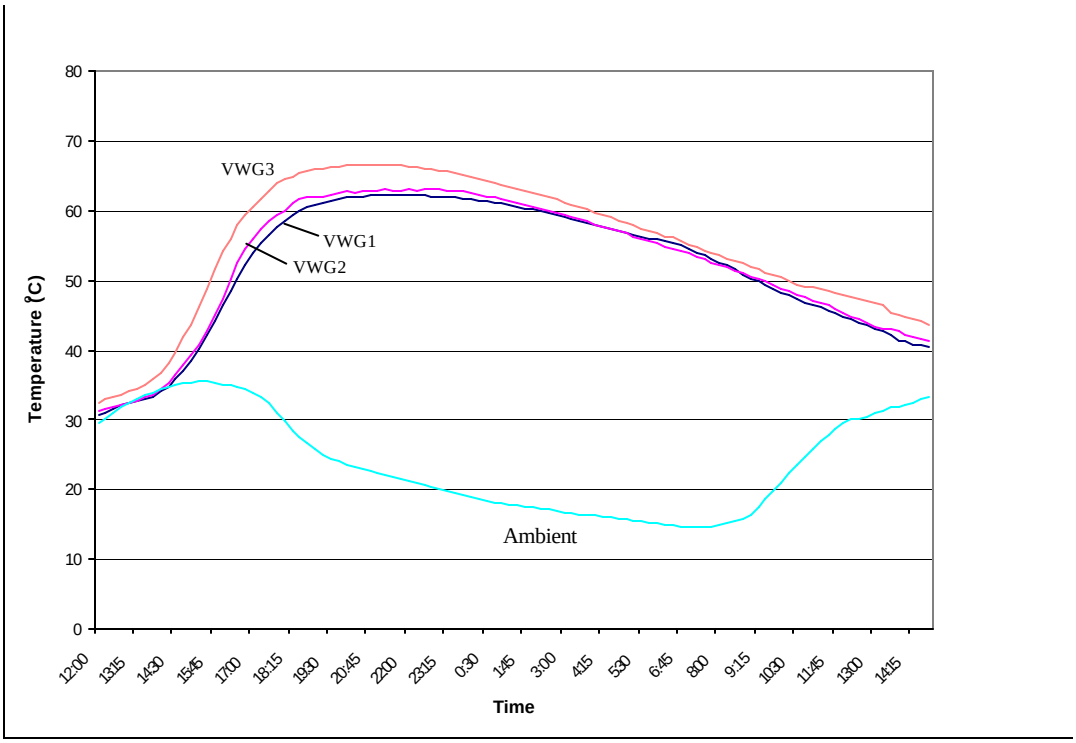

Figure 3.52 VWG Temperatures for Girder D4 (see Figure 3.18 for gage location)

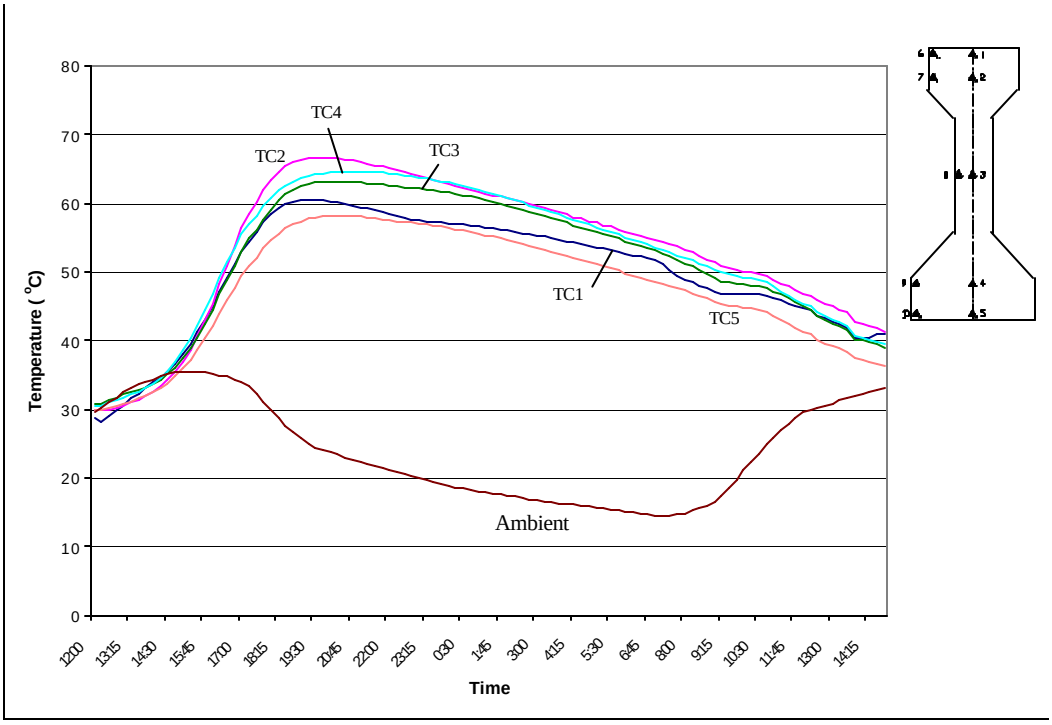

Figure 3.53 Thermocouples 1-5 for Girder D4 at Mid-span

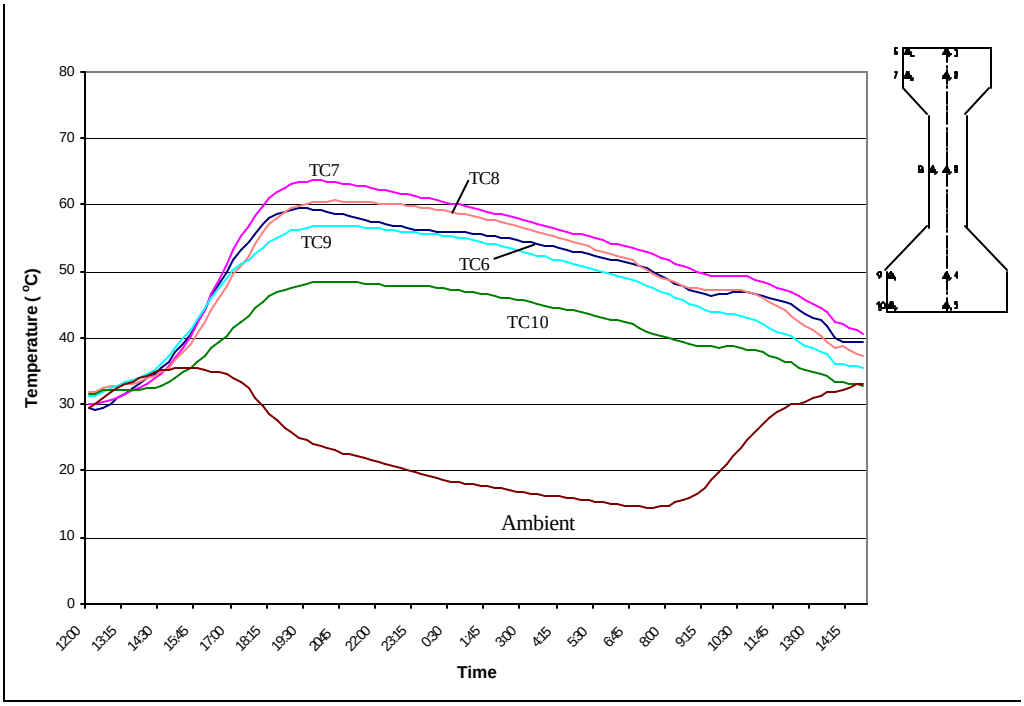

Figure 3.54 Thermocouples 6-10 for Girder D4 at Mid-span

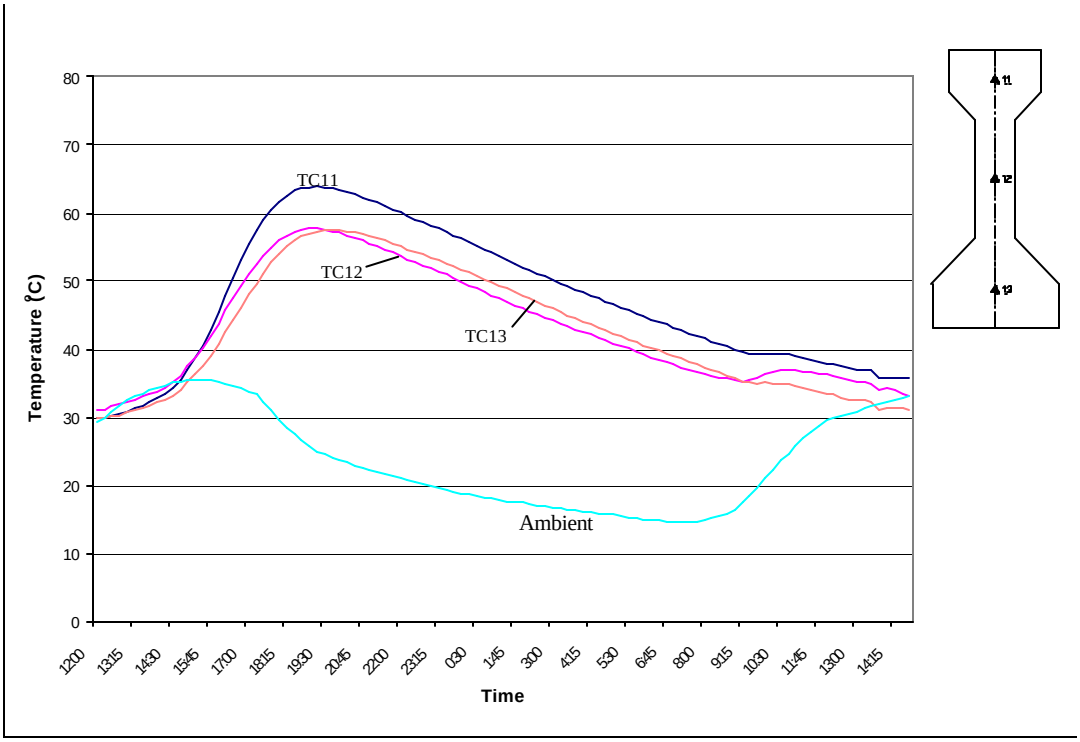

Figure 3.55 Thermocouples 11-13 for Girder D4 at L/50

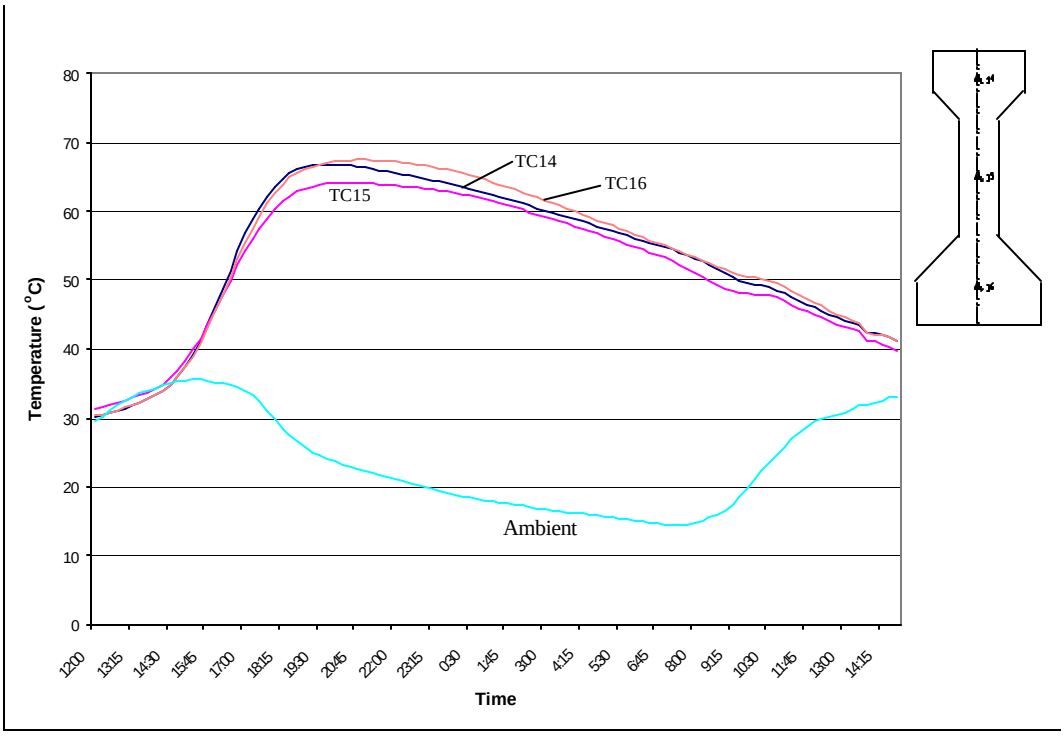

Figure 3.56 Thermocouples 14-16 for Girder D4 at L/4

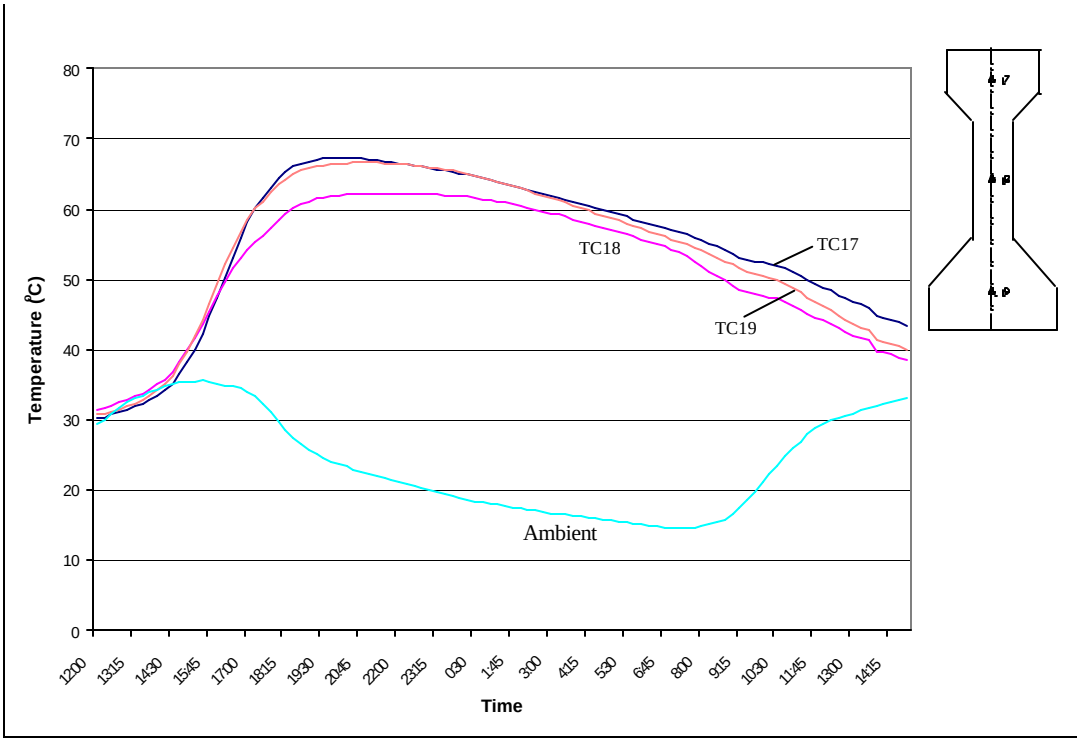

Figure 3.57 Thermocouples 17-19 for Girder D4 at 49L/50

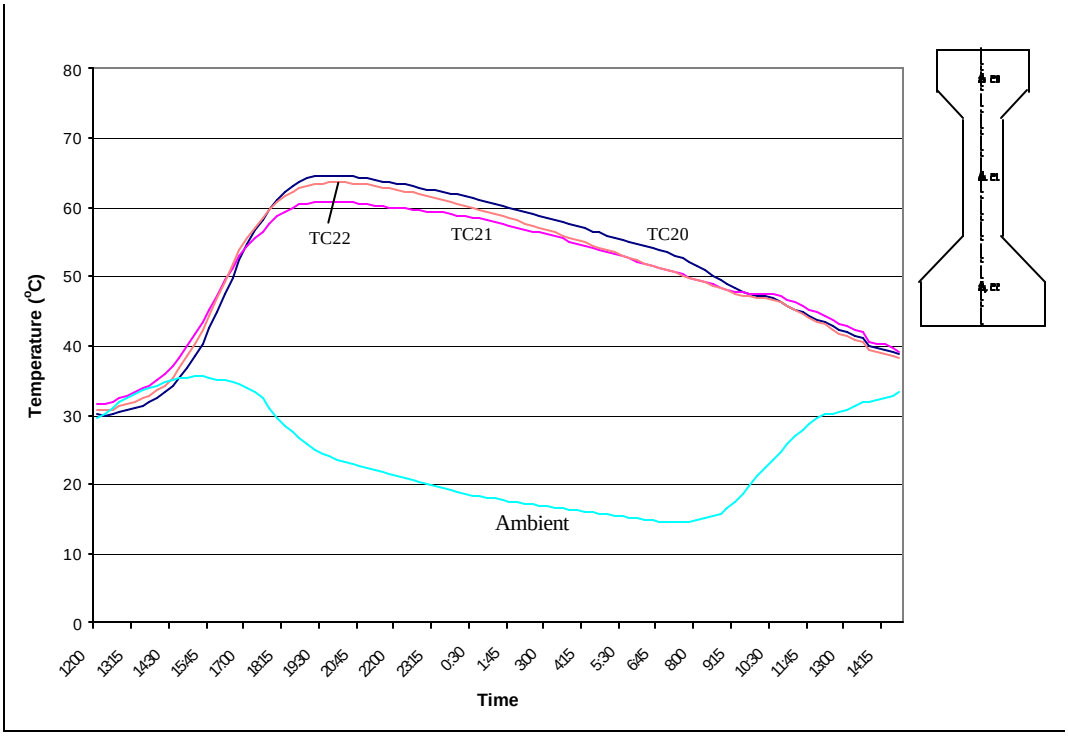

Figure 3.58 Thermocouples 20-22 for Girder D4 at 3L/4

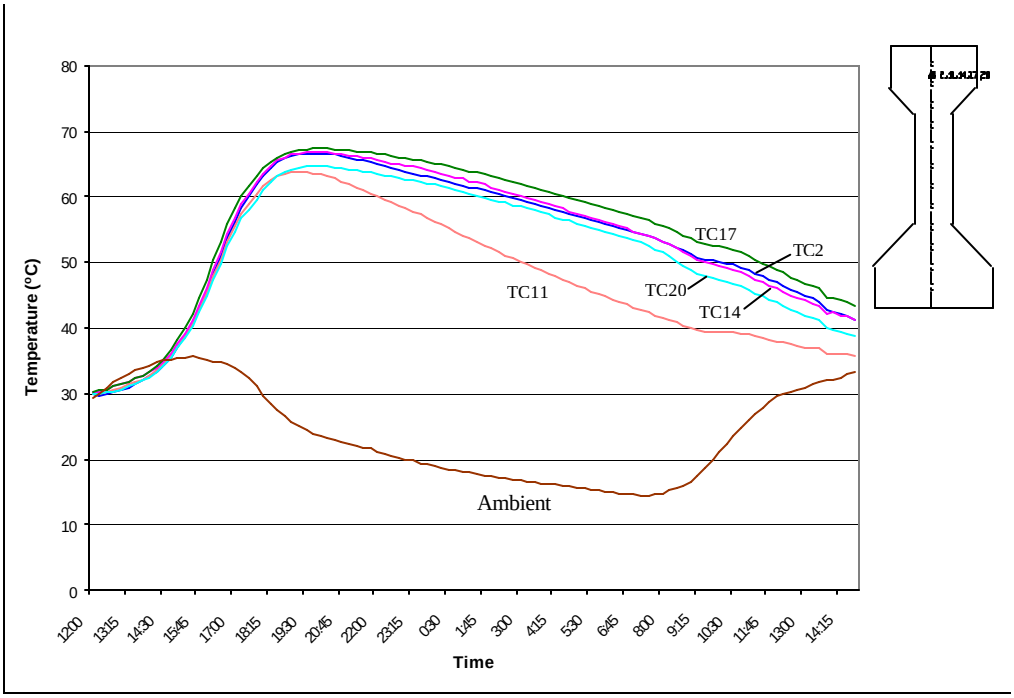

Figure 3.59 Thermocouples in Top Flange for Girder D4

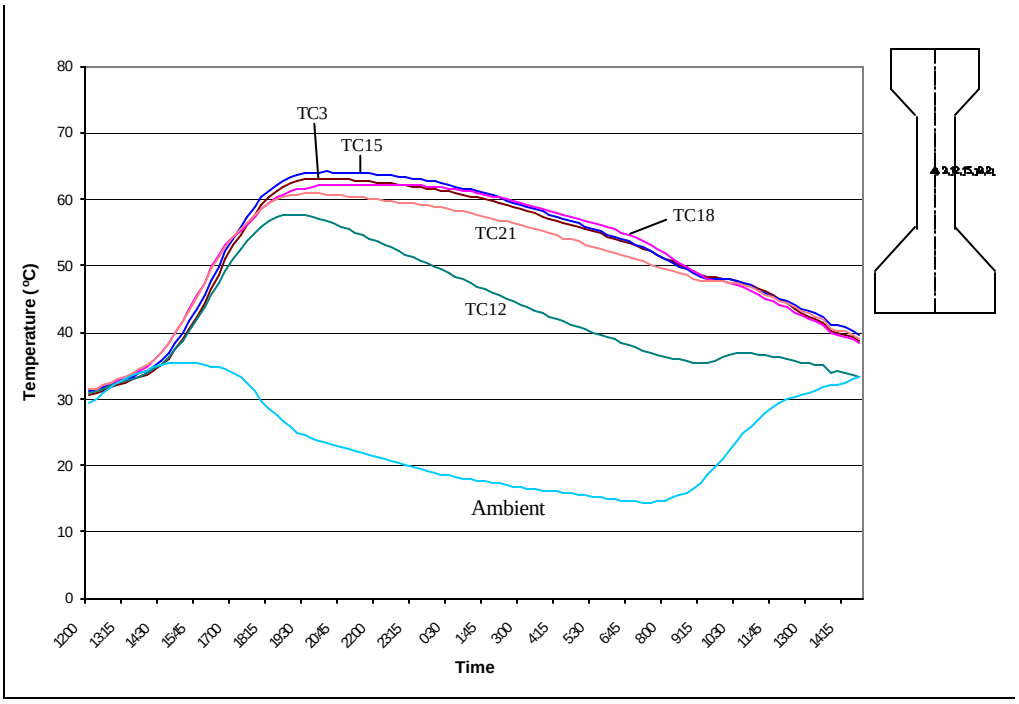

Figure 3.60 Thermocouples at Mid-height of Web for Girder D4

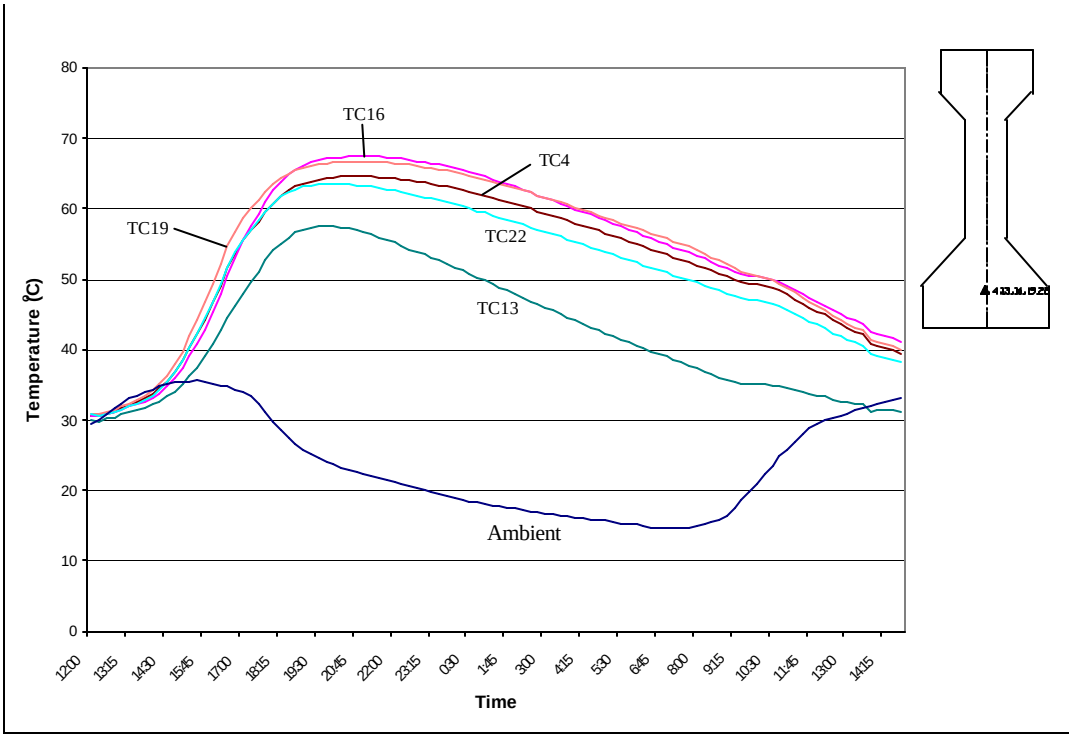

Figure 3.61 Thermocouples in Bottom Flange for Girder D4

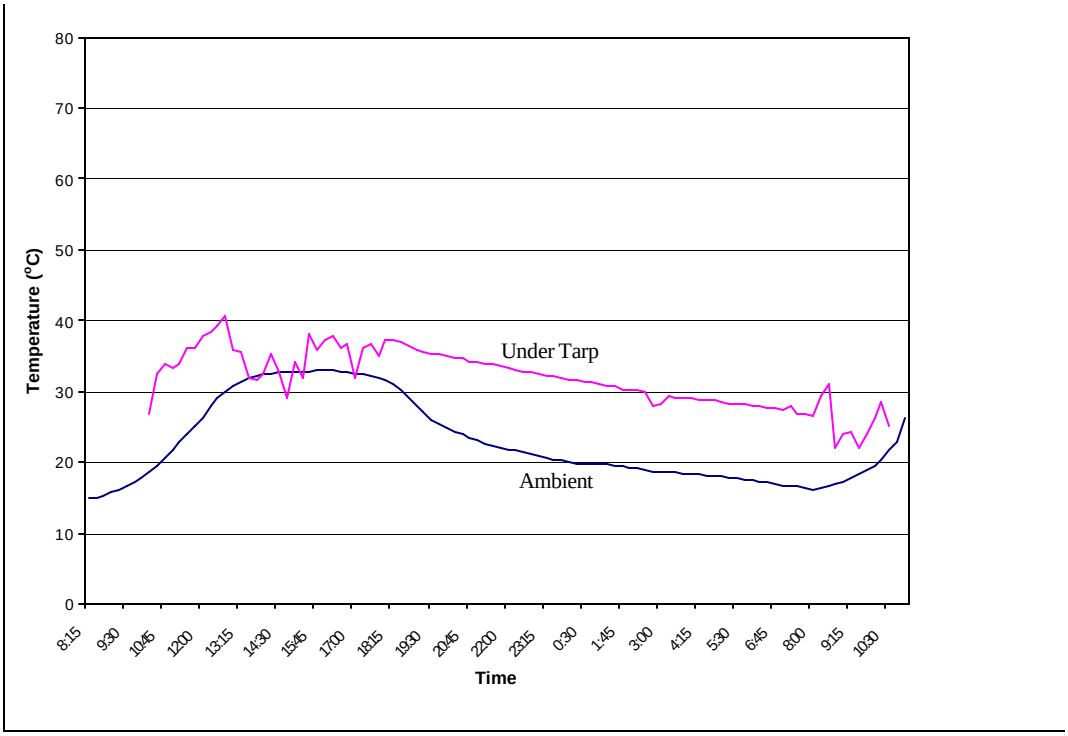

Figure 3.62 Reference Temperatures for Girder A4

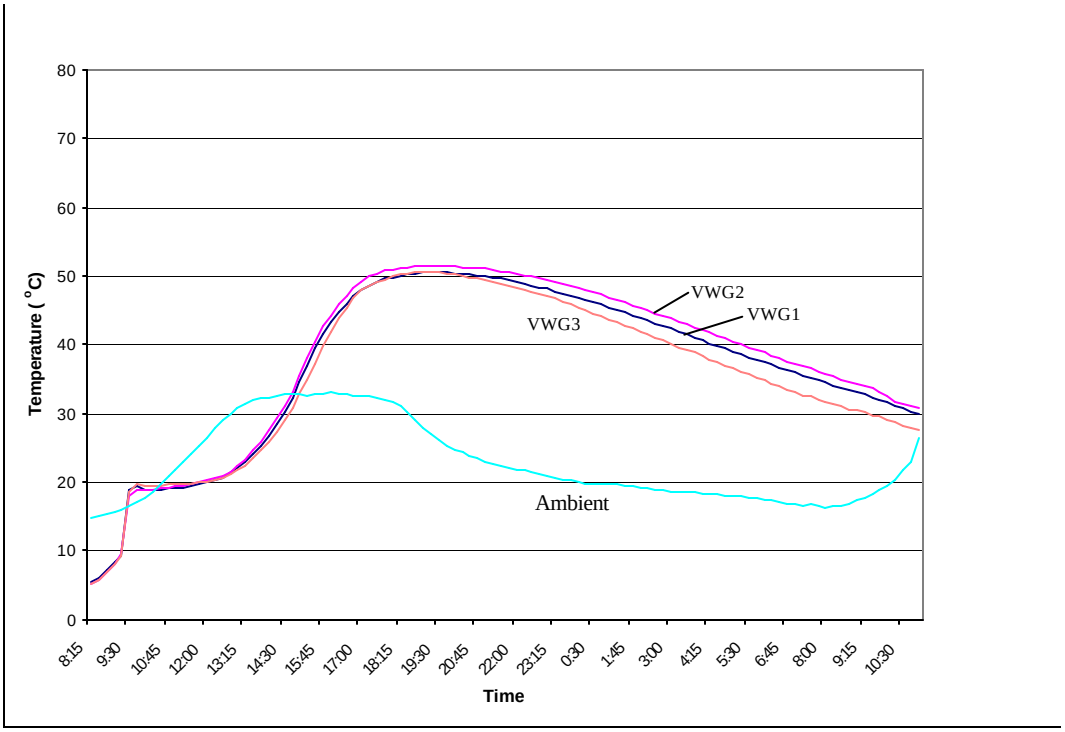

Figure 3.63 VWG Temperatures for Girder A4 (see Figure 3.18 for gage location)

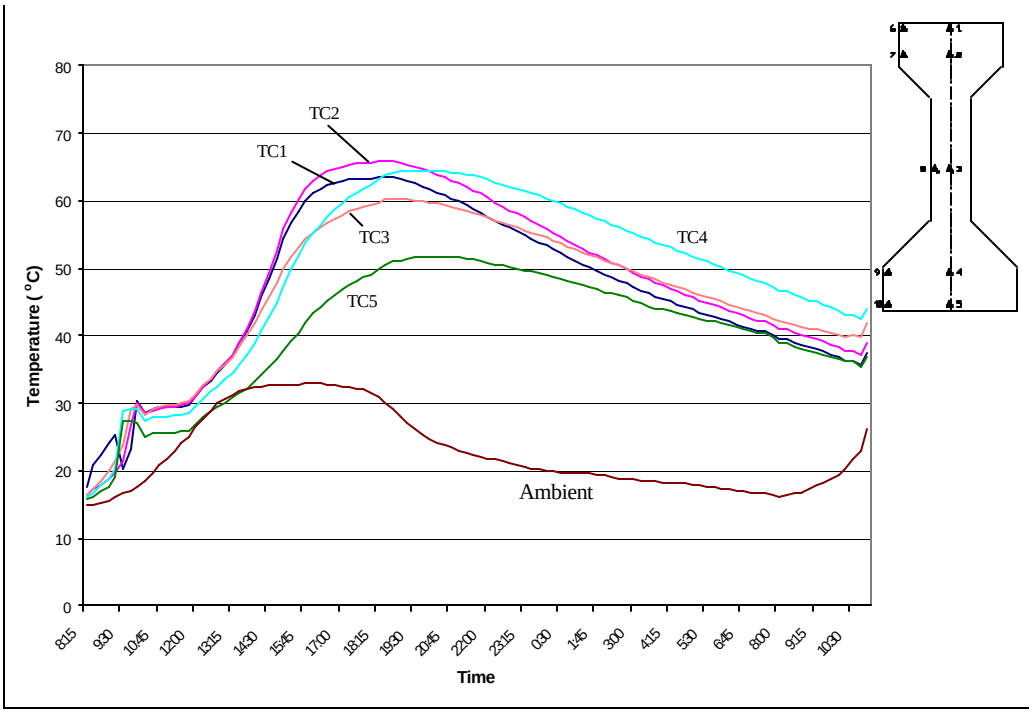

Figure 3.64 Thermocouples 1-5 for Girder A4 at Mid-span

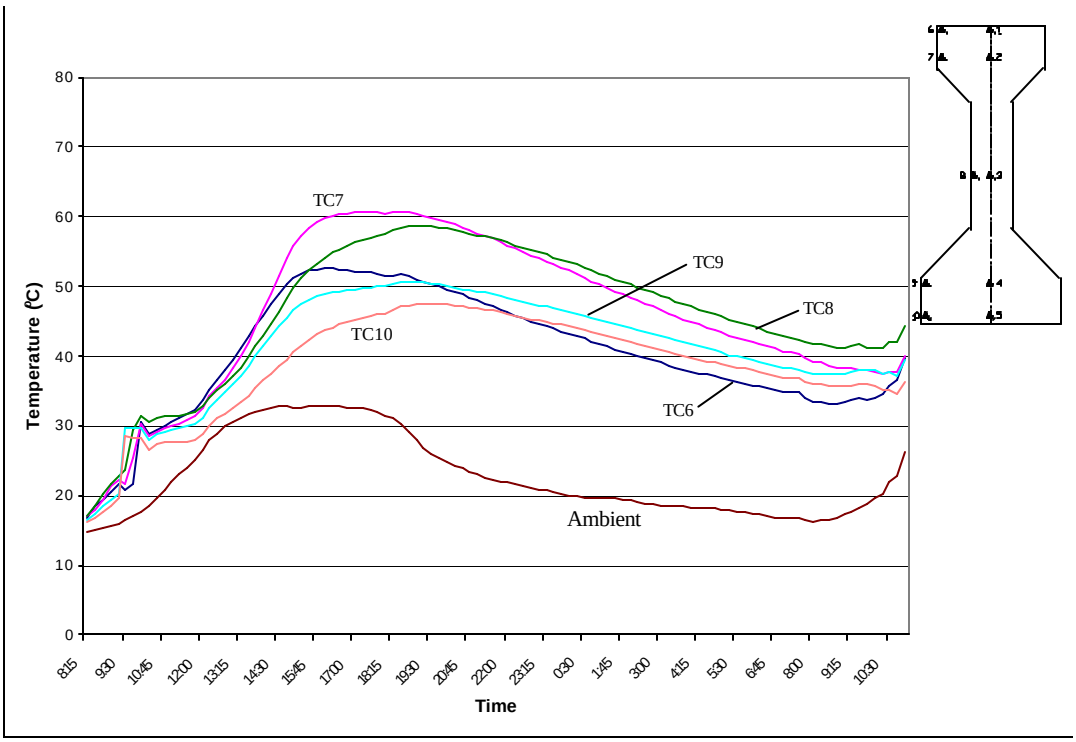

Figure 3.65 Thermocouples 6-10 for Girder A4 at Mid-span

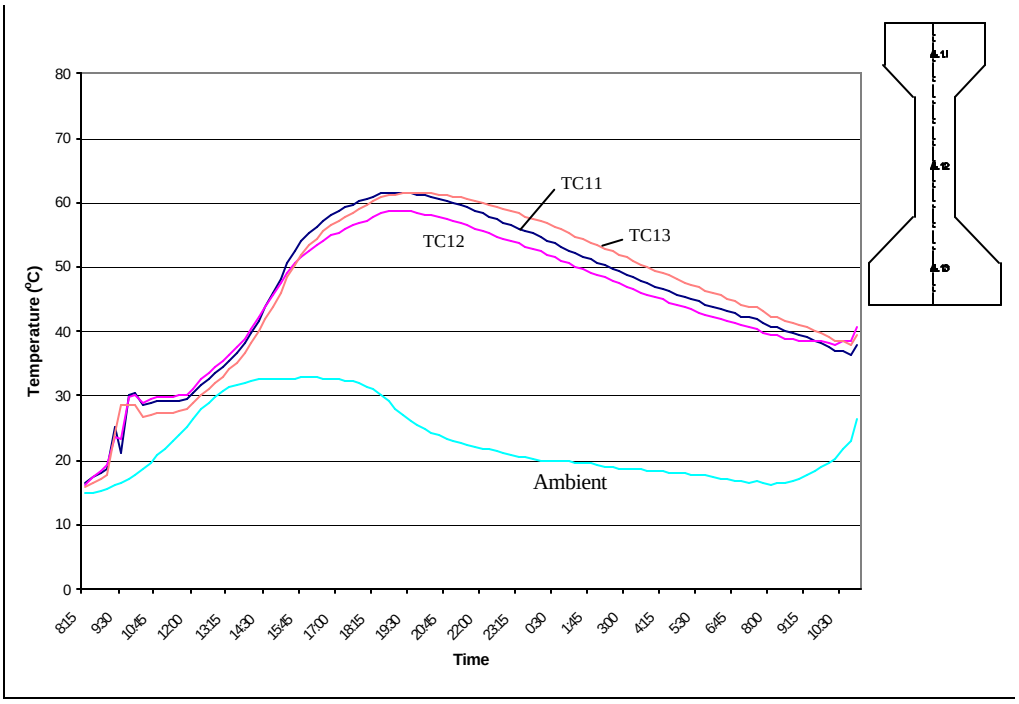

Figure 3.66 Thermocouples 11-13 for Girder A4 at L/50

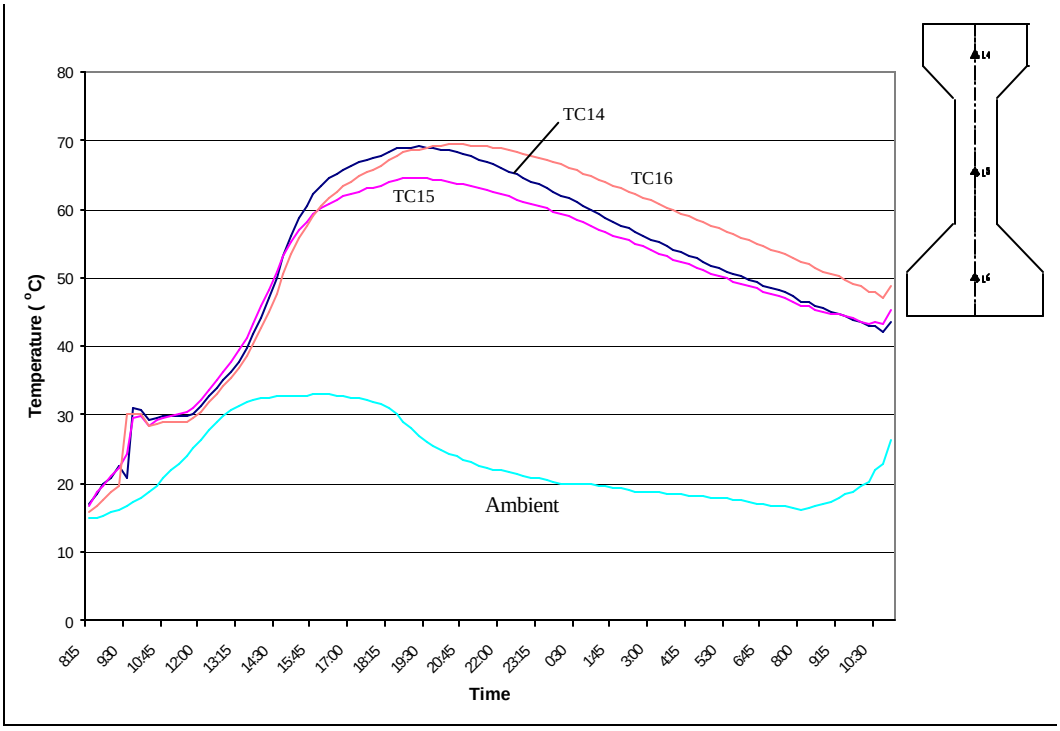

Figure 3.67 Thermocouples 14-16 for Girder A4 at L/4

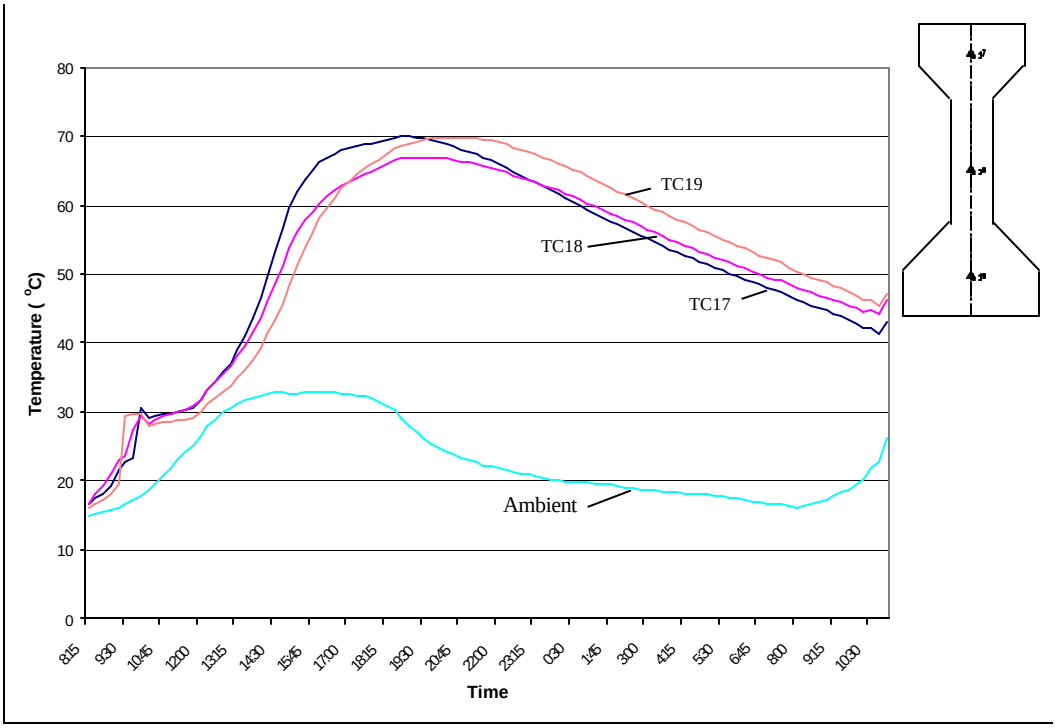

Figure 3.68 Thermocouples 17-19 for Girder A4 at 49L/50

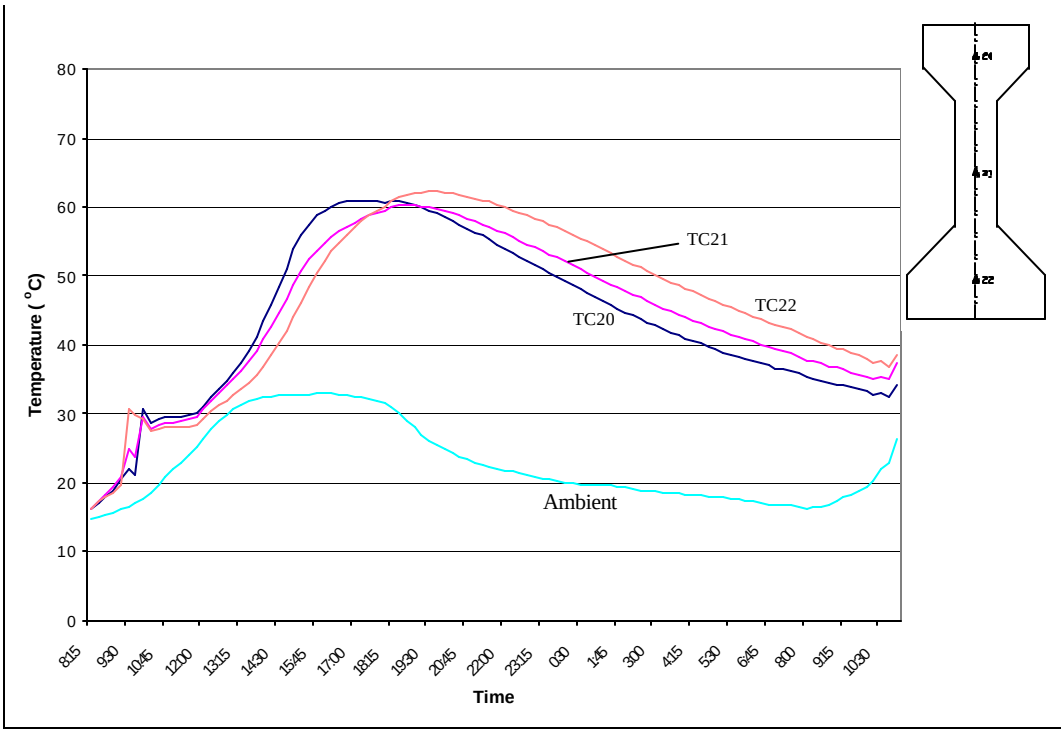

Figure 3.69 Thermocouples 20-22 for Girder A4 at 3L/4

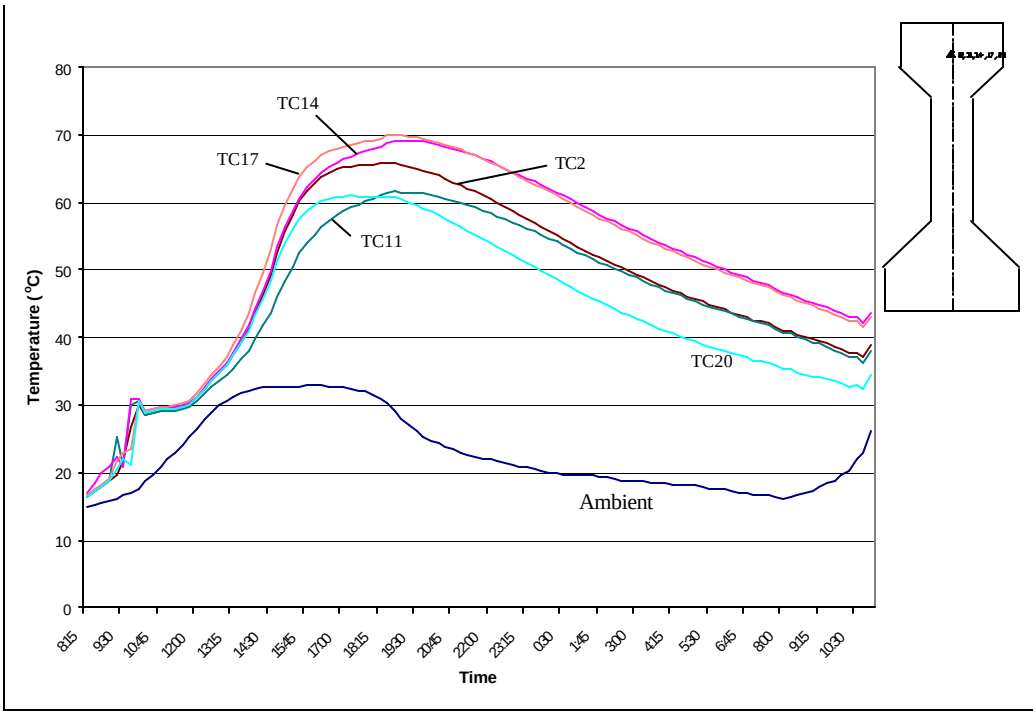

Figure 3.70 Thermocouples in Top Flange for Girder A4

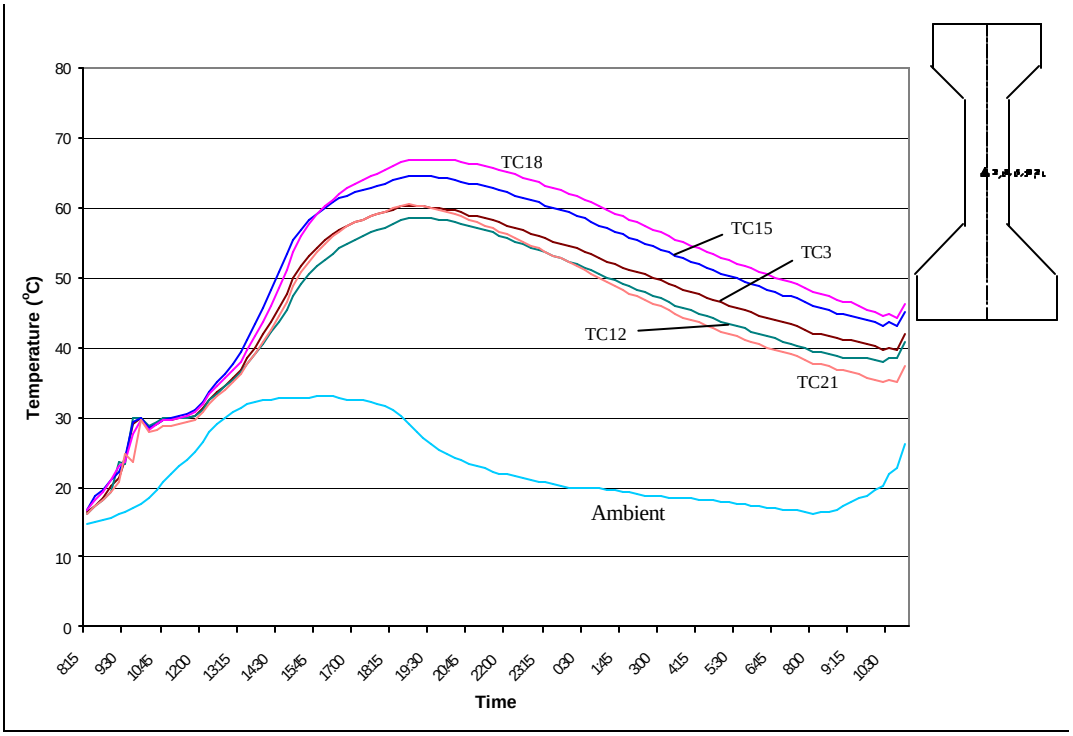

Figure 3.71 Thermocouples at Mid-height of Web for Girder A4

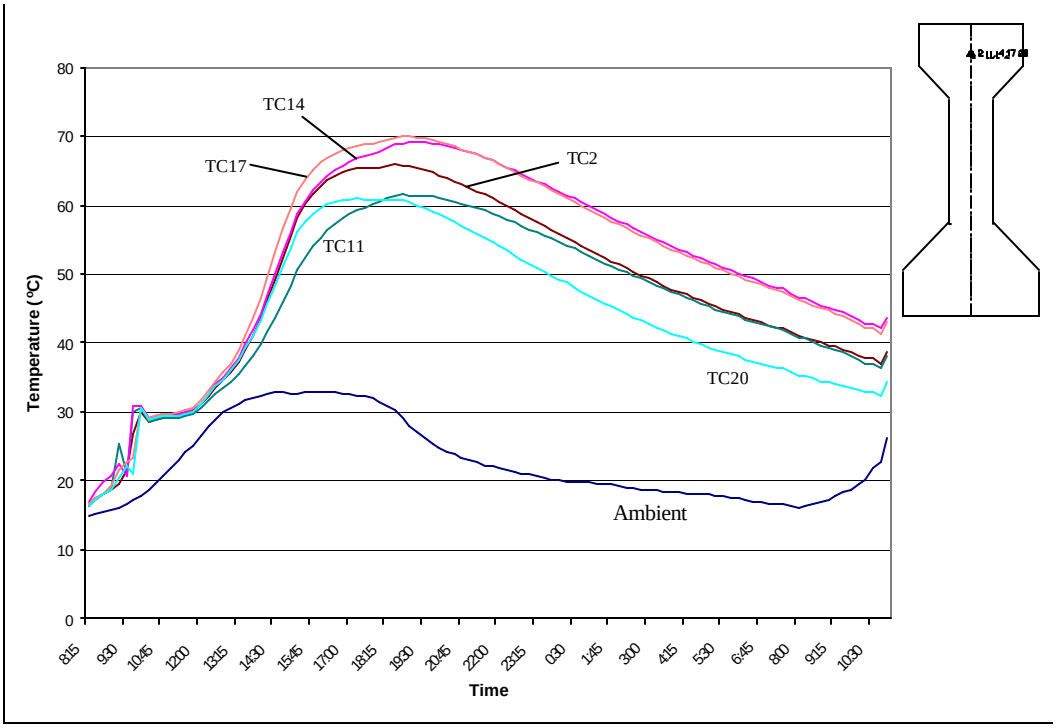

Figure 3.72 Thermocouples in Bottom Flange for Girder A4

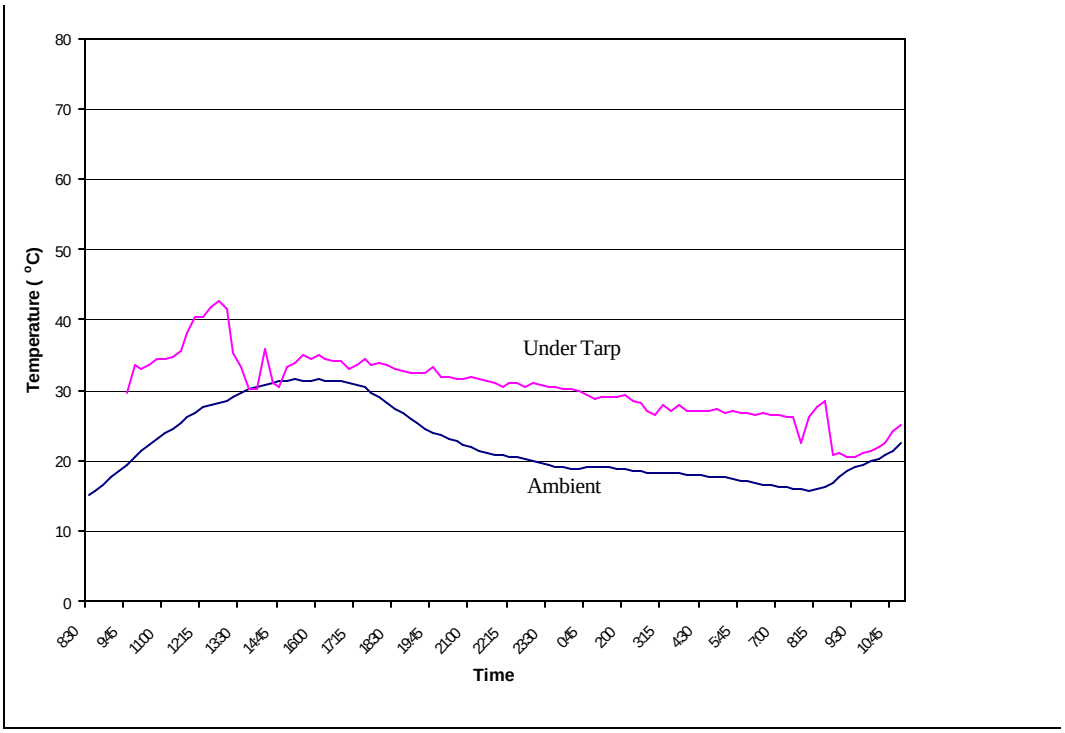

Figure 3.73 Reference Temperatures for Girder B4

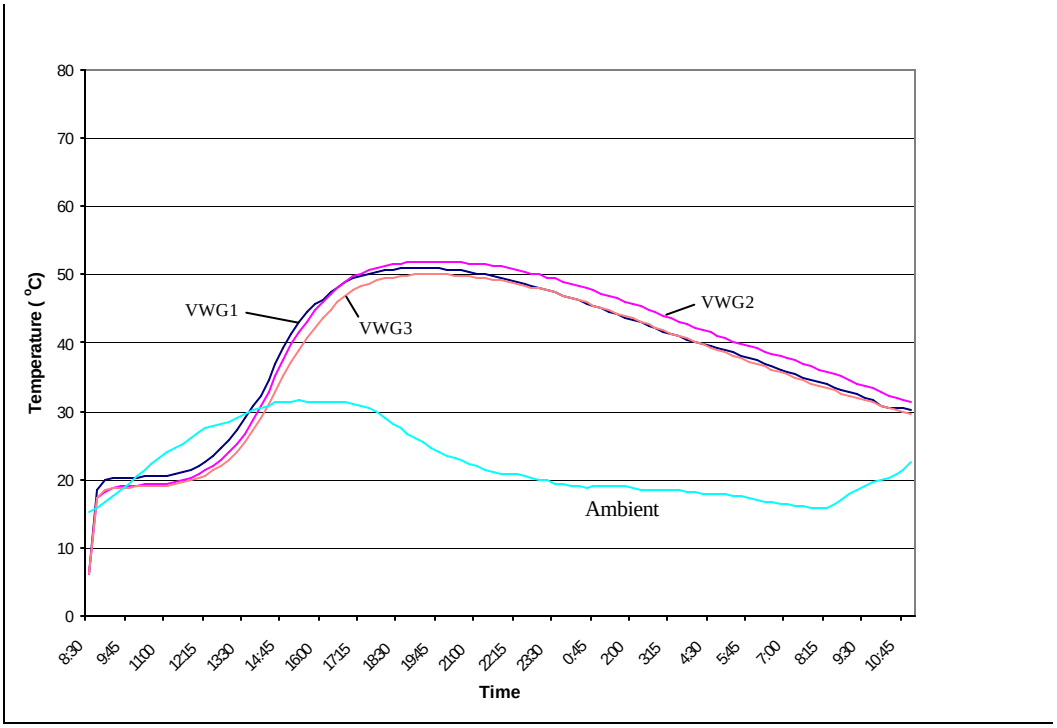

Figure 3.74 VWG Temperatures for Girder B4 (see Figure 3.18 for gage location)

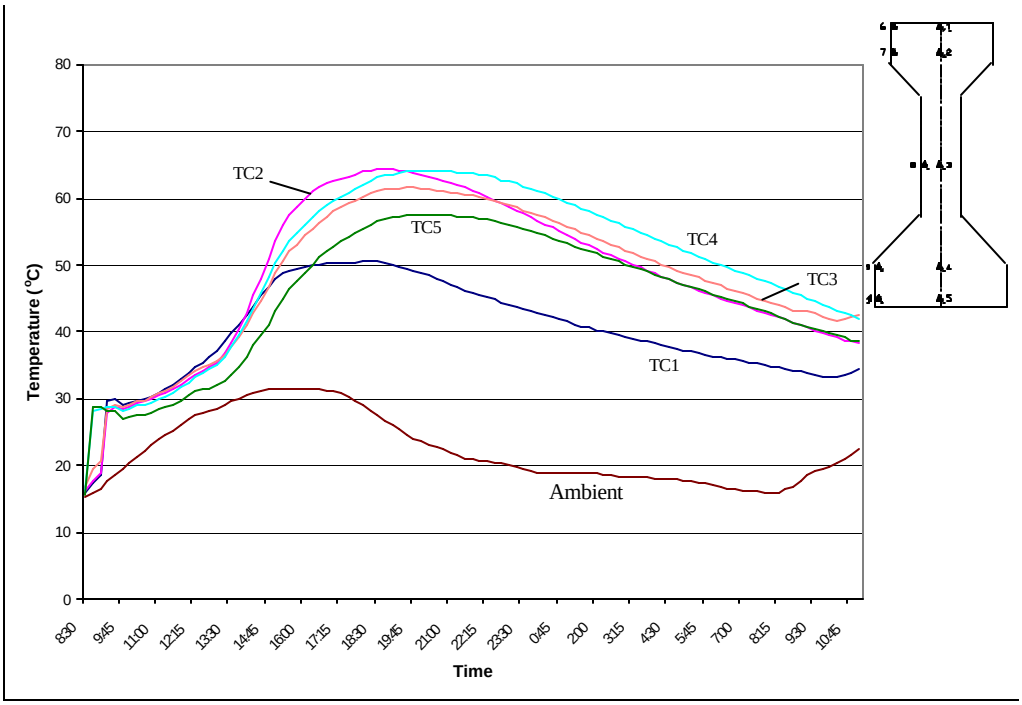

Figure 3.75 Thermocouples 1-5 for Girder B4 at Mid-span

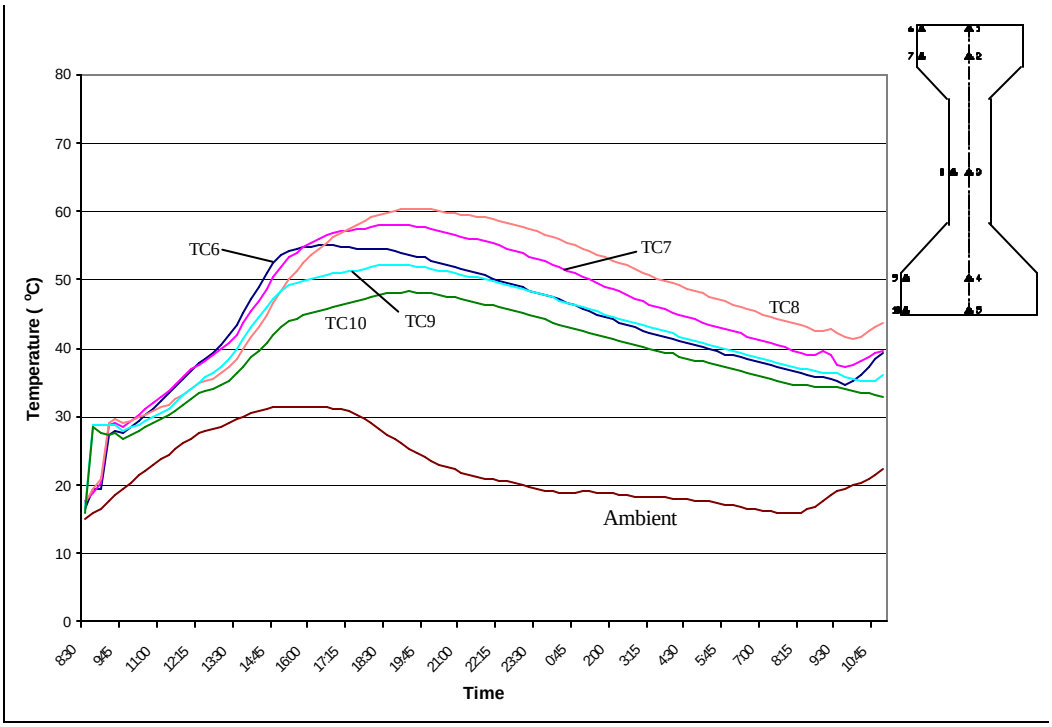

Figure 3.76 Thermocouples 6-10 for Girder B4 at Mid-span

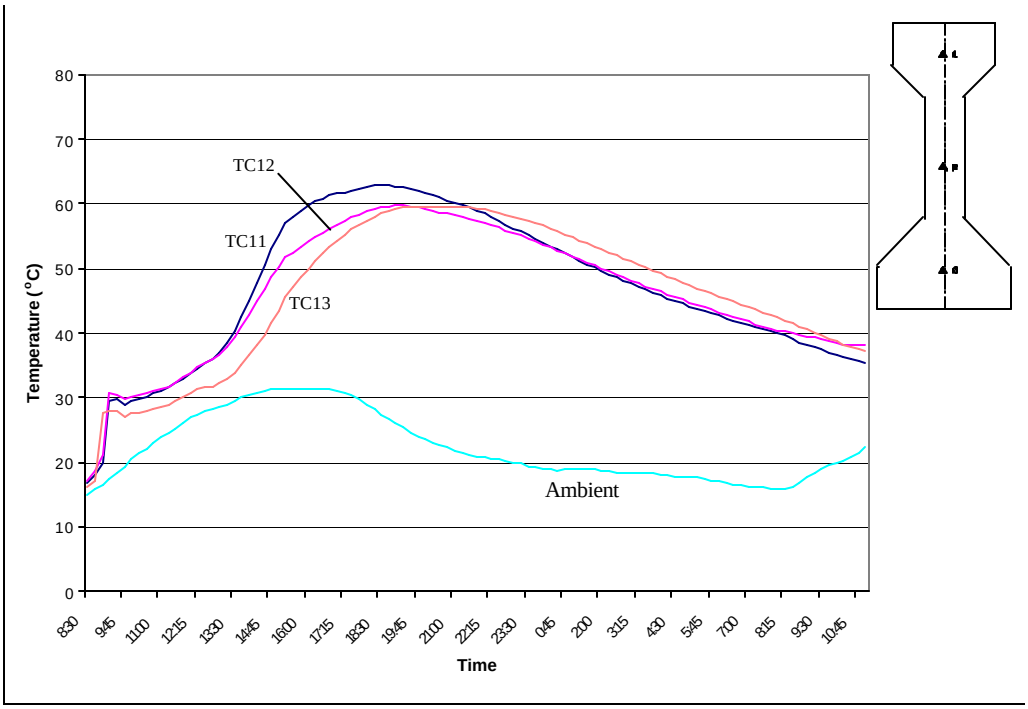

Figure 3.77 Thermocouples 11-13 for Girder B4 at L/50

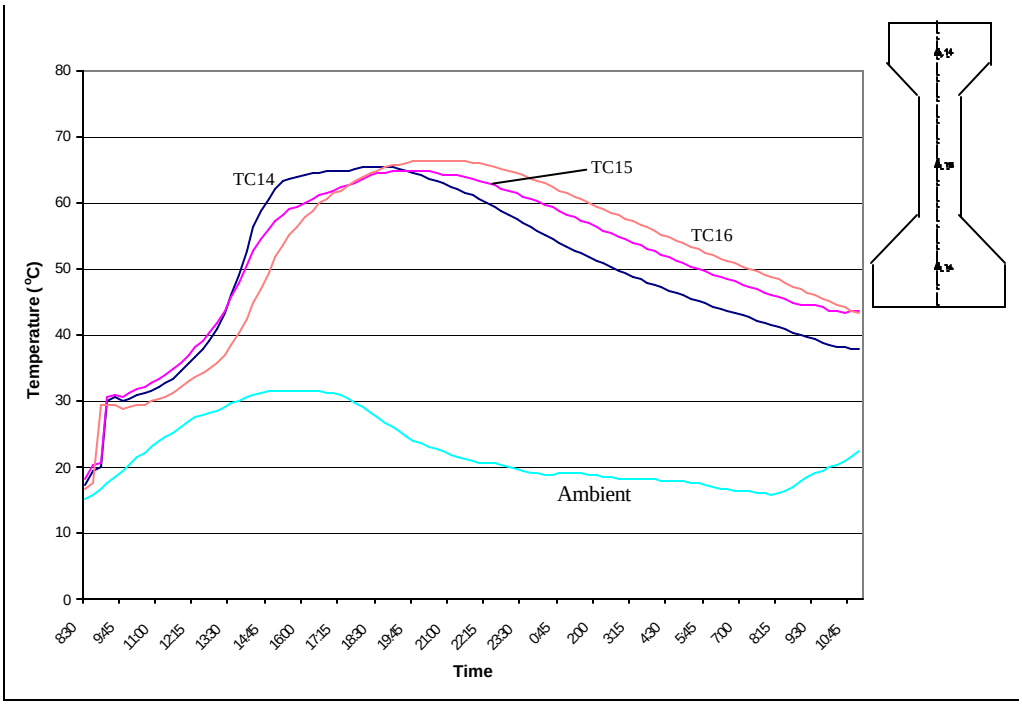

Figure 3.78 Thermocouples 14-16 for Girder B4 at L/4

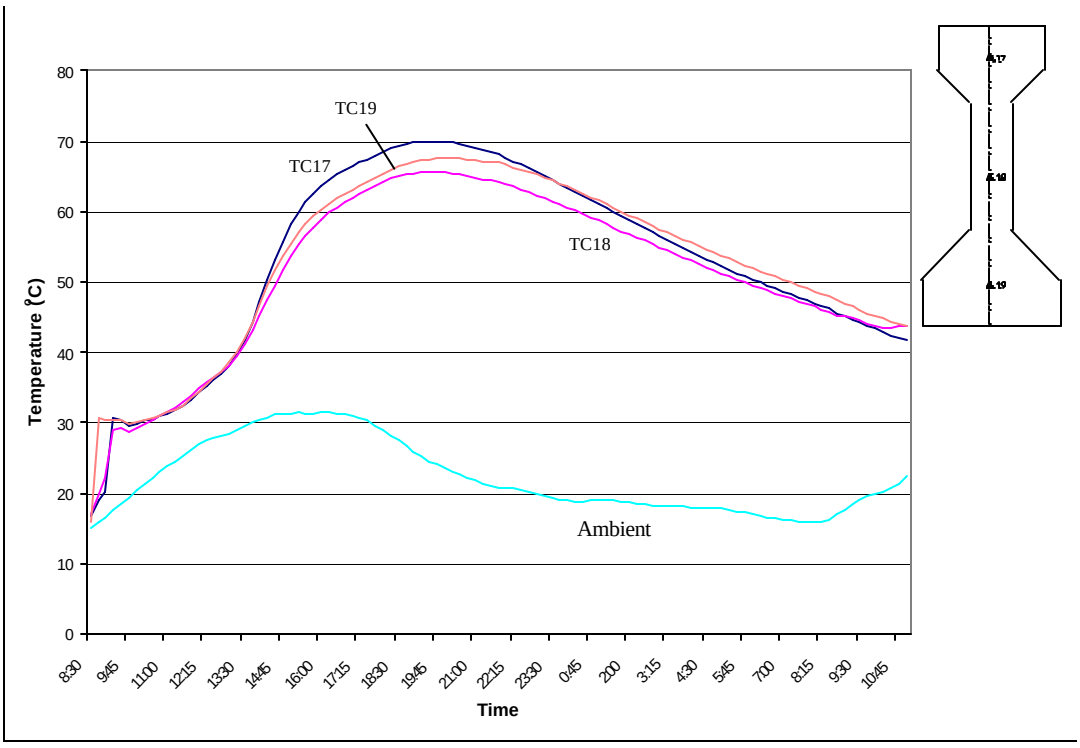

Figure 3.79 Thermocouples 17-19 for Girder B4 at 49L/50

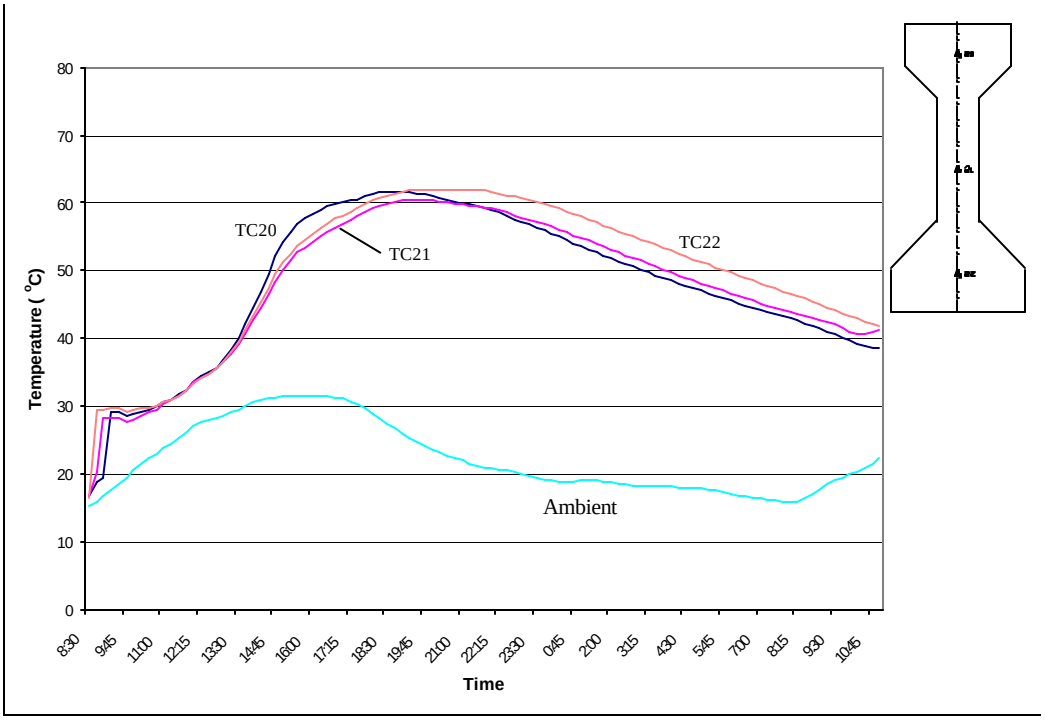

Figure 3.80 Thermocouples 20-22 for Girder B4 at 3L/4

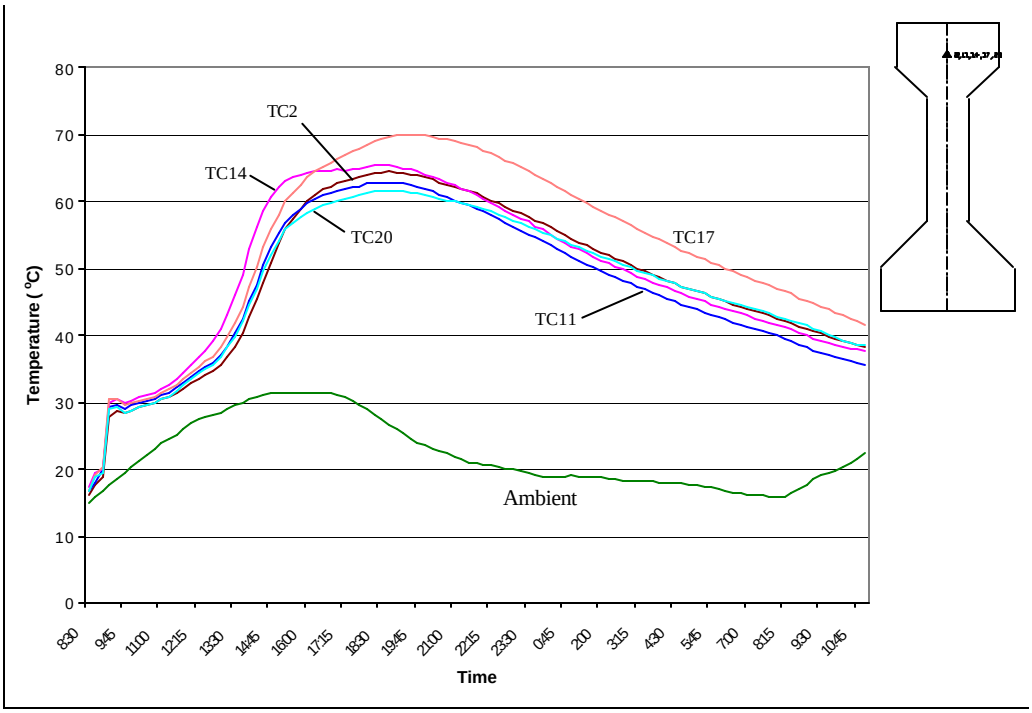

Figure 3.81 Thermocouples in Top Flange for Girder B4

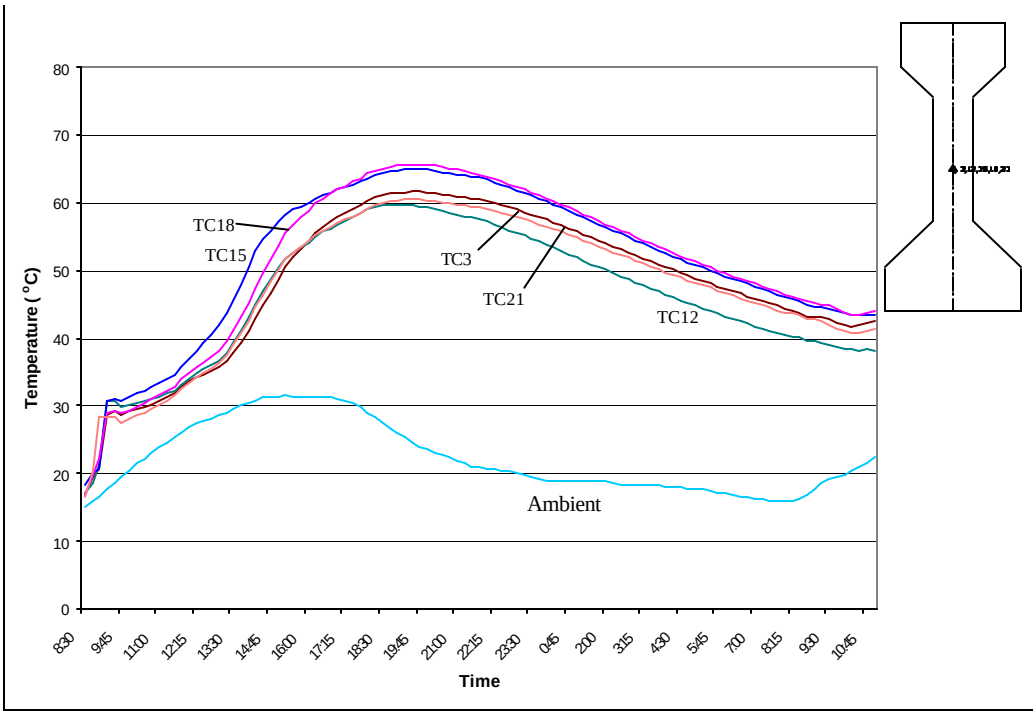

Figure 3.82 Thermocouples at Mid-height of Web for Girder B4

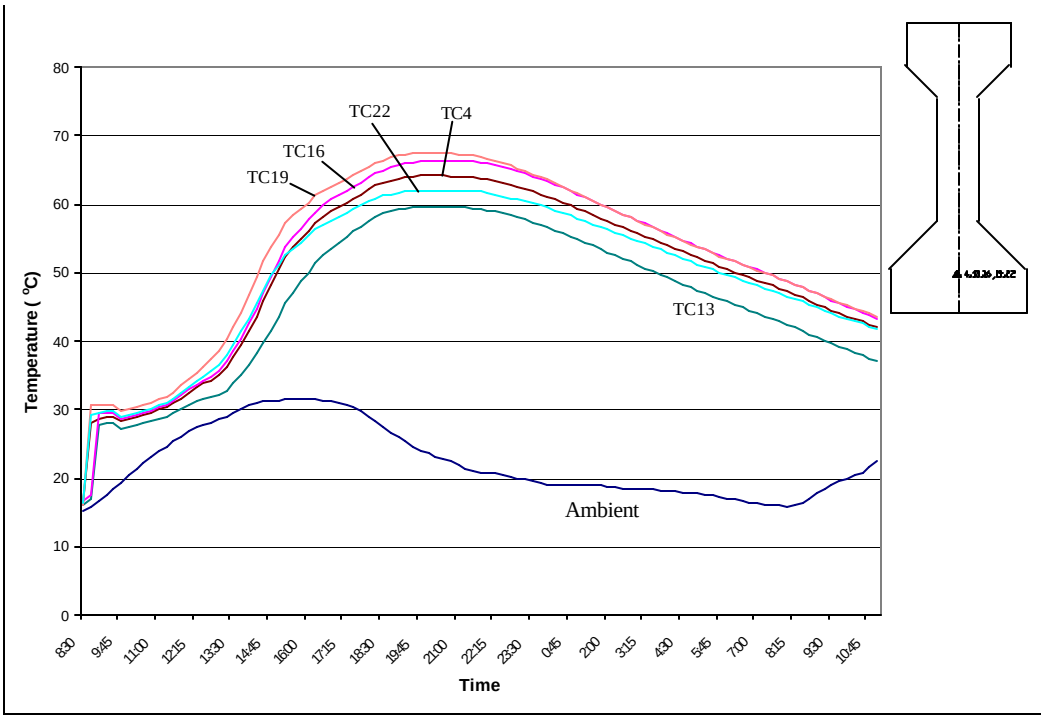

Figure 3.83 Thermocouples in Bottom Flange for Girder B4

3.6.2 Concrete Strains During Curing

Concrete strains were recorded by using plane strain bars, embedded ERSGs and VWGs. The recorded strains are presented in Figures 3.84-3.95. The location of the plane strain bars is included in the figures, however, a more detailed discussion was presented in Section 3.3.3. The ERSGs on strain gage bars five and six for girder C4 were not functioning prior to casting (see Figure 3.86). These were most likely damaged during transportation or installation. Plane strain bar one in girder D4 was damaged at detensioning (see Figure 3.87). Plane strain bar one for both girders A4 and B4 recorded data until detensioning. The gages were damaged at detensioning (see Figures 3.92-3.93).

It is noticed in the figures that the strain values change as the heat of hydration takes place. As the concrete cures, the cement absorbs water and the gages experience compression. Then, after peak hydration, there is a decrease in compression strain. For both the Type III and the Type IV girders, the VWGs experience a greater compression strain during curing than do the embedded ERSGs. The behavior of the two gages is similar; there is simply a difference in magnitude. The extended usage range for the embedded ERSGs is –30 to +60ºC (–25 to +150ºF). For all four girders, the heat generated during hydration was greater than 60ºC at the location of the embedded ERSGs (and VWGs). It is suspected that the high heat of hydration may have affected the polymer, which encases the ERSG in the embedded ERSG. A change in the polymer's matrix would account for the difference in strain magnitudes between the VWGs and embedded ERSGs.

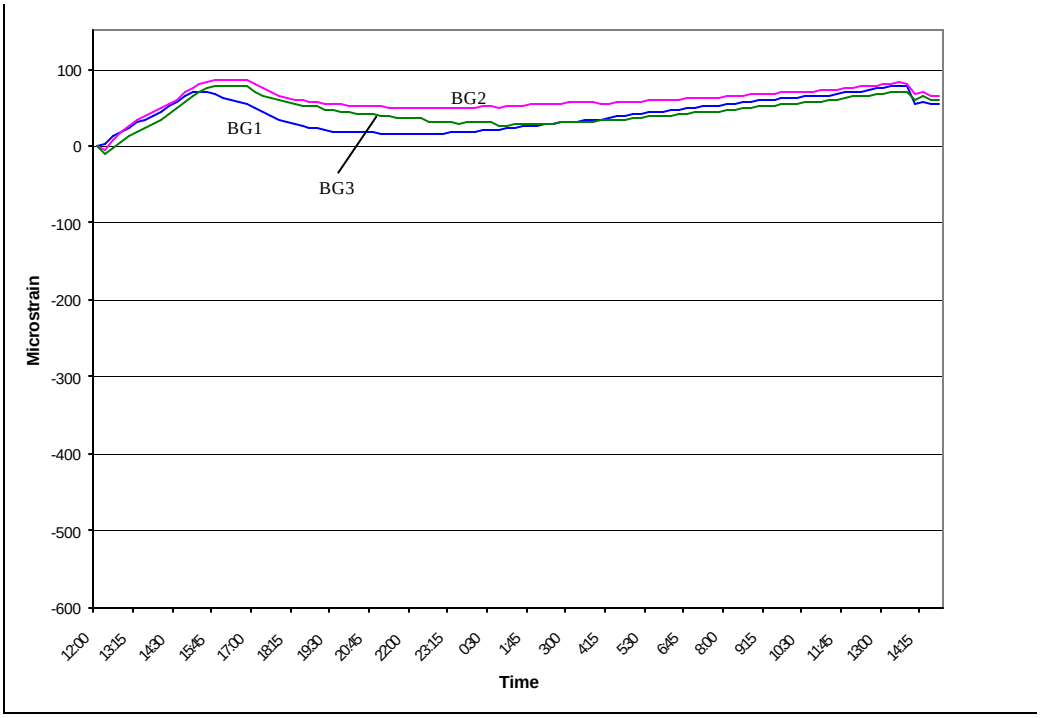

Figure 3.84 Embedment ERSG Readings for Girder C4

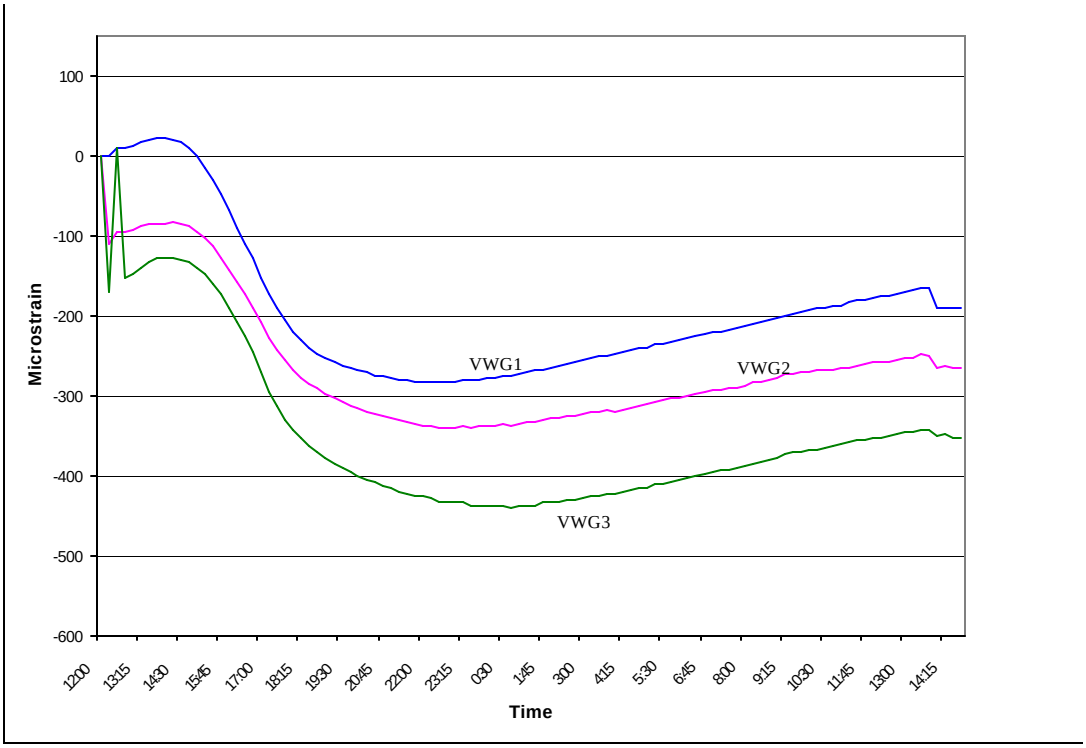

Figure 3.85 VWG Strains for Girder C4

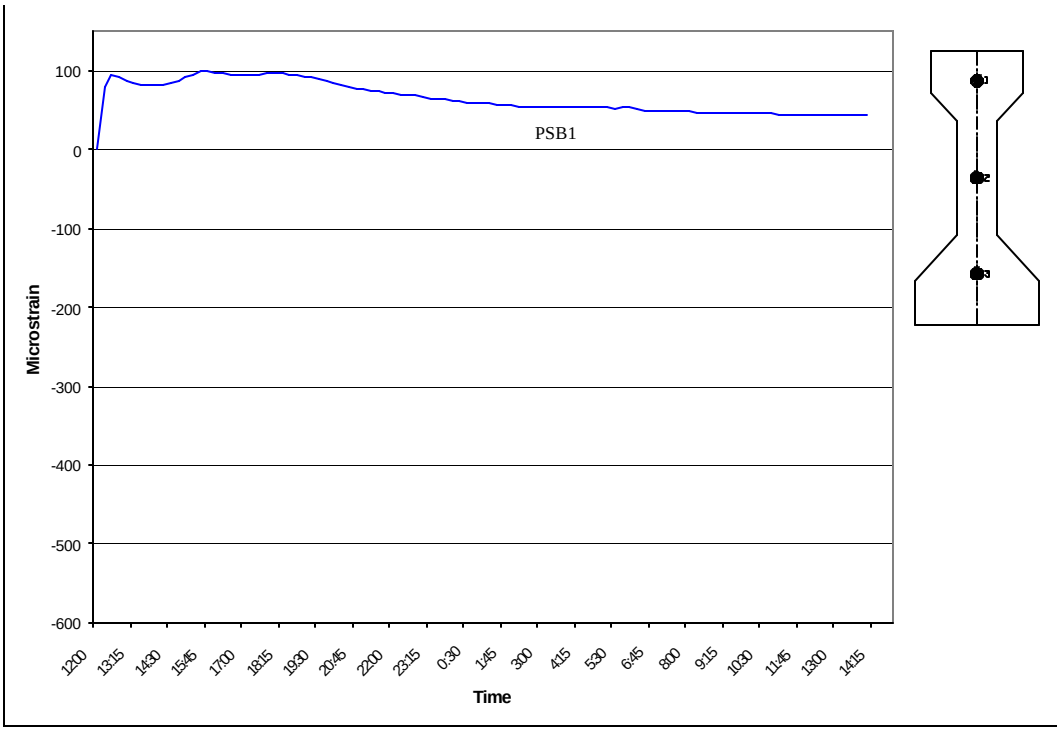

Figure 3.86 Plane Strain Bar Readings for Girder C4

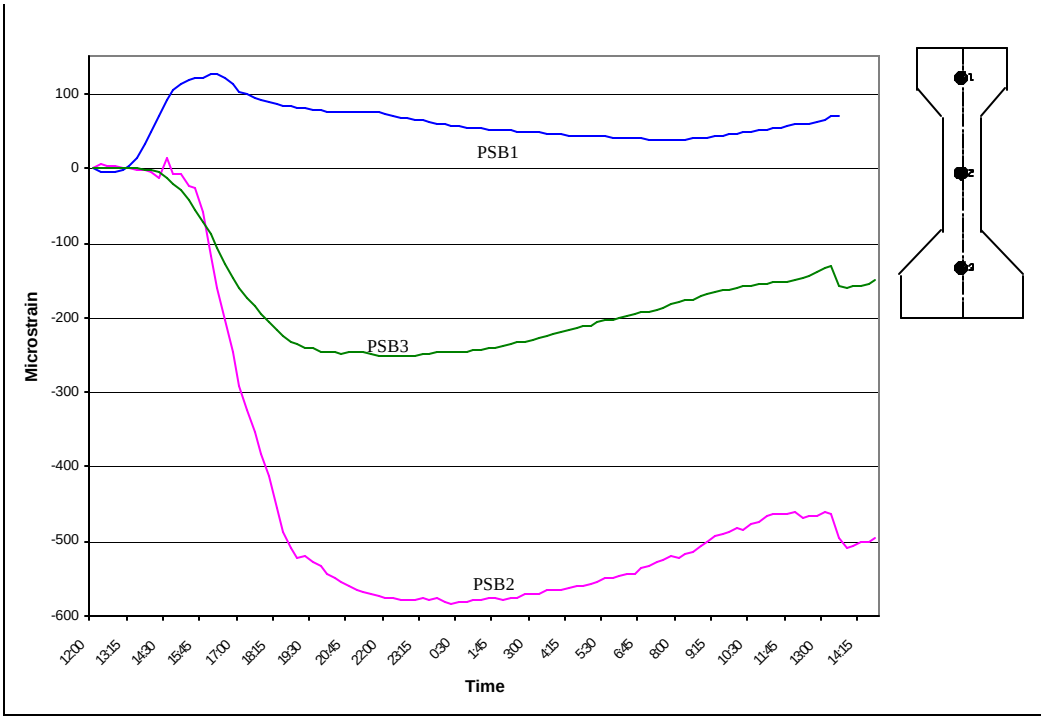

Figure 3.87 Plane Strain Bar Readings for Girder D4

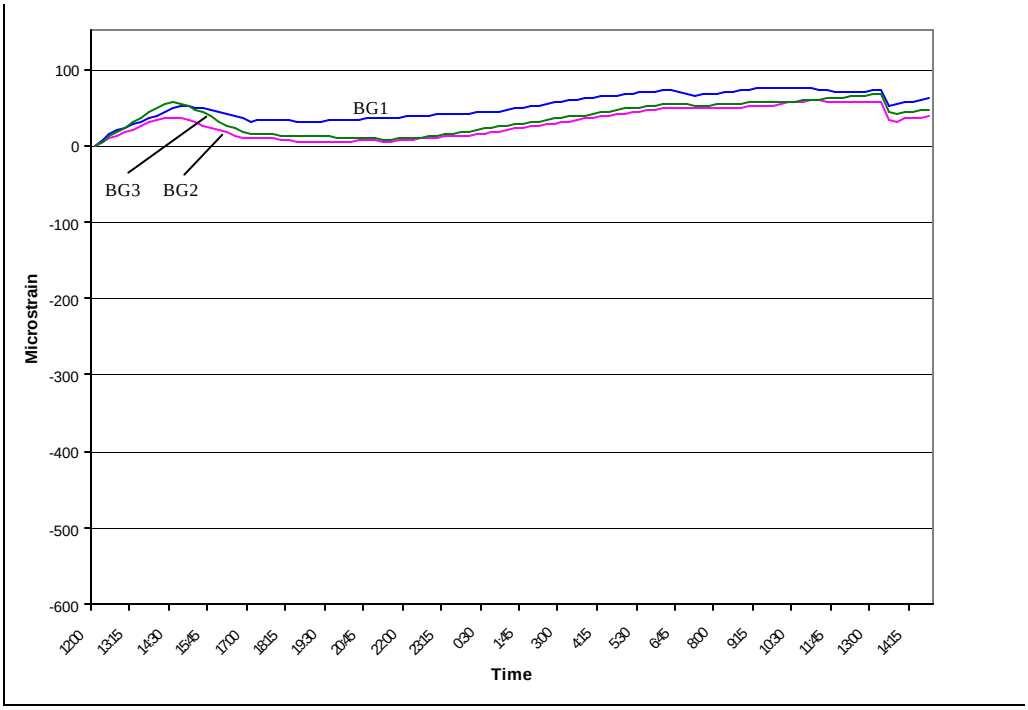

Figure 3.88 Embedment ERSG Readings for Girder D4

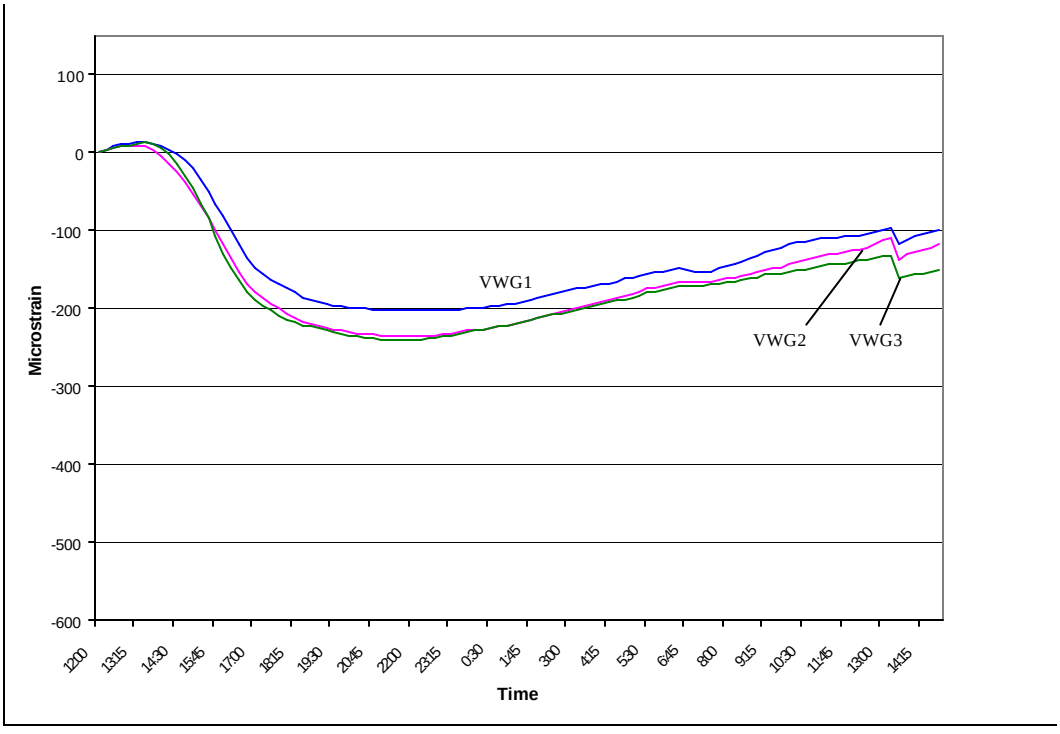

Figure 3.89 VWG Strains for Girder D4

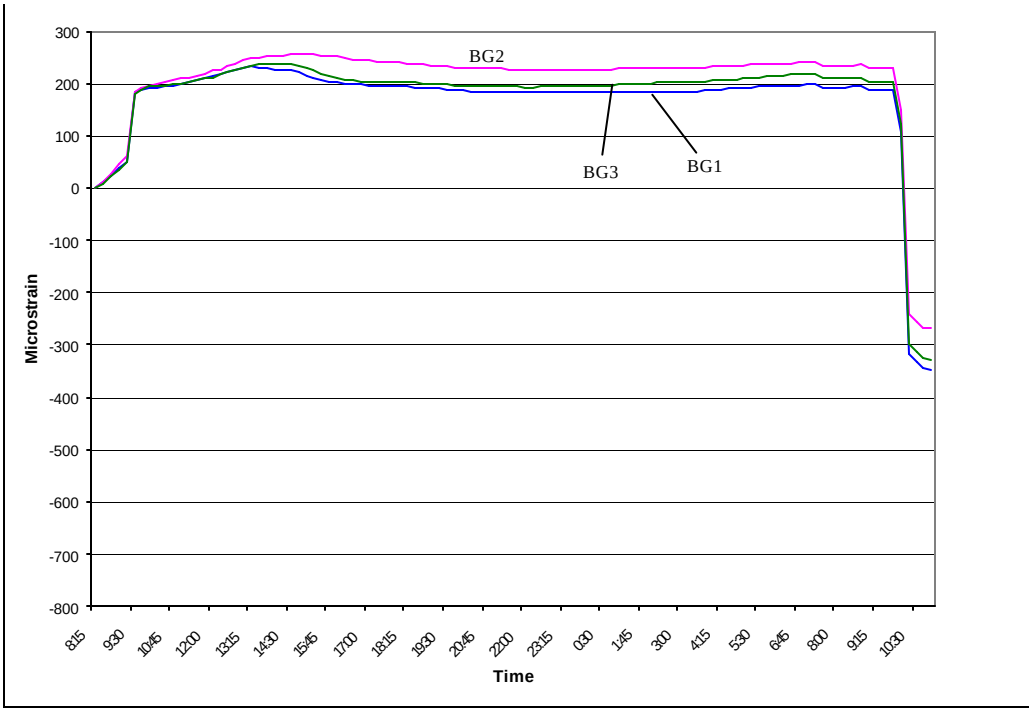

Figure 3.90 Embedment ERSG Readings for Girder A4

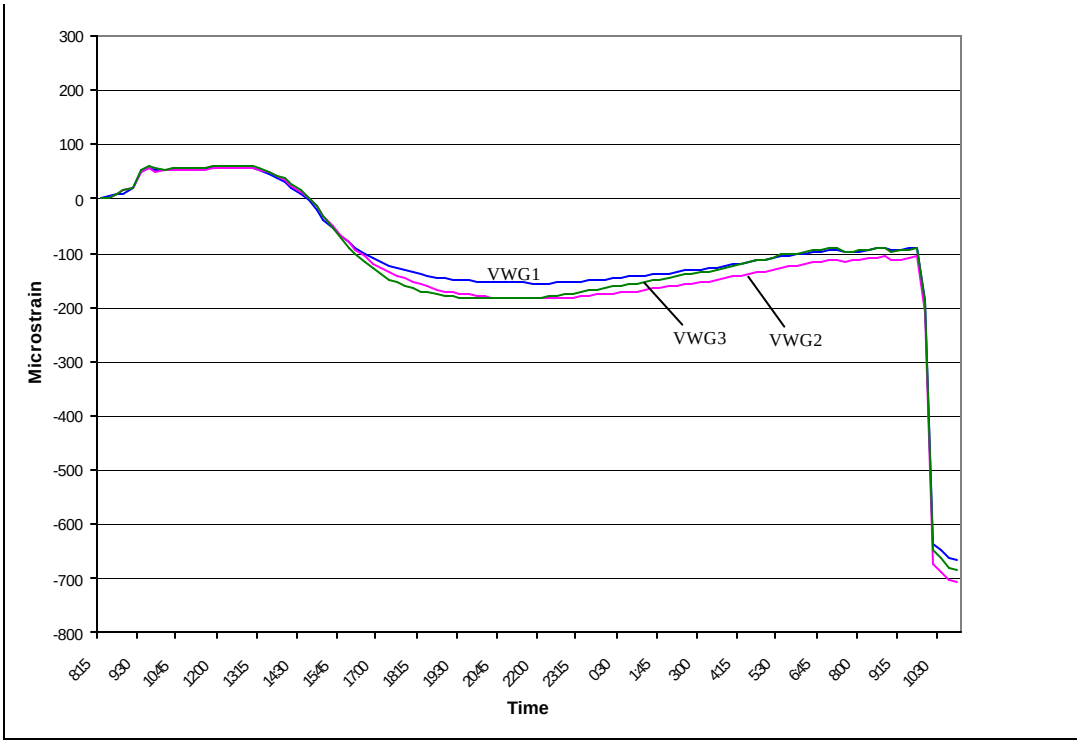

Figure 3.91 VWG Strains for Girder A4

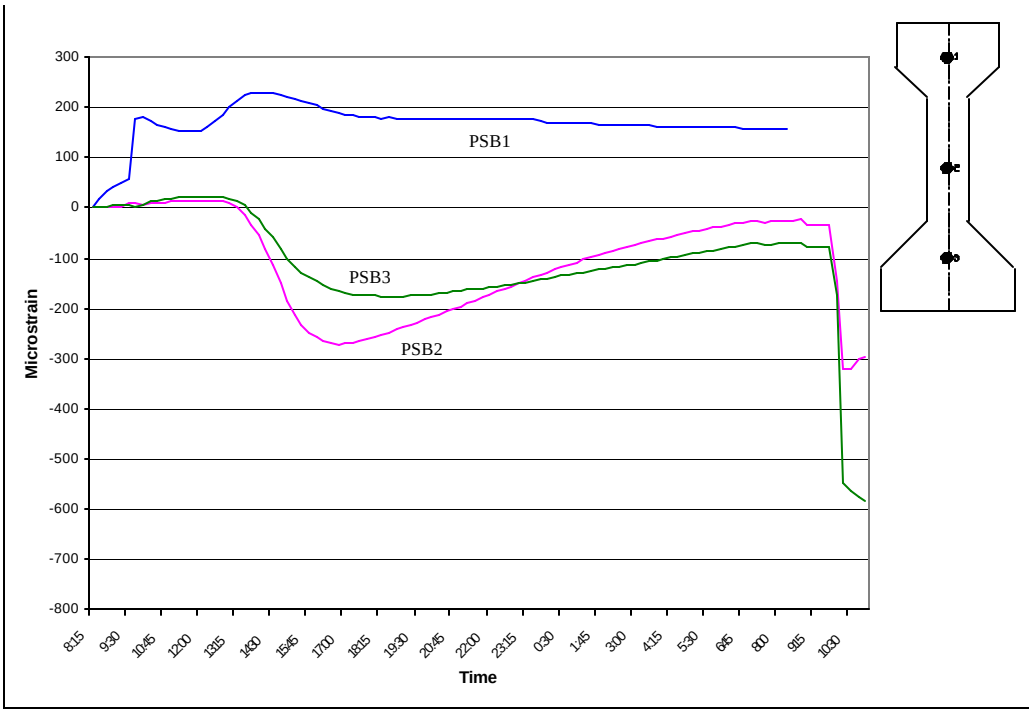

Figure 3.92 Plane Strain Bar Readings for Girder A4

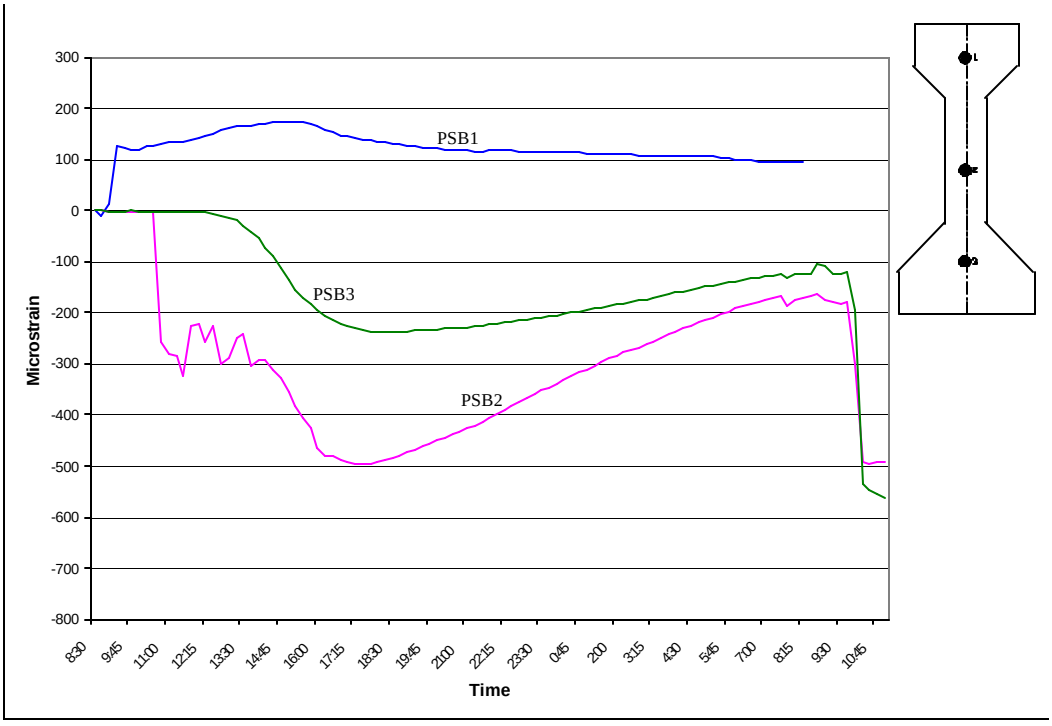

Figure 3.93 Plane Strain Bar Readings for Girder B4

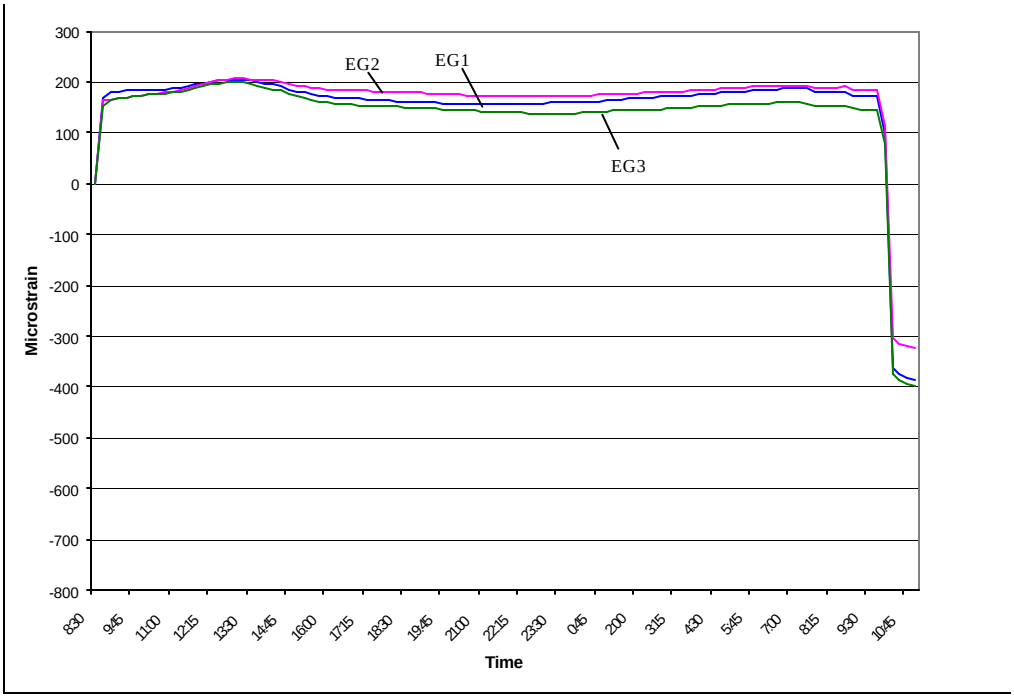

Figure 3.94 Embedment ERSG Readings for Girder B4

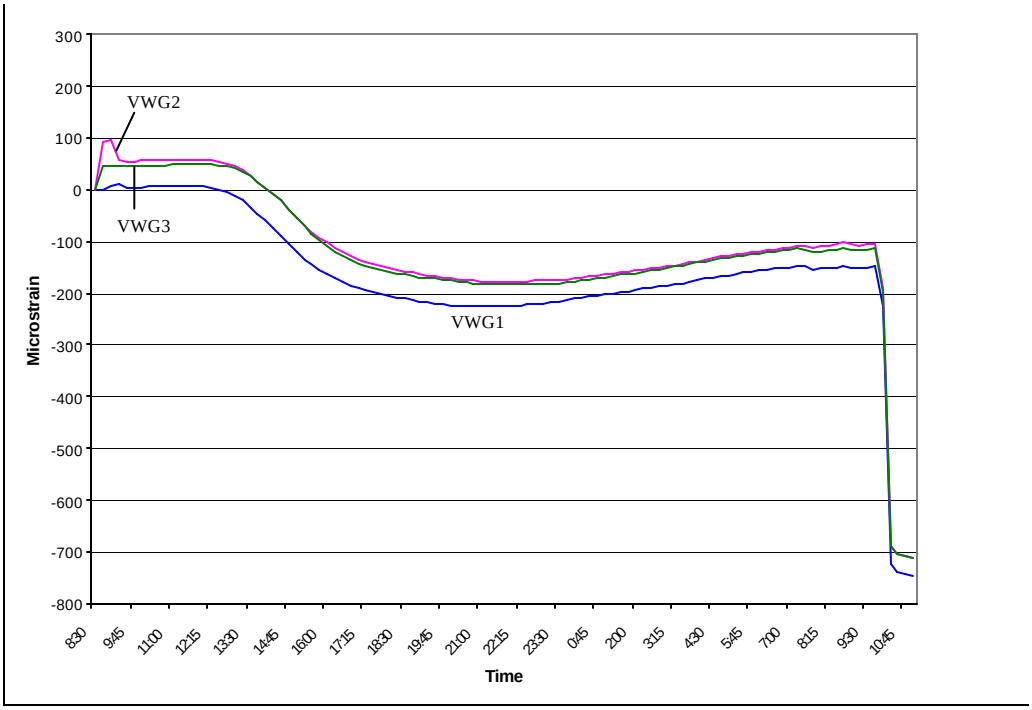

Figure 3.95 VWG Strains for Girder B4

3.7 Detensioning Strains

The difference between the strains measured just before detensioning and those measured just after represents the change in length per unit length of the girder at that location. Table 3.6 shows the strain value due to detensioning at each gage location. All gages are located at mid-span except VWG2/embedded ERSG2 and VWG3/ embedded ERSG3 (see Section 3.3.3). The location in the table is in reference to the cross-section.

Table 3.6 Detensioning Strains

Gage	Location	Strain (Microstrain)			
		Girder A4	Girder B4	Girder C4	Girder D4
SG1	Top	175	200	-	50
SG2	Middle	370	340	-	30
SG3	Bottom*	-	-	-	25
E. ERSG1	Bottom*	420	455	20	20
E. ERSG2	Bottom*	390	415	15	20
E. ERSG3	Bottom*	420	450	10	25
VWG1	Bottom*	450	500	20	15
VWG2	Bottom*	465	500	15	25
VWG3	Bottom*	460	490	5	25

- Indicates gage was damaged and does not function.
* Denotes center of gravity of prestressing steel.
E. Embedment.

By using Equation 3.4, the values shown in Table 3.6 can be compared with the values for loss due to elastic shortening found in Section 3.3.4. For example, the detensioning strain at the center of gravity of the prestressing steel in Girder A4 at midspan (VWG1) is 450 microstrain. This change in strain represents a loss of prestress of 12.8 ksi (using Equation 3.4), while the loss of prestress predicted in Section 3.3.4 was 18.1 ksi, as shown in Table 3.7. Similar values are listed for Girders B4, C4, and D4.

$$\Delta f_s = E_s e \qquad \text{(Eq. 3.4)}$$

where: Δf_s = loss of prestress in steel due to elastic shortening

E_s = modulus of elasticity of the prestressing strand (taken as 28,500 ksi)

e = measured detensioning strain

Table 3.7 Measured vs. Predicted Prestress Loss Due to Elastic Shortening

	Loss in Prestress (ksi)			
	Girder A4	**Girder B4**	**Girder C4**	**Girder D4**
Measured (Eq. 3.4)	12.8	14.3	0.6	0.4
Predicted (Eq. 3.1-3.3)	18.1	18.1	12.0	12.0
% Difference	29%	21%	95%	97%

Table 3.7 shows that the prestress loss due to elastic shortening based on the strain measurement is less than the predicted values presented in Section 3.3.4. Therefore, it appears that the total prestress loss for Type IV Girder given in Table 3.3 is slightly overestimated.

The strain values for the Type III girders (the last two columns of Table 3.6) are much smaller than expected. It indicates that the gages failed to record the entire compressive strain during detensioning. It is suspected that the failure in the strain measurement is due to inadequate consolidation of concrete around the embedded gages.

3.8 Camber

Camber was measured at mid-span of each girder, 1 hour and 24 hours after detensioning. Both readings were identical and are listed in Table 3.8. Figure 3.40 shows the camber of girder D4 as it separates from the casting bed.

Figure 3.96 Camber of Girder D4

The PCI Design Handbook gives expressions for determining the upward deflection that results from the prestressing force. Figures 3.97 gives the equation for calculating this deflection for the Type III girders and Figure 3.98 for the Type IV. These deflections do not take into account the weight of the girder itself. Equation 3.7 gives the downward deflection due to the dead weight of the girder. Subtracting the downward deflection from the upward deflection gives the predicted camber. Table 3.8 gives the calculated camber. The values for modulus of elasticity used in the calculations were the same predicted averages used in the calculation of prestress loss (see pages 65-66).

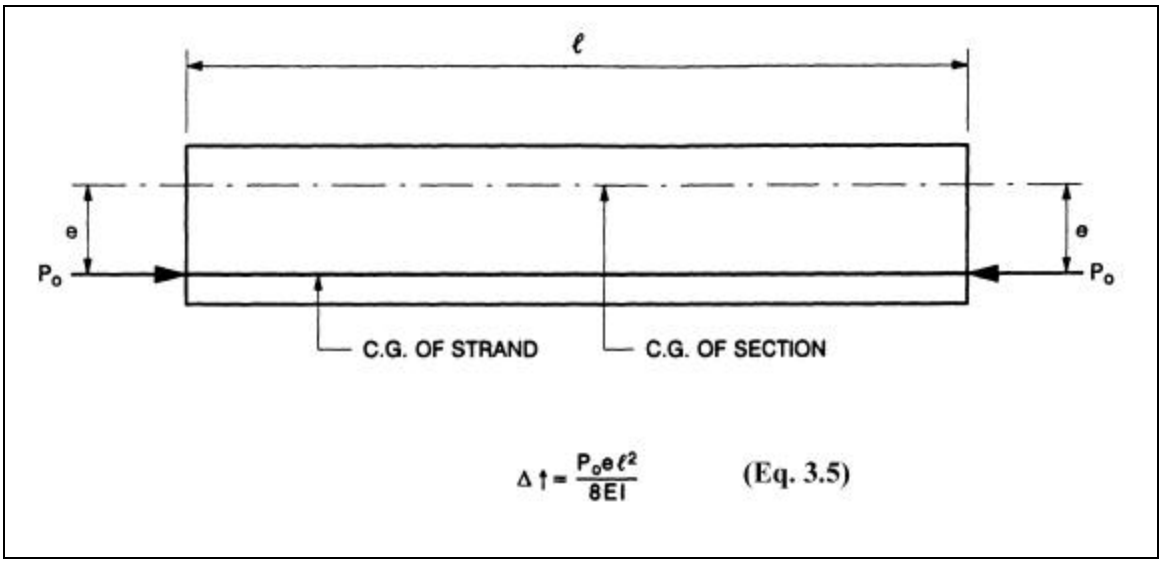

Figure 3.97 Camber Equation for a Straight Strand Profile

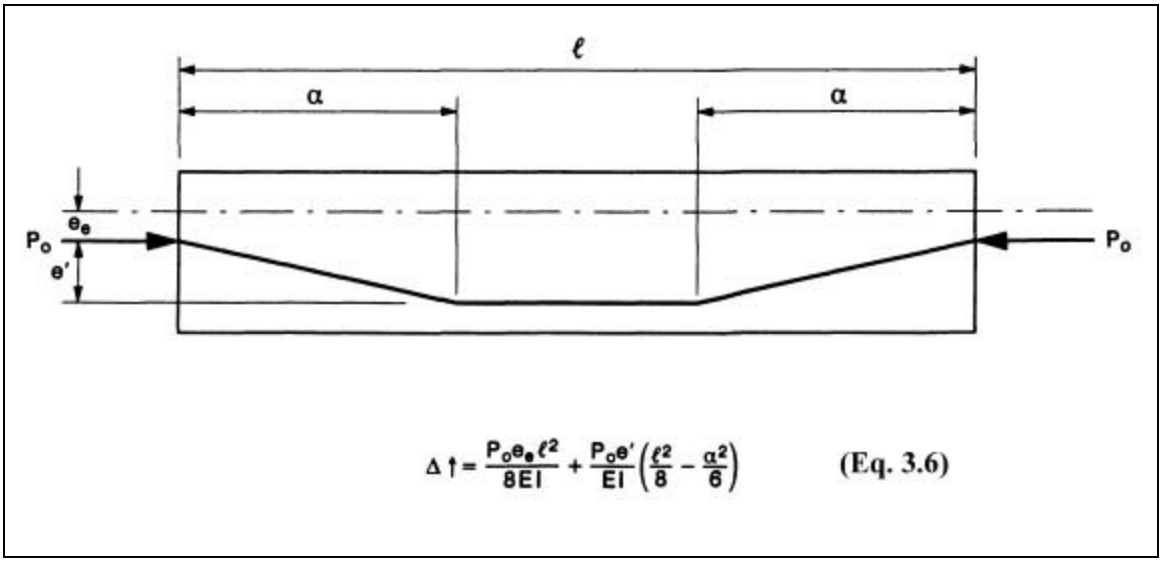

Figure 3.98 Camber Equation for a Two Point Depressed Strand Profile

$$\Delta\downarrow = \frac{5wl^4}{384E_{ci}I} \qquad \text{(Eq. 3.7)}$$

where: $w =$ weight of the concrete (lbs)
$l =$ length of the girder (inches)
$E_{ci} = E =$ modulus of elasticity at release (psi)
$I =$ gross section moment of inertia (inches^4)

Table 3.8 Girder Camber

	Type III Girders		Type IV Girders	
	Girder C4	**Girder D4**	**Girder A4**	**Girder B4**
Measured Camber (inches)	0.625	0.5	1.125	1.125
Predicted Camber (inches)	0.52	0.52	1.3	1.3
Percent Difference	17%	4%	13%	13%

4. CONCLUSIONS

This research examined the material properties and behavior of four prestressed HPC girders during casting and initial curing. Based on this research, the following conclusions can be drawn:

1. In general, the HPC used in this research was of good quality. Casting of a mock-up girder to demonstrate the constructability of the concrete was very helpful. The concrete performed well and met the expected results in compressive strength, modulus of rupture, coefficient of thermal expansion, and creep.
2. The modulus of elasticity of the concrete was lower than expected, most likely due to higher volume fraction of cement paste in the concrete, heat and air curing of the test specimens, and to a lesser extent the characteristics of the coarse aggregate.
3. The shrinkage of the concrete as measured by using the standard prisms stored in the laboratory exceeded the expected value by as much as 25 percent. However, the full-sized girder specimens placed in outdoor environment showed only 10 to 20 percent of the expected value. Such major differences reflect the effects of specimen size and the difference in the environmental conditions.
4. The results of the rapid chloride permeability test were higher than expected. The higher values of permeability are most likely the results of higher cement content of the HPC mix and the use of heat and air cure of the test specimens.

Both of these two factors could cause more and larger pore structures of the concrete paste, which would in turn increase the permeability of the concrete.

5. During concrete curing, the temperature measured by the embedded thermocouples showed that peak temperatures occurring 7 to 8 hours after casting never reached more than 80º C (176º F). Therefore, there was no danger of thermal cracking.

6. Based on the load cell readings (Tables 3.1 and 3.2), practically there were no changes of the initial prestressing force up to the time of detensioning. Therefore the measurement suggested that there was no loss of prestress due to strand relaxation prior to detensioning.

7. Upon detensioning, the transfer lengths for the 0.6 in. strand were found to be 28 and 26 inches, respectively, for Type III and Type IV girders. These values are slightly less than the standard design value of 50 times the strand diameter or 30 in.

8. During detensioning, the embedded gages recorded compressive strains of 20 microstrain on average for the Type III girders and 435 microstrain on average for the Type IV girders at the mid-span. It appeared that the gages in the Type III girders failed to record the full compressive strain during detensioning possibly due to inadequate consolidation of concrete around the embedded gages. The response of the gages in the Type IV girders were consistent with the predicted values of elastic shortening.

9. The calculated prestress loss due to elastic shortening was 12.0 ksi for the Type III girders and 18.1 ksi for the Type IV girders.
10. Total prestress loss was 26.0 ksi (12.9%) for the Type III girders and 38.1 ksi (19.1%) for the Type IV girders. Elastic shortening and creep were the major contributors to the total loss. The loss due to shrinkage was almost insignificant, since the shrinkage strain measured from the full-sized girder specimens was much less than normally expected.
11. The predicted camber compared closely with the measured camber. The close prediction was possible because the use of load cells at the anchoring end of the prestressing bed provided a more accurate value of the prestressing force at transfer than the normally assumed prestressing force based on estimated loss of prestress.
12. Prefabricating the instrumentation assemblies in the laboratory was very beneficial. The prefabricated assemblies eased the transportation to the job site, improved the field installation process, and provided excellent protection for the gages and lead wires.
13. The use of an embedded vibrating wire gage in a concrete cylinder to measure the concrete strain variation when the cylinder is subjected to a heating and cooling cycle is a simple, novel and economical method to determine the coefficient of thermal expansion of concrete.
14. Measuring the transfer length of the prestressing strand by using a small diameter steel bar instrumented with strain gages and embedded at the end of

a prestressed concrete girder is another original and simple technique developed in this research.

RECOMMENDATIONS

This project has demonstrated that HPC technology can be successfully implemented for highway bridge construction in North Carolina. There were no insurmountable technical problems, although certain material properties could be improved for future projects of similar type. Based on the experience gained in this project, the following recommendations can be made:

1. NCDOT should continue to identify appropriate projects to make use of HPC so as to take its full economic advantage.
2. Develop an improved Q/A program, which will include a pre-bid conference with prospective bidders, and required periodic meetings with the contractor to review progress of work and to resolve any technical issues.
3. Review the current special provisions of specifications on HPC and consider the need for introducing requirements on certain material characteristics in addition to the current requirements on compressive strength for concrete at prestress transfer and at 28 days. The additional requirements may include a maximum amount of cementitious materials used in the concrete mix proportion, a maximum water-cementitious materials ratio, a minimum requirement for the modulus of elasticity of concrete, a maximum limit on concrete permeability, and a higher limit on concrete slump after addition of superplasticizer.
4. Review and evaluate all available data on shrinkage of large-sized concrete members exposed to natural environment, and determine how such data can

be utilized in the determination of loss of prestress.

5. Review and evaluate all available data on loss of prestress in girders made of HPC, and develop an improved approach for estimating the loss of prestress.
6. Conduct pertinent studies on high strength flowable self-consolidating concrete for applications in prestressed concrete bridge construction.

IMPLEMENTATION

The investigators will make presentations on the findings of this research to representatives of NCDOT so that the information and data developed in this project can be incorporated into future HPC bridge projects. It is also anticipated that technical papers based on this research will be prepared by the principal investigators for presentations at national meetings of technical societies such as TRB and ACI .

REFERENCES

ACI Committee 318, "Building Code Requirements for Reinforced Concrete (ACI 318-99) and Commentary – ACI 318 R-99," ACI International, Farmington Hills, MI, 1999, 353 pp.

Alshamsi, Abdullah M., "The Influence of Silica Fume and Curing Temperatures on the Strength of HSC," *High Performance Concrete: Design and Materials and Recent Advances in Concrete Technology*, Proceedings of the ACI International Conference, Malaysia, ACI SP-172, ACI International, Farmington Hills, MI, 1997, pp. 57-66.

Anon., "Acoustic Strain Gauges Ease Bridge Monitoring," *Civil Engineering*, Vol. 67, September 1997, p. 83.

Anon., "Fiber Optics Monitors Composite Bridge," *Civil Engineering*, Vol. 67, December 1997, p. 74.

Collins, Michael P. and Mitchell, Denis, *Prestressed Concrete Structures*, Copywell, Ontario, 1997, pp. 57-65.

Ehlen, Mark A., "Life-Cycle Costs of New Construction Materials," *Journal of Infrastructure Systems*, Vol. 3, No. 4, December 1997, p. 54.

French, Catherine, Shield, Carol, and Ahlborn, Theresa, "Tests of Two High Performance Concrete Prestressed Bridge Girders," *Proceedings of the PCI/FHWA International Symposium on High Performance Concrete*, PCI, Chicago, IL, October 1997, pp. 394-405.

Fuhr, Peter L., Huston, Dryver R., and MacCraith, Brian, "Embedded Fiber Optic Sensors for Bridge Deck Chloride Penetration Measurement," *Optical Engineering*, Vol. 37, No. 4, April 1998, pp. 1221-1228.

Gilliland, James A. and Dilger, W. H., "Monitoring Concrete Temperature During Construction of the Confederation Bridge," *Canadian Journal of Civil Engineering*, Vol. 24, 1997, pp. 941-950.

Gowripalan, N. and Zou, X. W., "Flexural Behavior and Ductility of Prestressed Beams with High-Strength Concrete," *High Performance Concrete: Design and Materials and Recent Advances in Concrete Technology*, Proceedings of the ACI International Conference, Malaysia, ACI SP-172, ACI International, Farmington Hills, MI, 1997, pp. 573-599.

Halkyard, Terry, "Workshop Showcases High-Performance Concrete Bridges," *Focus*, FHWA, Washington D. C., May 1996, pp. 4-5.

Helland, Steinar, "Application of High-Strength Concrete in Norway," *High Strength Concrete: An International Perspective*, ACI SP-167, ACI, Farmington Hills, MI, 1997, pp.27-53.

Lachemi, Mohamed, Bois, Axel-Pierre, Miao, Buquan, Lessard, Michel, and Aitcin, Pierre-Claude, "First Year Monitoring of the First Air-Entrained High-Performance Bridge in North America," *ACI Structural Journal*, V. 93, No. 4, July-August 1996, pp. 379-386.

Naaman, Antoine E, *Prestressed Concrete Analysis and Design Fundamentals*, Irwin/McGraw Hill, 1982, p.65.

Nagataki, Shigeyoshi, "High-Strength Concrete in Japan: History and Progress," *High Strength Concrete: An International Perspective*, ACI SP-167, ACI International, Farmington Hills, MI, 1997, pp.1-15.

Oh, Byung Hwan and Kim, Eui Sung, "Realistic Evaluation of Transfer Lengths in Pretensioned, Prestressed Concrete Members," ACI Structural Journal, Vol. 97, No. 6, Nov-Dec 2000, pp. 821-830.

Pauw, A., "Static Modulus of Elasticity of Concrete as Affected by Density," *ACI Journal*, Vol. 57, No. 6, Dec. 1960, pp. 679-688.

PCI Design Handbook Precast and Prestressed Concrete, 5th Edition, Precast/Prestressed Concrete Institute, Chicago, 1999.

Price, Ken D., He, Eddie Y., Haines, Steve R, and Paulik, Arnaud Y., "High Performance Bridges," *High Strength Concrete: First International Conference*, ASCE, 1999, pp. 610-621.

Shah, S.P. and Ahmad, S.H., *High Performance Concrete: Properties and Applications*, McGraw-Hill, Inc, 1994, pp. 54-59, 354-363.

Shah, Surendra P., "Material Aspects of High Performance Concrete," *High Strength Concrete: First International Conference*, ASCE, 1999, pp. 504-511.

Shahawy, Mohsen A. and Aarockiasamy, M., "Field Instrumentation to Study the Time-Dependent Behavior in Sunshine Skyway Bridge - I," *Journal of Bridge Engineering*, Vol. 1 No. 2, ASCE, May 1996, pp. 76-86.

Shahawy, Mohsen A.; Aarockiasamy, M., "Field Instrumentation to Study the Time-Dependent Behavior in Sunshine Skyway Bridge - II," *Journal of Bridge Engineering*, Vol. 1 No. 2, ASCE, May 1996, pp. 87-97.

Tarricone, P., “Bridges Under Surveillance,” *Civil Engineering*, ASCE, May 1990, pp. 111-113.

Vanikar, Suneel, “What is High-Performance Concrete?” *Focus*, FHWA, Washington D. C., May 1996, p. 4.

Warren, Bruce, *Development of a Data Acquisition System for an Instrumented Highway Structure*, MSCE Thesis, North Carolina State University, 2000. 139 pp.

Yamada, Minoru and Matsuura, Hideki, “High Strength Concrete for Prestressed Concrete,” *High Strength Concrete: First International Conference*, ASCE 1999, pp. 363-376.

Zia, Paul, Ahmad, Shuaib, and Leming, Michael, *High Performance Concrete State-of-the Art Report (1989-1994)*, FHWA-RD-97-030, FHWA, Washington D.C., 1997. (http://www.tfhrc.gov/structur/hpc2/contnt.htm)

APPENDIX

PRESTRESS LOSS CALCULATIONS

	A_t	I_t	F	e	M_{DL}	f_c by Eq. 3.1	ε_s	ε_c	E_{ci}
	(in^2)	(in^4)	(kips)	(in)	(ft-kips)	(ksi)	microstrain	microstrain	(ksi)
Type III Girder	570.4	130,490	786.6	8.8	241	1.647	45	445	3,900
Type IV Girder	825.1	279,590	1,382.4	18.1	885	2.608	85	615	4,100

	Loss Due to Elastic Shortening (ksi)	Loss Due to Shrinkage (ksi)	Loss Due to Creep (ksi)	Total Loss (ksi)
	(Eq. 3.2)	(Eq. 3.3a)	(Eq. 3.3b)	
Type III Girder	12.0	1.3	12.7	26.0
Type IV Girder	18.1	2.4	17.5	38.1